UNIVERSITY OF CALIFORNIA

Santa Barbara

Computational Mechanistic Study of the Reactivity of Metal Oxide Catalyst towards Olefins

A dissertation submitted in partial satisfaction of the

requirements for the degree Doctor of Philosophy

in Chemical Engineering

by

Anthony Mark Fong

Committee in charge:

Professor Baron Peters, Chair

Professor Susannah Scott

Professor Brad Chmelka

Professor Horia Metiu

March 2015

The dissertation of Anthony Mark Fong is approved.

_____

Professor Susannah Scott

_____

Professor Brad Chmelka

_____

Professor Horia Metiu

_____

Professor Baron Peters, Committee Chair

December 2014

Computational Mechanistic Study of the Reactivity of Metal Oxide Catalysts to Olefins

by

Anthony Mark Fong

ACKNOWLEDGEMENTS

This work would not have been possible without the support of my advisor, Baron Peters. I would like to thank him for his generous patience with me over these past five years. I would also like to thank Susannah Scott, particularly for the discussions I have had with Baron and her. This work would not have been possible without her insight, guidance, and expertise. I am also thankful to my other committee members, Brad Chmelka and Horia Metiu. Their advice and knowledge were helpful in completing the necessary work for my thesis.

In addition, I am grateful to the Peters Group for all of their help. I would like to thank Nathan Duff for his maintenance of the cluster. My work would not have been possible without his diligence and deep knowledge. I also owe much thanks to Sam Ivry and Chris Yuan for their help in running some of my calculations.

Finally, I would like to acknowledge the support of my parents. I am indebted to their sacrifices and encouragement.

Curriculum Vita

Anthony Mark Fong
December 2014

Education

B.S. Chemical Engineering, University of California, Berkeley, May 2009
Ph.D. Chemical Engineering, University of California, Santa Barbara, December 2014 (expected)

Professional Employment

Spring 2013 TA for Thermodynamics, Chem. Eng. 110B, UC Santa Barbara

Spring 2012 TA for Chemical Engineering Laboratory, Chem. Eng. 180A, UC Santa Barbara

Winter 2011, Spring 2012, Spring 2013: Teaching Assistant, Department of Chemical Engineering, University of California, Santa Barbara

Publications

B. R. Goldsmith, A. Fong, B. Peters, B. "Understanding reactivity with reduced potential energy landscapes: recent advances and new directions." In K. Han & T. Chu, *Reaction Rate Constant Computations: Theories and Applications* (pp. 213-232). Cambridge, U.K., Royal Society of Chemistry (2013)

Presentations

A. Fong, S.L. Scott, B. Peters, "Computational Mechanistic Study of the Philips Ethylene Polymerization Catalyst." Institute of Pure and Applied Mathematics, UCLA, (6/2014)

A. Fong, S.L. Scott, B. Peters, "Computational Mechanistic Study of the Philips Ethylene Polymerization Catalyst."AIChE Annual Meeting, Atlanta, Georgia, (11/2014)

ABSTRACT

Computational Mechanistic Study of the Reactivity of Metal Oxide Catalysts to Olefins

by

Anthony Mark Fong

Two heterogeneous catalysts, the Phillips ethylene polymerization catalyst and supported rhenium olefin-metathesis catalyst, are computationally investigated.

The mechanism of ethylene polymerization by the Phillips catalyst remains unknown despite numerous hypotheses and studies since its discovery sixty years ago. This work uses density functional and small chromasiloxane cluster models to compare initiation, propagation, and termination pathways for several previously proposed mechanisms and for two newly proposed mechanisms. Where possible, complete catalytic cycles and predicted kinetics, molecular weights, and site abundances are compared to properties of the Phillips catalyst. Prohibitively high activation barriers for propagation rule out chromacycle ring expansion and Green-Rooney mechanisms (alternating alkylidene/chromacycle). A new oxachromacycle ring expansion mechanism has a favorable plausible propagation barrier, but initiation for the oxachromacycle expansion is prohibitively slow. Chain growth is fast on a recently proposed bridging hydroxyl $Si(OH)Cr^{III}$-alkyl site that is initiated by proton transfer from ethylene. However, the initiation step is extremely slow and uphill, and termination is even faster than propagation, so essentially all sites remain trapped in a dormant state. A new $Si(OH)Cr^{II}$-alkyl site also has a small barrier for Cossee-Arlman type

chain growth, but it forms only oligomers because termination by proton transfer back to the alkyl chain is faster than propagation, and initiation is slow. Only the monoalkylchromium(III) site $(\equiv SiO)_2Cr$-alkyl is viable as an active site for polymerization, however the nature of the initiation mechanism remains unknown.

CH_3ReO_3 (MTO) interacting with the surface of extensively chlorinated γ-Al_2O_3 is a highly active catalyst for olefin metathesis. Its activity, selectivity and stability exceed that of any other reported MTO-based catalyst as measured in propene metathesis at 0 °C, including MTO/SiO_2-Al_2O_3 and MTO/$ZnCl_2$/γ-Al_2O_3, and are far higher than MTO/γ-Al_2O_3. DFT calculations support facile Cl-O ligand exchange between MTO and Cl-Al_2O_3. The calculations further suggest that chlorination at Re promotes active site formation via tautomerization.

TABLE OF CONTENTS

LIST OF FIGURES

LIST OF TABLES

Chapter 1

Introduction

Many heterogeneous catalysts are important to industrial processes because of their high activity and ability to be separated readily from products after reaction. Examples include iron for ammonia synthesis,[1] zeolites for catalytic cracking of gas oil,[2] and supported transition metals for olefin polymerization.[3]

However, many of these systems, such as the Phillips catalyst or supported MTO for olefin metathesis, have a low fraction of active sites. This complicates characterization of the active species, because spectroscopic signals may correspond to the major fraction of inactive sites.[4] Without a molecular understanding of these systems, the relationship between catalyst design and product is unknown. For instance, impregnating titanium into the silica support during preparation of the Phillips catalyst decreases the molecular weight of the polethylene, which determines whether the final polymer is suitable for blow molding, films, or other applications. Without the activation mechanism for the catalyst, the origin of the catalyst behavior is unknown.

Computational modeling with density functional theory (DFT) can potentially address this problem by testing various proposed active mechanism. Through quantum chemistry and solution to the Schrödinger equation, the total energy of a reaction intermediate or

transition state can be computed. From there, computed reaction and activation energies can be used to determine which pathways and candidate active site are the most likely. While DFT functionals are improving,[5] prediction of rates are still not sufficiently accurate. However, theoretical calculations can still play an important role in finding trends, and add or refute support to experimental results.

In the following chapters, such simulation results are presented for supported metal oxide heterogeneous catalysts. Chapter 2 involves an investigation of the Phillips oliefin polymerization catalyst. Reaction barriers and energies are reported for four pathways involving a Cr(II) site. Two additional pathways are investigated for a Cr(III) site. A Cossee-Arlman mechanism on a (≡SiO2)Cr(III) site was found to be most favorable, and a microkinetic model is presented, along with a prediction of reaction rate and predicted molecular weights. A recently proposed Cr(III) mechanism involving initiation by proton transfer is analyzed and shown to be unlikely.

In Chapter 3, activation of methyltrioxorhenium (MTO) supported on chlorinated alumina, a heterogeneous catalyst for olefin metatheis, is investigated. Multiple pathways for proton transfer from the methyl of MTO to either a lone metal oxo or an oxo bridging between the metal and aluminum are considered. The most favorable proton transfers were found to occur after chlorination of rhenium.

References

1. Jennings, J. R., *Catalytic ammonia synthesis : fundamentals and practice*. Plenum Press: New York, 1991; p xx, 451 p.
2. Rahimi, N.; Karimzadeh, R., Catalytic cracking of hydrocarbons over modified ZSM-5 zeolites to produce light olefins: A review. *Applied Catalysis a-General* **2011,** *398* (1-2), 1-17.

3. Hoff, R. E.; Mathers, R. T., *Handbook of transition metal polymerization catalysts*. Wiley: Hoboken, N.J., p xxi, 575 p.
4. McDaniel, M. P., A Review of the Phillips Supported Chromium Catalyst and Its Commercial Use for Ethylene Polymerization. *Advances in Catalysis, Vol 53* **2010,** *53*, 123-606.
5. Minenkov, Y.; Singstad, A.; Occhipinti, G.; Jensen, V. R., The accuracy of DFT-optimized geometries of functional transition metal compounds: a validation study of catalysts for olefin metathesis and other reactions in the homogeneous phase. *Dalton Transactions* **2012,** *41* (18), 5526-5541.

Chapter 2

Computational Analysis of Ethylene Polymerization Mechanism for the Phillips (Cr/SiO_2) Catalyst

2.1. Introduction

The Phillips catalyst (Cr/SiO_2), discovered serendipitously in 1951, is still used today in the annual production of nearly half of the world's supply of high density polyethylene.[1] Typical properties of Phillips polyethylene are a weight-averaged molecular weight of ca. 10^5 g/mol, a dispersity of D = 4-100, and a polymerization rate of 2-5 x 10^3 C_2H_4 molecules s^{-1} Cr^{-1} at 373 K and 40 atm C_2H_4 pressure.[1] The polyethylene properties can be adjusted for pipe extrusion, film blowing, or other applications by modifying the catalyst. For example, increasing the catalyst calcination temperature, which enhances the activity, usually lowers the polymer average molecular weight.[2] The presence and amount of additional catalyst components (such as alkylaluminum reagents) change the polymer density.[1, 3] Incorporating titanium into the silica support causes chain transfer to accelerate and the molecular weight distribution, which determines toughness and creep resistance, to broaden.[1, 4, 5] Although numerous other methods for tailoring specific polymer attributes are known, there is little molecular-level understanding of how they work, nor even any consensus on the nature of the minority Cr active sites.

The mystery of how the inorganic precursor sites of the Phillips catalyst (CrO_x/SiO_2) spontaneously initiate polymerization has resisted sustained investigation by many research groups over several decades. Unlike other catalysts for α-olefin polymerization, the silica-supported chromate ester sites that are believed to be present in the pre-catalyst do not require an external source of alkyl or hydride groups to create the first polymer chain (Figure 2.1). Nevertheless, in the most widely-accepted mechanistic model, ethylene inserts into a Cr-H or Cr-C bond (Figure 2.2), resulting in a new alkylchromium site that polymerizes ethylene by repeated insertion of monomer.[6] Through β-H transfer to an incoming ethylene molecule, the growing polymer chain is eventually expelled, and a newly-formed alkylchromium continues the polymerization process. This mechanism is well-established for Ziegler-Natta catalysts, which either possess pre-existing alkyl ligands or acquire them from alkylating agents (co-catalysts).[7]

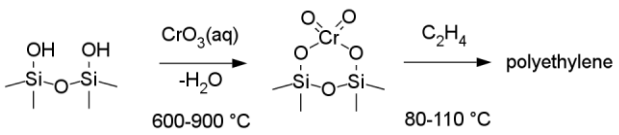

Figure 2.1: Supporting CrO_3 on amorphous silica leads to formation of grafted chromate esters, whose exposure to ethylene at ca. 100 °C results in spontaneous active site formation during a pronounced induction period, and subsequent polymer growth.

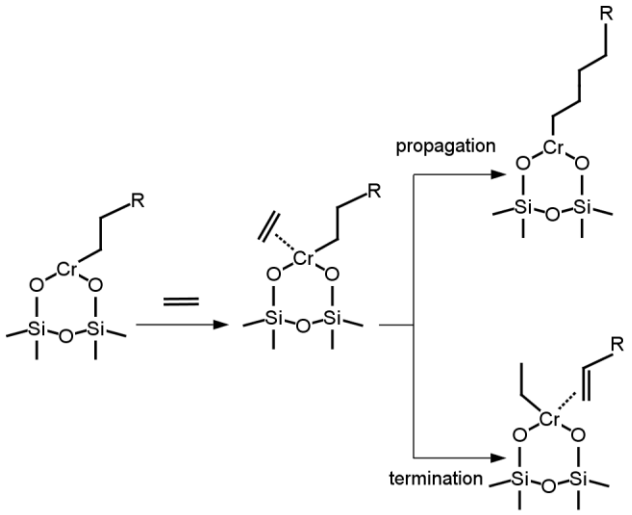

Figure 2.2: Proposed Cossee-Arlman mechanism for Phillips polymerization by minority alkylchromium(III) sites formed *in situ* under reaction conditions. R is either H or an alkyl group.

For the Phillips catalyst, such a mechanism requires that an alkyl ligand (most likely with an odd number of H atoms) be formed from ethylene alone, with its even number of H atoms. This dilemma is known as the "missing hydrogen" problem.[1, 6, 8] In principle, the silica support could supply the additional proton from one of its surface hydroxyl groups. However, calcining the support to *remove* most of these hydroxyl groups as water is necessary, and higher calcination temperatures actually cause the polymerization activity to increase.[2] Isotopic labeling experiments[9] as well as first-principles calculations[10] are consistent with chain propagation by a Cossee-Arlman mechanism once the alkyl group is established, although the evidence consists largely of analogy to Ziegler-Natta catalysts,[6] or elimination of other possible mechanisms.[9-11] There is still no mechanism that explains the initial alkyl ligand creation.

Several alternative mechanisms that circumvent the "missing hydrogen" problem have been proposed (Figure 2.3), although each faces its own challenges. For instance, polyethylene chains could potentially grow by repeated ring expansion of a chromacycle

(**M**),[12] or by alternation of carbene and chromacyclobutane intermediates (**C**).[13] Neither mechanism requires an external source of hydrogen or alkyl groups. However, isotopic labeling experiments[9, 11] suggest that neither is correct. Using first principles calculations, Espelid and Børve[10] computed large barriers for both mechanisms, and concluded that neither was a likely mode of polymerization.

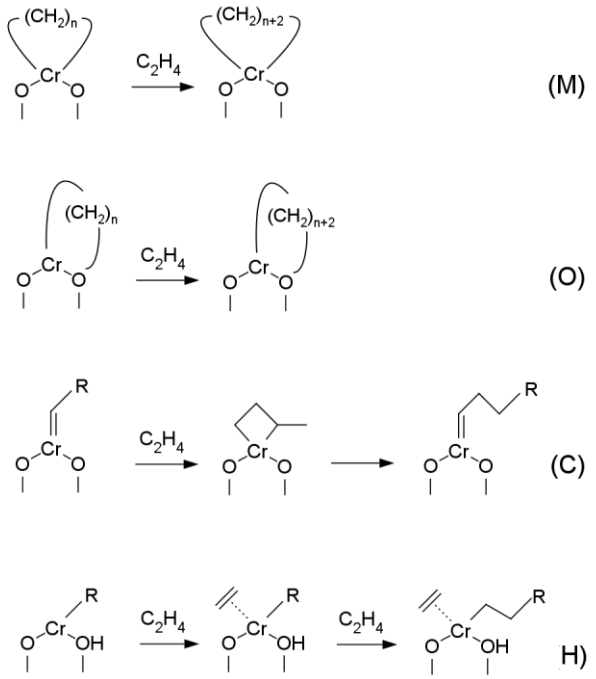

Figure 2.3: Four alternative propagation mechanisms proposed for ethylene polymerization by the Phillips catalyst. Chromacycle (M): ethylene inserts into either of two equivalent Cr-C bonds in a ring that includes a Cr(IV) ion. Oxachromacycle (O): polymer grows by insertion into the Cr-C bond of a ring that includes a support O and a Cr(II) ion. The ring is initially formed by addition of ethylene across a Cr-O bond. Carbene (C): an alkylidenechromium(IV) site undergoes ethylene cycloaddition to give a substituted chromacyclobutane, which then reverts to an alkylidene via a 1,3-H shift. Cossee-Arlman with Cr(II) (H): ethylene inserts into the Cr-C bond of an alkylchromium(II) site.

This study investigates yet two more polymerization mechanisms, which do not require an external source of hydrogen or alkyl group. First, the oxachromacycle mechanism (designated **O**) resembles the chromacycle mechanism except that the ring includes a Cr-O bond. Second, we consider proton transfer initiation and a Cossee-Arlman polymerization at

a Cr(II) site (designated **H**).[19] For both of these mechanisms, the chromium oxidation state is also +2, consistent with that in the pre-reduced Phillips catalyst that initiates polymerization spontaneously without an induction period.[20, 21]

Most recently, Delley et al.[14, 15] also suggested that an inorganic Cr(III)/SiO_2 catalyst polymerizes ethylene after activation via proton transfer from ethylene to a bridging oxygen. Delley et al. propose that the proton transfer step creates an Si(OH)Cr-vinyl site, then grows a polymer by a Cossee-Arlman mechanism, and then terminates via proton transfer back to the alkyl chain which restores the Cr(III)/SiO_2 as shown in Figure 2.4.

In this work, we examine the six hypothetical mechanisms. Specifically, we investigate the barriers to initiation, the kinetics of polymerization, the molecular weight, and termination pathws that do and do not leave a site ready for polymerization. All mechanisms are examined with a single range-separated DFT model chemistry to enable direct comparisons.

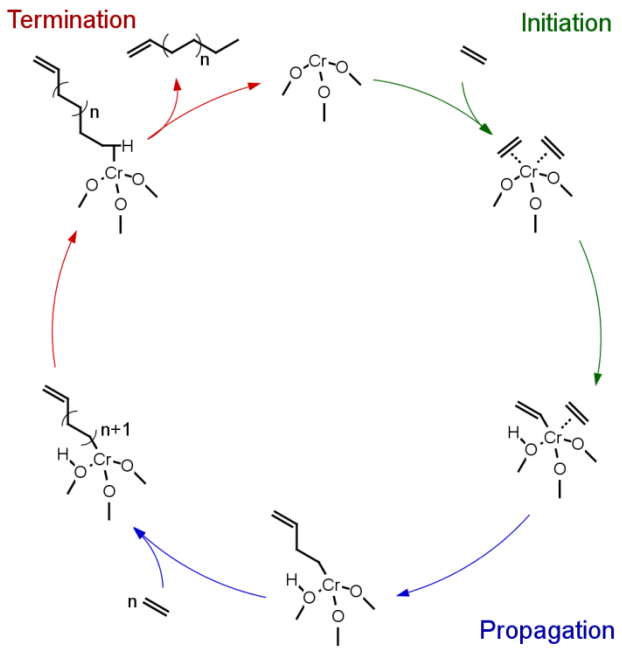

Figure 2.4: Mechanism proposed by Delley et al.[14, 15, 18] for ethylene polymerization over Cr(III)/SiO_2.

2.2. Methods and Models

All calculations were performed with Gaussian09.[22] Energies, gradients, and Hessian matrices for all structures were calculated with the range-separated density functional, ωB97X-D,[23] recommended from benchmarking studies for barrier heights[24-27] and geometries of transition metal catalysts.[28] The basis set used for Cr is def2-TZVP,[29, 30] while the basis set used for C, H, O, and Si is TZVP.[31] For all calculations, the highest spin contaminant was annihilated. The geometries of all minimum-energy structures were optimized with the Berny algorithm[32] in Gaussian09. For convergence, the maximum and RMS forces were set to 4.50 x 10^{-4} and 3.00 x 10^{-4} Hartrees/Bohr, respectively, while the maximum and RMS displacements were set to 1.80 x 10^{-3} and 1.20 x 10^{-3} Bohr, respectively. Transition state structures were calculated using a memory-enhanced eigenvector-following algorithm.[33] The norm of the mass-weighted gradient was limited to 3.00 x 10^{-4} Hartrees/(Bohr•amu$^{1/2}$), while the tolerance for energy was 1.00 x 10^{-5} Hartrees. Finally, every converged transition state was required to have only one imaginary frequency. Thermal corrections were computed for the Gibbs' free energies of reaction and activation for all elementary steps. Gibbs' free energies include rotation, vibration, and translation[34] at the experimental operating temperature of about 373.15 K.[1, 35, 36] Free energies for gaseous species were calculated at a standard state pressure of 1 atm.

The active site precursor was modeled as the energy-minimized *bis*(silanolato)monochromium(II) cluster shown in Figure 2.5 and Table 2.1. This structure represents the product of chromate ester reduction by either CO or ethylene.[20, 37-39] In the optimized, quintuplet-spin ground state of the cluster model, Cr(II) is bonded to two silanolate oxygens at a distance of 1.82 Å, and each oxygen is also bonded to silicon. A third

bridging oxygen is located between the two silicon atoms to complete a six-membered chromasiloxane ring, a strained geometry correlated with high polymerization activity.[40] Finally, the silicon atoms are capped with hydroxyl groups, whose positions were optimized in the original cluster, then fixed in all subsequent calculations. This anchoring of the terminal hydroxyl groups approximates the rigidity of the solid catalyst support. The structure of our final cluster is similar to that used in a previous study by Espelid and Børve.[10] Our O-Cr-O and Si-O-Si angles (109.8 º and 139.3 º) are considerably smaller than those used previously (116 º and 141-147 º). Si-O-Si amorphous silicas are typically 148-152 º,[41, 42] but Demmelmaier et al. found that Phillips active sites are associated with strained rings such as the 6-membered ring used here.[40]

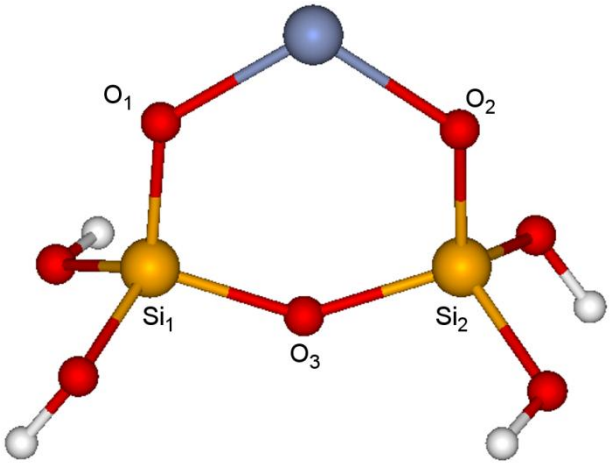

Figure 2.5: Structure of the optimized chromium(II) cluster [5]I. Color scheme: Cr(blue), O(red), Si(orange), H(white).

In order to evaluate the mechanism proposed by Delley et al.,[14, 15, 18] a *tri*(silanolato)monochromium(III) cluster shown in Figure 2.6 and Table 2.1 was also modeled. The cluster consists of one six-membered ring containing chromium, which is connected through oxygen bridges to a second six-membered ring containing only silicon and oxygen. The cluster is capped with fluorine atoms, which are not held in space. All

reported results are again computed with the ωB97X-D functional and the def2-TZVP basis set for Cr and TZVP basis set for C, H, O, Si, and F. To reproduce the B3LYP[43, 44] calculations of Delley et al. and to investigate certain additional pathways, structures were optimized with the LANL2DZ[45-47] basis set for Cr and 6-311G(d,p)[48, 49] basis set for C, H, O, Si, and F with energy refinement using the LANL2TZ(f)[45, 50, 51] basis set for Cr and 6-311++G(d,p)[48, 49, 52] basis set for C, H, O, Si, and F. Dispersion correction was also included using Grimme's DFT-D3 with Becke-Johnson damping.[53, 54] Finally, all free energies were calculated at 373.15 K, but results at 298.15 K for are available in Table B.1.

Table 2.1. Key inter-atomic distances (Å) and bond angles (°) for the Cr(II) cluster ^{5}**I**. [a]Values in this column were computed by Espelid and Børve.[10] [b]Values in this column were computed by Delley et al.[15]

Parameter	^{5}**I**	^{4}**D.I** (ωB97X-D)	^{4}**D.I** (B3LYP-D3)
*r*Cr-O1	1.82 (1.82)[a]	1.791	1.805 (1.805)[b]
*r*Cr-O4	--	1.781	1.798 (1.798)
∠O1-Cr-O2	110 (116)	104	103
∠O1-Cr-O4	--	114	113
∠Cr-O1-Si1	127	125	126
∠Cr-O4-Si3	--	130	132
∠Si1-O3-Si2	139	132	132
∠Si1-O6-Si5	--	137	139

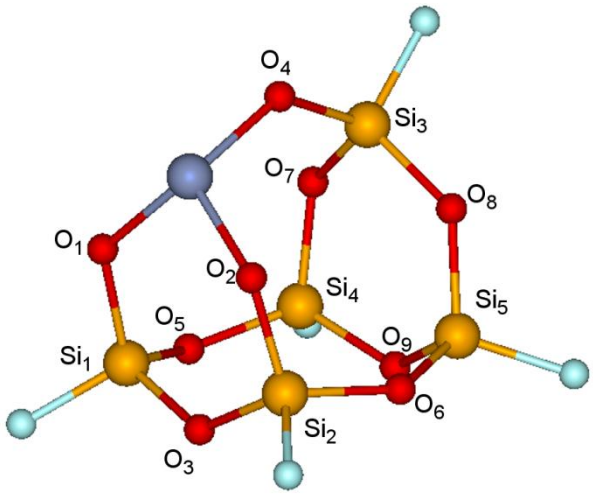

Figure 2.6: Structure of the optimized chromium(III) cluster [4]D.I. Color scheme: Cr(blue), O(red), Si(orange), F(teal).

All calculated minimum-energy species are named using the notation $^{\#}$X.Y, where # is the spin multiplicity, X denotes the mechanism, and Y is a Roman numeral. For instance, ^{5}**M.IV** refers to the fourth quintuplet-spin species in the metallacycle mechanism. ^{3}**M.IV** refers to the same structure re-optimized with a triplet spin multiplicity. Some species appear in multiple mechanisms, such as ^{5}**I** (Figure 2.5), which refers to the initial Cr(II) species in a quintuplet spin state. Thus, the name for this bare site does not include an X designation. Transition states were described using a similar notation, $^{\#}$TS[X.Y_1-X.Y_2], where TS denotes a transition state structure; Y_1 and Y_2 refer to reactant and product, respectively.

Some results in this present paper pertain to mechanisms studied computationally by Schmid and Ziegler,[55] or Espelid and Børve.[10] The ωB97X-D functional we used is more accurate relative to what was available and feasible at the time of their studies. [24-27] Furthermore, we analyzed alternate spin states, and computed free energy barriers, which are necessary to estimate rates of reactions. Nevertheless, the general agreement between their

findings and ours, where overlap exists, adds confidence both to the previous conclusions and to our results for the new mechanisms.

2.3. Results and Discussion

2.3.1 Ethylene binding to the bare chromium(II) site

Prior to polymerization, ethylene can form several different coordination complexes with the bare Cr(II) site ^{5}**I** (Figure 2.7). The quintuplet-spin complex ^{5}**II** is formed when ethylene binds *trans* to one of the silanolate ligands. The C-C bond is elongated by only 0.02 Å, at a Cr-C distance of 2.40 Å. The structural parameters, summarized in Table B.2 in Appendix A, compare well with previous computational results reported by Espelid and Børve.[10] However, the O-Cr-O angle, which is correlated with site activation,[40] is slightly smaller (104 vs. 107 °). Unsurprisingly, the binding energy of -84 kJ/mol calculated here differs from their -68 kJ/mol. We investigated whether the discrepancy is due to the different choice of functionals. When we repeated the calculation with the BVP86 functional[56, 57] used previously, we obtained a binding energy of -80 kJ/mol, similar to our original result. However, we compute a smaller energy change of only -65.1 kJ/mol for ethylene binding to an eight-membered chromasiloxane ring with a much larger O-Cr-O angle (135 º), suggesting that the ring geometry is primarily responsible for the discrepancy (Figure A.1 and Table B.3). Our choice of more electronegative terminal OH groups (compared to H-termination of the cluster in previous work)[10] may also influence the ethylene binding energy.

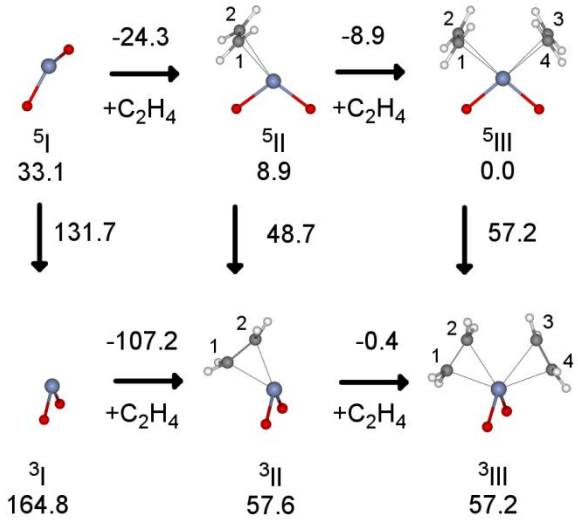

Figure 2.7: Structures for ethylene complexes of the Cr(II) cluster, as well as their free energies (kJ/mol) relative to the *bis*(ethylene) complex, ^{5}III, at 373 K. Numbers above or to the right of arrows correspond to reaction free energies. Si atoms and the rest of the siloxane cluster are omitted for clarity. Species in the upper and lower rows correspond to quintuplet and triplet spins, respectively. ^{5}I, bare Cr(II) site; ^{5}II, *mono*(ethylene) complex; ^{5}III, *bis*(ethylene) complex. Free energy differences between spin states are also shown. Color scheme: Cr (blue), O (red), H (white), C (gray).

Upon computing the entropy change, we obtained an overall free energy change for binding the first ethylene to ^{5}**I** of -24 kJ/mol at 373 K. Coordination of a second ethylene occurs with a free energy change of only -9 kJ/mol (^{5}**III**). This weaker interaction results in an increase in the average Cr-C distance, from 2.40 Å in ^{5}**II** to 2.48 Å in ^{5}**III** (Table B.2). Steric crowding around the metal appears to hinder further ethylene binding; a stationary point for a third coordinated ethylene was not found, although weakly bound *tris*- and *tetrakis*(ethylene) complexes have been reported with $Cr(OH)^{+}$ and other models with considerably smaller ligand sets.[58, 59] Therefore, the *bis*(ethylene) complex ^{5}**III** is the most likely stable intermediate present prior to initiation of polymerization. It also represents our chosen reference point of free energy, relative to which the energies of most other species will be reported.

For both *mono* and *bis*(ethylene) complexes ^{5}**II** and ^{5}**III**, analogs with triplet spins also exist. These species, called ^{3}**II** and ^{3}**III** in Figure 2.7, are higher in energy than the corresponding quintuplet forms. For instance, ^{3}**III** is 57 kJ/mol higher in free energy than ^{5}**III**. In both complexes, the ethylene molecules bind in *cis* fashion, but differ in their orientation relative to the OCrO plane. However, it is clear that Cr(II) ethylene complexes prefer the higher spin multiplicity.

2.3.2. Chromacycle propagation mechanism

Homogeneous organochromium catalysts have been reported to oligomerize ethylene via a metallacycle mechanism,[60, 61] in which ethylene inserts repeatedly into an expanding ring system that includes the Cr ion.[62] Because the ring always contains an even number of H atoms, no external source of H is required. Thus, it is a possible propagation mechanism for the Phillips catalyst whose activity does not require an alkylating co-catalyst, which led Groppo et al. to assign the observed IR bands of $–CH_2–$ groups (in the absence of discernable vibrations attributable to $–CH_3$ groups) to an expanding chromacycle.[63] However, McGuinness et al. ruled out a chromacycle polymerization mechanism after copolymerizing ethylene with isotopically-labeled decenes.[9]

Chromacycle ring expansion was modeled starting with a four-carbon-containing chromacyclopentane ring, formed by cycloaddition of two coordinated ethylenes in ^{5}**III**.[10, 38] The most stable form of this ring has a triplet spin configuration (^{3}**M.IV** in Figure 2.8), with a free energy of +9 kJ/mol relative to ^{5}**III**. Free energies for the quintuplet and singlet spin forms are significantly higher, at 101 and 156 kJ/mol, respectively. This preference for the triplet spin state in the metallacycle raises the issue of spin conservation, because the initial state is the quintuplet-spin *bis*(ethylene) complex ^{5}**III**. The issue was addressed in previous

computational work on the model ethylene dimerization catalyst [$Cr(OH)^{+}$], which also prefers different spins in the corresponding chromacycle and bis(ethylene) complexes.[59] In that case, spin crossover to the triplet state was assumed to precede metallacycle formation.

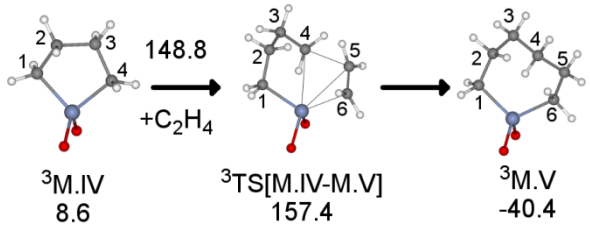

Figure 2.8: Structures of stationary points in the chromacycle mechanism, and free energies (kJ/mol) relative to the *bis*(ethylene) complex, ^{5}III, at 373 K. ^{3}M.IV, chromacyclopentane; ^{3}TS[M.IV-M.V], transition state for insertion of ethylene into the Cr-C4 bond; ^{3}M.V, chromacycloheptane.

Optimizing the minimum on the seam of crossing, an essential part of the initiation step, was not undertaken for our system, because subsequent propagation via chromacycle expansion is slow (*vide infra*), effectively ruling out this mechanism. In the late transition state **^{3}TS[M.IV-M.V]**, the Cr-C4 distance increases dramatically to 2.99 Å to accommodate the incoming monomer (Table B.4). This elongation compares well with the 3.02 Å reported by Zhong et al.[38] but contrasts with the much smaller value of 2.21 Å reported by Espelid and Børve.[10] However, we all calculate prohibitively large activation energies of 112 kJ/mol (Zhong et al.), 119 kJ/mol (Espelid and Børve), and 89 kJ/mol (this work). When the loss of entropy of the free ethylene molecule is included, we obtain a total free energy barrier of 149 kJ/mol, resulting in an extremely small rate constant of only 1 x 10^{-8} s^{-1} $site^{-1}$ atm^{-1} at T = 373 K. Although the chromacycloheptane product **^{3}M.V** is 49 kJ/mol lower in free energy relative to **^{3}M.IV**, the high insertion barrier shows that the chromacycle mechanism is not a viable route for polymer chain growth.

Despite the impracticality of ring expansion as a polymerization mechanism, Espelid and Børve did not rule out a chromacycle as a relevant intermediate in side-reactions.[10] They suggested that any chromacycloheptane that does form may undergo intramolecular β-H transfer to give 1-hexene (98 kJ/mol activation energy), faster than subsequent ethylene insertion (122 kJ/mol activation energy). We observed similar trends in the activation energies for termination and a second ethylene insertion (114 and 129 kJ/mol, respectively, Figure 2.9). We observed an even larger difference upon including entropy in the free energy barriers for β-H transfer and insertion: 114 and 189 kJ/mol, respectively (geometries in Table B.5). This preference for termination might explain reports of 1-hexene formation in polymerization experiments with the Phillips catalyst.[64, 65] Such reactions have been widely observed with homogeneous chromium catalysts that trimerize ethylene selectively.[60, 66, 67]

Nevertheless, the very slow rate we calculate for ring expansion of the chromacyclopentane suggests that even chromacycloheptane is unlikely to form on this type of site. Espelid and Børve noted that the activation energy for ethylene insertion on a model chromacyclopentane attached to a four-membered chromasiloxane ring with a very small, strained O-Cr-O angle was reduced by 46 kJ/mol, to 73 kJ/mol.[10] At the same time, the termination barrier was reduced by only 13 kJ/mol, to 85 kJ/mol. However, including the entropy of immobilizing the free monomer prior to the insertion step leads to a free energy of activation for ring expansion that is still larger than that of termination. Nevertheless, rare sites similar to the one studied by Espelid and Børve may be responsible for the co-production of α-olefins, suggesting that a future analysis of structure sensitivity in the active site may be fruitful.

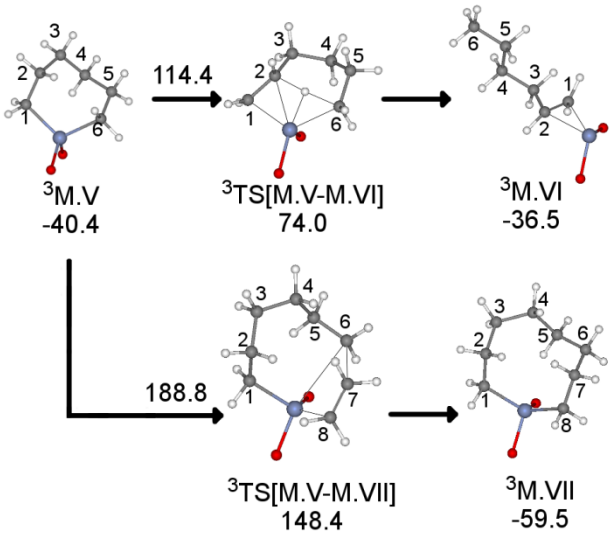

Figure 2.9: Structures of stationary points in chromacycle propagation and termination by β-H transfer, and free energies (kJ/mol) relative to the *bis*(ethylene) complex, ^{5}III, at 373 K. ^{3}M.V, chromacycloheptane; ^{3}TS[M.V-M.VI], transition state for intramolecular β-H transfer; ^{3}M.VI, coordinated 1-hexene; ^{3}TS[M.V-M.VII], transition state for ethylene insertion into the Cr-C6 bond; ^{3}M.VII, chromacyclononane.

2.3.3. Oxachromacycle mechanism

This new mechanism is adapted from one originally suggested by Baker and Carrick for the homogeneous catalyst bis(triphenylsilyl)chromate.[68] In that system, the first ethylene insertion was suggested to occur at one of the two Cr-O bonds (Equation 2.1), followed by ethylene insertion into the resulting Cr-C bond. To the best of our knowledge, the viability of such a mechanism has not been evaluated computationally for the heterogeneous Phillips catalyst.

$$(Ph_3SiO)_2Cr + n C_2H_4 \rightarrow Ph_3SiOCr(CH_2CH_2)_nOSiPh_3 \qquad (2.1)$$

The reaction is initiated from the *bis*(ethylene) complex ^{5}**III** when a coordinated ethylene adds across the Cr-O1 bond (Figure 2.10). In contrast to Baker and Carrick's proposal, while the Cr-O1 distance lengthens from 1.88 to 1.96 Å (Table B.6), the bond does not break. Instead, O1 becomes tri-coordinate (Cr, C, Si), forming the oxachromacyclobutane intermediate ^{5}**O.IV**. Overall, the initiation step associated with the

late transition state **^{5}TS[III-O.IV]** occurs with an activation free energy of 81 kJ/mol and a reaction free energy of 68 kJ/mol. In the oxachromacycle, the Cr(II) site is a quintuplet, in contrast to the triplet Cr(IV) center in the chromacycle **^{3}M.IV**. Since the triplet and singlet configurations for the ethylene-oxachromacyclobutane complex **O.IV** are 144 and 320 kJ/mol higher in energy relative to **^{5}III**, reaction paths relevant to their corresponding spins were not considered further.

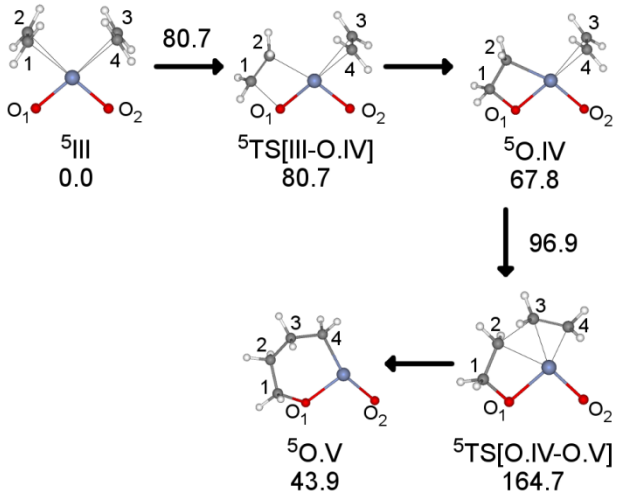

Figure 2.10: Stationary points for the oxachromacycle mechanism, and free energies (kJ/mol) relative to that of the *bis*(ethylene) complex ^{5}III, at 373 K. ^{5}TS[III-O.IV], transition state for ethylene insertion into the Cr-O bond; ^{5}O.IV, ethylene-oxachromacyclobutane complex; ^{5}TS[O.IV-O.V], transition state for ethylene insertion into the Cr-C2 bond; ^{5}O.V, oxachromacyclohexane.

For quintuplet **^{5}O.IV**, the remaining bound ethylene ligand then inserts into the newly-formed Cr-C2 bond (Table B.7). The barrier to form the oxachromacyclohexane **^{5}O.V** is 97 kJ/mol (corresponding to k = 0.2 s^{-1} atm^{-1} $site^{-1}$ at 373 K), which is significantly lower than the insertion barrier for the chromacyclopentane **^{3}M.IV** (149 kJ/mol, see Figure 2.8). This may be a consequence of lower steric hindrance in **^{5}O.IV**, due to the smaller Cr coordination number. However, since the preceding step (**^{5}III** → **^{5}O.IV**) is endothermic, the effective barrier to transform the *bis*(ethylene) complex **^{5}III** into the oxachromacyclohexane **^{5}O.V** is

165 kJ/mol, corresponding to a very low effective rate constant of 7 x 10^{-11} s^{-1} atm^{-1} $site^{-1}$ at 373 K. Thus for the model we investigated, the oxachromacycle does not appear to be a viable intermediate for polymerization.

2.3.4. Green-Rooney (carbene) mechanism

In principal, polymer chain growth can be accomplished by an olefin metathesis-type mechanism involving alternating carbene and substituted chromacyclobutane intermediates, also known as the Green-Rooney mechanism.[69] A version adapted for the Phillips catalyst is depicted in Figure 2.11. Because all of the intermediates have an even number of hydrogen atoms, this mechanism also avoids the missing hydrogen problem. Although exceedingly rare in molecular catalysis,[70, 71] the Green-Rooney mechanism was proposed for the Phillips catalyst by Kantcheva et al.,[13] who assigned IR signals to the Cr=C and C-H methyl stretches of an ethylidene intermediate such as ^{3}**C.IV**. Nait Ajjou and Scott prepared a silica-supported *bis*(neopentyl)chromium(IV) catalyst, which undergoes α-H elimination to give a neopentylidene complex capable of initiating ethylene polymerization ethylene.[64] Furthermore, Fang et al. detected olefins with an odd number of carbons, which may arise from olefin metathesis over a carbene intermediate.[72]

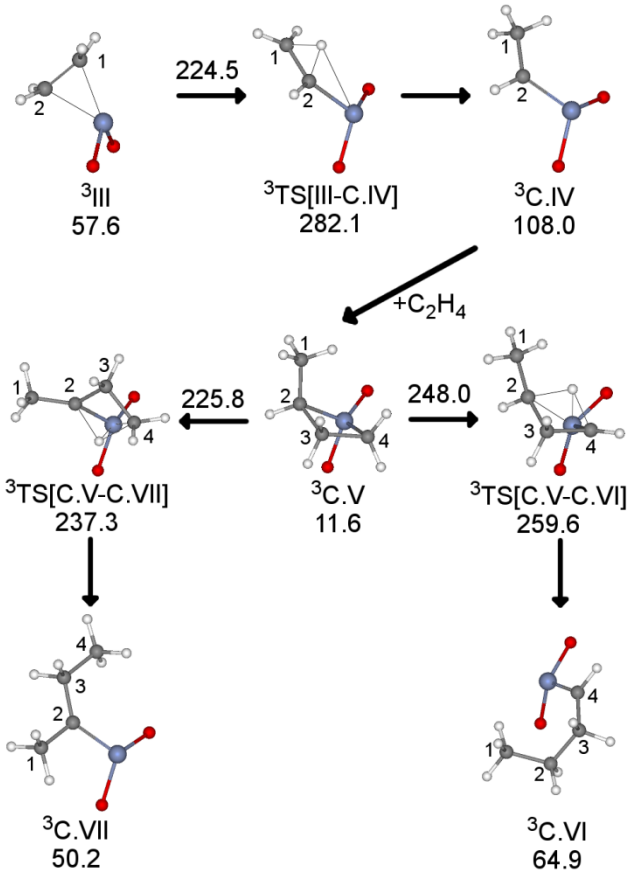

Figure 2.11: Structures of stationary points in the Green-Rooney (carbene) mechanism, and free energies (kJ/mol) relative to that of the *bis*(ethylene) complex ^{5}III, at 373 K. ^{3}III, triplet-spin *bis*(ethylene complex); ^{3}C.IV, ethylidenechromium; ^{3}C.V, (2-methyl)chromacyclobutane; ^{3}TS[C.V-C.VI], transition state for 1,3-H transfer from C4 to C2; ^{3}C.VI, butylidenechromium; ^{3}TS[C.V-C.VII], transition state for 1,3-H transfer from C2 to C4; ^{3}C.VII, (1-methyl)propylidenechromium.

The initiating ethylidenechromium(IV) site **^{3}C.IV** could form by rearrangement of the bound ethylene ligand in **^{3}III**, resulting in a change in formal oxidation state from Cr(II) to Cr(IV). We calculate a barrier for this step of 225 kJ/mol, similar to the 214 kJ/mol reported by Zhong et al.[38] Like the chromacycle **^{3}M.IV**, a triplet spin state is preferred for **^{3}C.IV** (Geometries in Table B.8). Relative to the *bis*(ethylene) complex **^{5}III**, the free energy of **^{3}C.IV** and free monomer (included for stoichiometry) is a high 108 kJ/mol. Quintuplet and singlet spin configurations are 151 and 234 kJ/mol higher in free energy relative to **^{5}III**, respectively.

Chain propagation, which involves [2+2] cycloaddition of ethylene followed by intramolecular 1,3-H-transfer within the chromacyclobutane intermediate, is slow overall. The first step, which generates the substituted metallacycle **^{3}C.V**, is barrierless and has a favorable free energy change of -96 kJ/mol, but subsequent H-transfer to generate one of two possible carbenes **^{3}C.VI** or **^{3}C.VII** is predicted to be extremely sluggish. For instance, when hydrogen is transferred from the unsubstituted α-carbon (C4) of **^{3}C.V** to the methyl-substituted α-carbon (C2), the barrier is an enormous 248 kJ/mol (**^{3}TS[C.V-C.VI]** in Figure 2.11). Several previous computational studies reported similarly high barriers, in the range 231 - 241 kJ/mol.[10, 38, 55] The alternative, H transfer from C2 to C4 to give (1-methyl)propylidene **^{3}C.VII**, is slow as well. The free energy change for the reaction is 39 kJ/mol, with a barrier of 226 kJ/mol. The slightly lower values, relative to those for the path to generate **^{3}C.VI**, are due to the increased stability of the more substituted carbene **^{3}C.VII**. Nevertheless, the high barriers for both H-transfer reactions show that polymerization by the Phillips catalyst is unlikely to involve a carbene intermediate. Geometries for intermediates in both pathways are compiled in Tables B.9 and B.10.

These findings are consistent with a previous experimental study, in which McDaniel did not observe the expected H/D scrambling for polymerization of CHD=CHD by a Green-Rooney mechanism.[11] The isotopically-labeled ethylene produced a polymer containing only CHD units, although the Green-Rooney mechanism should cause scrambling of the label (producing CH_2 or CD_2 units) via H/D transfer in the transition state (Figure 2.12). Furthermore, only small kinetic isotope effects have been reported for C_2D_4 polymerization.[9, 73] A sizeable primary effect is expected for the Green-Rooney mechanism,

because the rate-determining step involves H/D transfer in the transition states **^{3}TS[C.V-C.VI]** and **^{3}TS[C.V-C.VII]**.

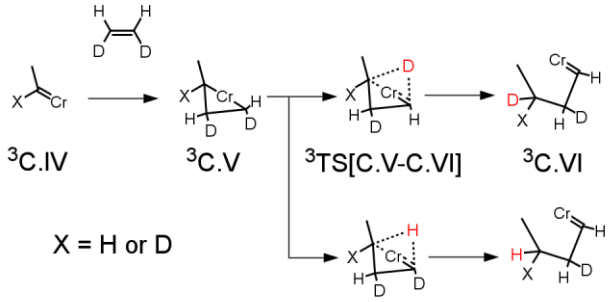

Figure 2.12: Green-Rooney mechanism for polymerization of *cis*-ethylene-l,2-d_2, showing the expected scrambling of the isotope label. This scrambling is not observed for the Phillips catalyst.

2.3.5. Cossee-Arlman chain growth at a monoalkylchromium(II) site initiated through proton transfer

In contrast to the metallacycle and oxametallacycle mechanisms described above, the growing polymer chain in a Cossee-Arlman mechanism[7] is σ-bonded to the active site at only one end. When a coordinated monomer inserts into the Cr-C σ-bond, the length of the polymer chain is extended by two methylene units. A possible Cossee-type site involving Cr(II) is shown in Figure 2.13 as **^{5}H.VI**. The growing alkyl ligand attached to Cr(II) is terminated by a vinyl end-group, -$(CH_2CH_2)_n$CH=CH_2.

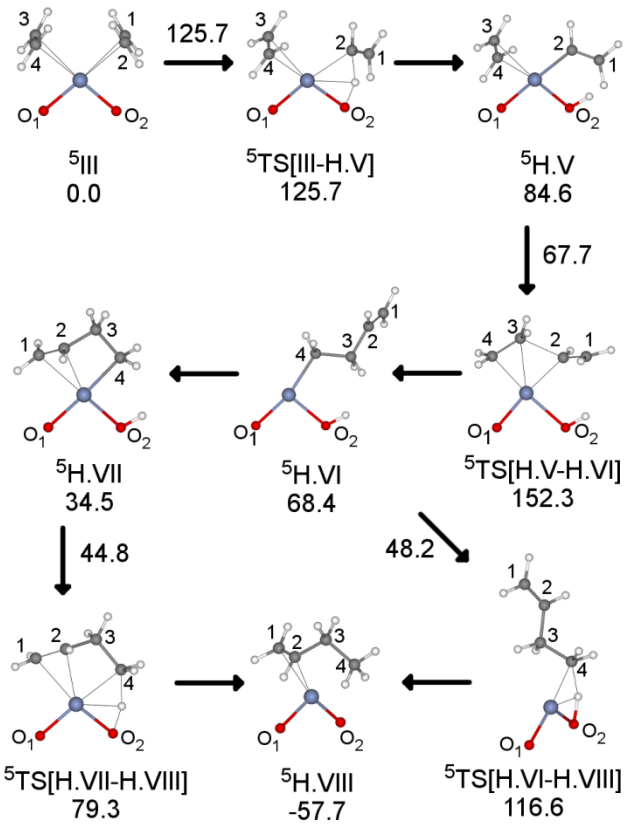

Figure 2.13: Stationary points for the Cossee-Arlman mechanism on a Cr(II) site, and free energies (kJ/mol) relative to that of the *bis*(ethylene) complex ^{5}III, at 373 K. ^{5}TS[III-H.V], transition state to transfer H to O2; ^{5}H.V, (ethylene)(vinyl)chromium(II); ^{5}TS[H.V-H.VI], transition state for ethylene insertion into the Cr-C2 bond; ^{5}H.VI, butenylchromium(II) with uncoordinated vinyl chain end; ^{5}H.VII, butenylchromium(II) with coordinated vinyl chain-end; ^{5}TS[H.VII-H.VIII], transition state for H transfer from O2 to C4, with coordinated vinyl end-group; ^{5}H.VIII, 1-butene complex; ^{5}TS[H.VI-H.VIII], transition state for H transfer from O2 to C4 without vinyl end-group coordination.

To maintain an even number of hydrogen atoms in the active site and thereby avoid the missing hydrogen problem, the reaction may be initiated by proton transfer from one of the ethylene ligands in the *bis*(ethylene) complex **^{5}III** to a silanolate oxygen.[19] A similar proton transfer initiation pathway involving Cr(III)/SiO_2 was investigated by Delley et al.,[14, 15, 18] and the Cr(III) case will be analyzed below. The free energy barrier for proton transfer at Cr(II)/SiO_2 to create an Si(OH)Cr^{II}-vinyl site (vinylchromium(II)) is 126 kJ/mol, and the free energy of the vinylchromium(II) site **^{5}H.IV** is +85 kJ/mol relative to **^{5}III**. Like the other

Cr(II) species considered in this study, its preferred spin multiplicity is quintuplet. Relative to **^{5}III**, triplet and singlet forms have much higher energies (176 and 246 kJ/mol, respectively). Bond lengths and angles appear in Table B.11.

Propagation proceeds by monomer insertion into the Cr-C σ-bond. At the transition state **^{5}TS[H.V-H.VI]**, the Cr-C2 bond of **^{5}H.V** stretches slightly, from 2.09 to 2.13 Å (Table B.12), while incipient Cr-C4 and C2-C3 bonds appear at 2.12 and 2.02 Å, respectively. The reaction and activation free energies for formation of the butenylchromium(II) intermediate **^{5}H.VI** are -16 and +68 kJ/mol, respectively, relative to **^{5}H.V**. However, the transition state **^{5}TS[H.V-H.VI]** is a high 152 kJ/mol relative to the stable starting point **^{5}III**, suggesting that overall formation of **^{5}H.VI** from **^{5}III** would be extremely slow (k = 4 x 10^{-9} s^{-1} $site^{-1}$) at 373 K.

If a faster initiation path to **^{5}H.VI** were accessible, the low propagation barrier of 68 kJ/mol might suggest that long polymer chains could be formed via the Cossee-Arlman mechanism at these sites. However, growth at a vinylchromium(II) site is not viable, because **^{5}H.VI** tends to favor chain termination prior to additional insertion. The butenyl ligand may coordinate to Cr(II) via its vinyl end-group (**^{5}H.VII**), while the bridging silanol prepares to transfer H back to C4, causing the Cr-C σ-bond to break in **^{5}TS[H.VII-H.VIII]** (Table B.13). The resulting coordinated 1-butene complex **^{5}H.VIII** is formed with reaction and activation free energies of -92 and 45 kJ/mol, respectively. When the vinyl end does not coordinate to Cr(II), it models the behavior of a much longer polymer chain whose bending and attachment to Cr comes at the expense of configurational entropy. In this case, H transfer to C4 (**^{5}TS[H.VI-H.VIII]**) occurs with a slightly higher barrier of 48 kJ/mol. Since

the propagation barrier (~86 kJ/mol) is higher than either termination barrier, this active site cannot account for the formation of long polymer chains by the Phillips catalyst.

Formation of an alkoxy complex such as **^{5}H.IX** by ethylene insertion into the O-H bond of the coordinated silanol of **^{5}H. V** (Figure 2.14) would effectively prevent the silanol proton from migrating and thereby terminating the growing polymer chain. Unfortunately, although the alkoxy complex is only 8 kJ/mol higher in energy relative to **^{5}H.V**, the barrier to its formation is a prohibitive 215 kJ/mol (Geometries in Table B.14). To explore the effect of ring strain, the energy of a transition state with a six-membered ring, **^{5}TS[H.V-H.X]**, was also calculated. Unfortunately, it is similarly very high in free energy (Figure 2.14).

The tendency of Cr(II) sites in the Phillips catalyst to catalyze ethylene oligomerization rather than polymerization was also observed by Theopold, who found only propylene and other short-chain α-olefins in the homogeneous reaction of $Cp^{*}Cr^{II}$(dmpe)Me [dmpe = bis(dimethylphosphino)ethane] with ethylene.[74] On the other hand, $[Cp^{*}Cr^{III}(dmpe)Me]PF_6$, was found to be capable of ethylene polymerization. These results suggest that while Cr(II) sites may be precursors of the Phillips catalyst active sites, the actual active site may not necessarily have this oxidation state. Merryfield et al. also observed XPS spectra consistent with a Cr(II) precursor, but observed partial oxidation after exposure to ethylene.[20] However, they also reported that the results may have been measuring the more prevalent inactive sites.

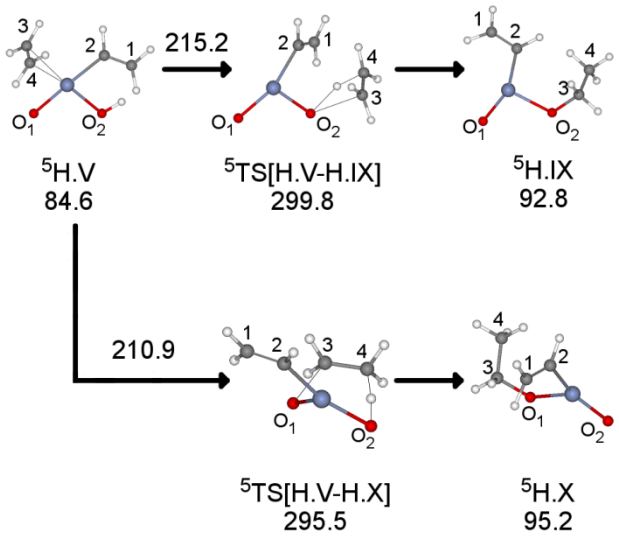

Figure 2.14: Stationary points for formation of a bridging alkoxy ligand at a monoalkylchromium(II) site, and free energies (kJ/mol) relative to that of the *bis*(ethylene) complex ^{5}III, at 373 K. ^{5}H.V, (ethylene)(vinyl)chromium; ^{5}TS[H.V-H.IX], transition state to form alkoxy at O2; ^{5}H.IX, (alkoxy)(vinyl)chromium with alkoxy at O2; ^{5}TS[H.V-H.X], transition state to form alkoxy at O1; ^{5}H.X (alkoxy)(vinyl)chromium with alkoxy at O1.

2.3.6. Cossee-Arlman chain growth at a monoalkylchromium(III) site initiated through proton transfer

Recently, Delley et al.[15] computationally studied a Cr(III)/SiO_2 site (Figure 2.4), which was proposed to initiate through a proton transfer mechanism like the Cr(II) system of the previous section. Delley et al. performed DFT calculations for the initiation, propagation, and termination steps using the B3LYP-D3 functional with a triple-ζ basis and pseudopotentials. Delley et al. also reported IR spectra with peaks at 3605 and 3640 cm^{-1}, which they interpreted as evidence for $Si(OH)Cr^{III}$-alkyl sites during polymerization. Delley et al. did not use their calculations to predict overall rates or molecular weights. Nor did Delley et al. compute site abundances to check the interpretation of their spectra. This section presents these additional analyses of the kinetics along with independent DFT results using the ωB97X-D functional. As shown in the Table B.1, the ωB97X-D results are very similar to the B3LYP-D3 results of Delley et al. at 298 K. Note that Delley et al. only

reported Gibbs free energies at 298K. Our results, as in the rest of the manuscript, are reported at the more typical catalyst operation temperature of 373 K.

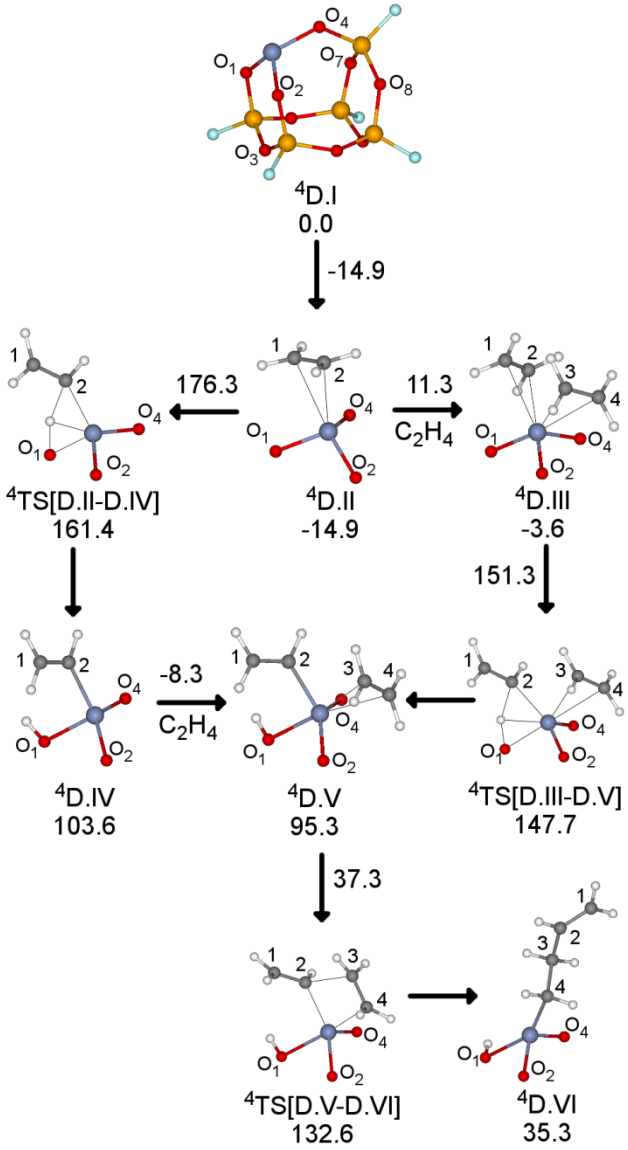

Figure 2.15: Stationary points for the Cossee-Arlman mechanism on a Cr(III) site, and free energies (kJ/mol) relative to that of the bare site, ^{4}D.I, at 373 K. ^{4}D.II, *mono*(ethylene) complex; ^{4}D.III, *bis*(ethylene) complex; ^{4}TS[D.II-D.IV], transition state to transfer H to O1 from *mono*(ethylene) complex; ^{4}D.IV, vinylchromium(III); ^{4}TS[D.III-D.V], transition state to transfer H to O1 from *bis*(ethylene) complex; ^{4}D.V, (ethylene)(vinyl)chromium(III); ^{4}TS[D.V-D.VI], transition state for ethylene insertion into the Cr-C2 bond; ^{4}D.VI, butenylchromium(III) with uncoordinated vinyl chain end.

The mechanism starts with the ethylene complexes **^{4}D.II** and **^{4}D.III**. Unlike the case in Cr(II), the *bis*(ethylene) complex **^{4}D.III** is slightly less stable than the *mono*(ethylene) complex **^{4}D.II**. At 373 K, the *bis*(ethylene) complex is 11 kJ/mol higher in free energy (Figure 2.15). However, proton transfer from the *mono*(ethylene) complex **^{4}TS[D.II-D.IV]** is prohibitively slow, with a barrier of 176 kJ/mol. However, there is a slightly more favorable path of initiation from the *bis*(ethylene) complex (**^{4}D.III** → **^{4}TS[D.III-D.V]** → **^{4}D.V**), which involves a barrier of about 151 kJ/mol (k_{init} = 5 x 10^{-9} site^{-1} s^{-1} and k_{-init} = 4 x 10^5 site^{-1} s^{-1} at 373 K). The additional monomer binds *trans* to the oxygen receiving the proton, while the *trans* Cr-O bond stretches from about 1.83 to 1.96 Å (Table B.15). The product, (ethylene)(vinyl)chromium(III) **^{4}D.V**, then inserts ethylene with a barrier of 37 kJ/mol (**^{4}TS[D.V-D.VI]**, geometry in Table B.16). Like Cr(II), Cr(III) initiates slowly through a proton transfer.

A typical propagation for the vinylchromium(III) (Figure 2.16) site is very similar to that of Cr(II). First, butenylchromium(III) **^{4}D.VI** binds ethylene forming the complex **^{4}D.VII**. The coordination is weak because the free energy change is +16 kJ/mol, K_{bind} = 6 x 10^{-3} atm^{-1} site^{-1}. Interestingly, Cr(III) distorts to an octahedral geometry in the complex **^{4}D.VII**, in which the Cr-O8 distance (refer to Figure 2.6 or **^{4}D.I** in Figure 2.15) shrinks from 3.68 in **^{4}D.VI** to 3.12 Å in **^{4}D.VII** (Table B.17). The distance then increases again to 3.80 Å in **^{4}TS[D.VII-D.VIII]** when ethylene inserts into the Cr-C4 σ bond, yielding hexenylchromium(III) **^{4}D.VIII**. The free energy barrier of 67 kJ/mol corresponds to a propagation rate coefficient k_{insert} of 3 x 10^3 site^{-1} s^{-1}. The overall free energy difference between **^{4}TS[D.VII-D.VIII]** and **^{4}D.VI** is 83 kJ/mol.

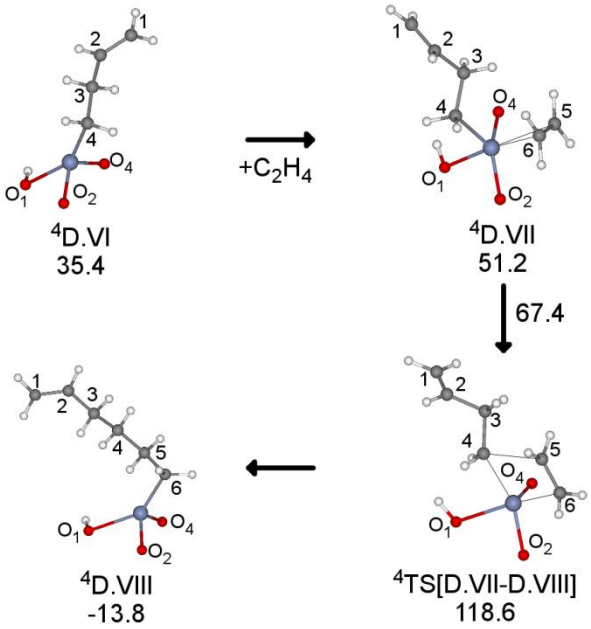

Figure 2.16: Stationary points for Cossee-Arlman propagation on a Cr(III) site, and free energies (kJ/mol) relative to that of the bare site, ^{4}D.I, at 373 K. ^{4}D.VI, butenylchromium(III) with uncoordinated vinyl chain end; ^{4}D.VII, (ethylene)(butenyl)chromium(III); ^{4}TS[D.VII-D.VIII], transition state for insertion of coordinated ethylene into the Cr-C4 bond; ^{4}D.VIII, hexenylchromium(III) with β-agostic interaction.

Delley et al. identified several termination mechanisms, the most favorable according to them involving proton transfer from O1 to C4 of the growing chain (Figure 2.17, middle path **^{4}D.VI → ^{4}TS[D.VI-D.X] → ^{4}D.X**). This particular reaction is similar to the reverse of initiation from a *mono*(ethylene) complex (Figure 2.15 **^{4}D.IV → ^{4}TS[D.IV-D.II] → ^{4}D.II**), except that the olefin in **^{4}D.X** is coordinated to chromium through its methyl and not vinyl end. The free energy barrier from **^{4}D.VI** is 99 kJ/mol ($k_{H\text{-}Xfer}$ = 9 x 10^{-2} site^{-1} s^{-1}), which is slightly higher than the overall 83 kJ/mol for propagation (Bond lengths and angles in Table B.18). On first inspection, it appears that polymers or long oligomers could form under this mechanism, unlike the case in Cr(II). The stationary rate of ethylene consumption is given by equation 2.2 (Appendix C.1):

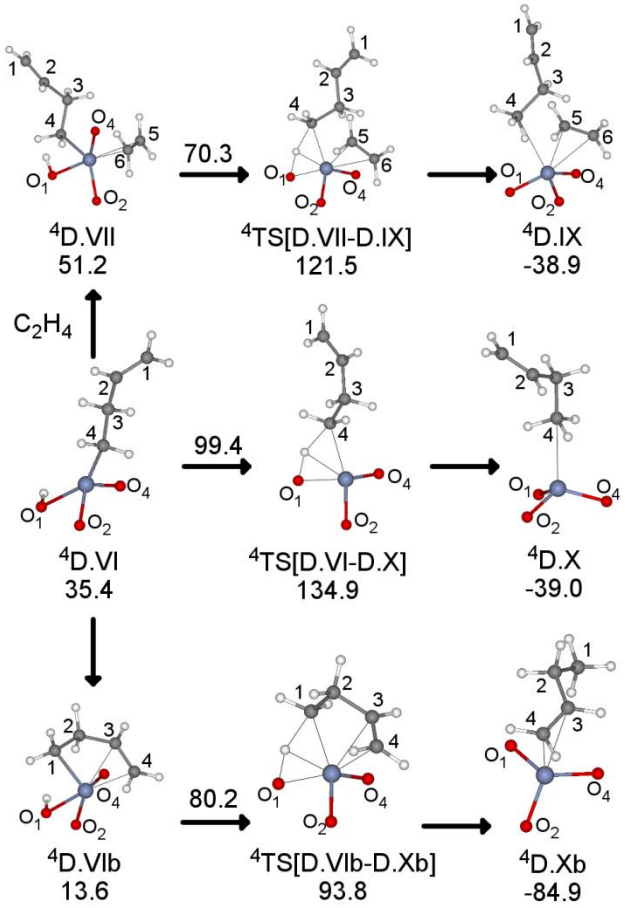

Figure 2.17: Stationary points for termination by proton transfer over a Cr(III) site, and free energies (kJ/mol) relative to that of the bare site, ^{4}D.I, at 373 K. ^{4}D.VII, (ethylene)(butenyl)chromium(III); ^{4}TS[D.VII-D.IX], transition state for proton transfer for ethylene complex; ^{4}D.IX, (ethylene)(1-butene) complex with methyl end of butene near Cr; ^{4}D.VI, butenylchromium(III); ^{4}TS[D.VI-D.X], transition state for direct proton transfer without ethylene assistance; ^{4}D.X, 1-butene complex with methyl end near Cr; ^{4}D.VIb, butenylchromium(III) with coordinated vinyl chain end; ^{4}TS[D.VIb-D.Xb], transition state for direct proton transfer with coordinate vinyl chain end and without ethylene assistance; ^{4}D.Xb, 1-butene complex with vinyl end near Cr.

$$-r_{C_2H_4} \approx k_{init} \frac{k_{insert}}{k_{H-Xfer}} \frac{k_{\pi-insert}}{k_{\pi-insert} + k_{-init}} K_{bind} P \tag{2.2}$$

At 373 K and 1 atm, this corresponds to 1 x 10^{-6} C_2H_4* site^{-1} s^{-1}, or 1 x 10^{-4} kgPE*(mol Cr)$^{-1}$h^{-1}. At the 343 K and 6 atm Delley et al. ran their experiments, the computed rate is 6 x 10^{-7} C_2H_4* site^{-1} s^{-1}, or 6 x10^{-5} kgPE*(mol Cr)$^{-1}$h^{-1}, which is far from the 10^2 kgPE*(mol

Cr)$^{-1}$h^{-1} they reported. Furthermore, the fraction of active sites is extremely low, given by equation 2.3:

$$\theta_{act} \approx \frac{k_i k_{\pi-insert}\left(1+K_{bind}P\right)}{k_{H-Xfer}\left(k_{\pi-insert}+k_{-init}\right)} \tag{2.3}$$

At 373 K and 1 atm, this corresponds to about 6 x 10^{-8}. At 343 K and 6 atm, the fraction reduces slightly to 10^{-8}, which is still significantly less than the 0.6 reported.

Futhermore, Delley et al. did not consider that ethylene can coordinate to chromium during the proton transfer (**^{4}D.VII** → **^{4}TS[D.VII-D.IX]** → **^{4}D.IX**), leading to a faster termination pathway. The transition state for ethylene-assisted termination **^{4}TS[D.VII-D.IX]** is lower in free energy than the previous **^{4}TS[D.VI-D.X]** by 13 kJ/mol. The free energy barrier of 70 kJ/mol ($k_{\pi,H\text{-}Xfer}$ = 10^3 site^{-1} s^{-1}) is also nearly the same as the corresponding propagation barrier, suggesting oligomers and instead of long polymers form (Bond lengths and angles in Table B.19).

The butenyl ligand in Cr(III) may similarly coordinate through its vinyl end in preparation for proton transfer (Table B.20). A butenylchromium(III) with coordinated vinyl chain end **^{4}D.VIb** is 22 kJ/mol lower in free energy than **^{4}D.VI** ($K_{vinyl\ coord}$ = 10^3) and 38 kJ/mol lower than complex **^{4}D.VII**. The free energy barrier for proton transfer is 80 kJ/mol ($k_{vinylH\text{-}Xfer}$ = 5 x 10 site^{-1} s^{-1}), which is slightly higher than the 70 kJ/mol for ethylene-assisted termination. However, the termination barrier to reach **^{4}TS[D.VIb-D.Xb]** is 28 kJ/mol lower in free energy than the ethylene-assisted termination transition state **^{4}TS[D.VII-D.IX]** and 25 kJ/mol lower than the propagation transition state **^{4}TS[D.VII-D.VIII]**. The product **^{4}D.Xb**, a 1-butene complex with the vinyl end near chromium, is also more stable than either **^{4}D.IX** or **^{4}D.X**. Implication of this pathway is that coordination of ethylene then follows, and another unfavorable proton transfer must occur with a large

barrier similar to the 151 kJ/mol from the *bis*(ethylene) complex (**^{4}D.III** → **^{4}TS[D.III-D.V]** → **^{4}D.V**).

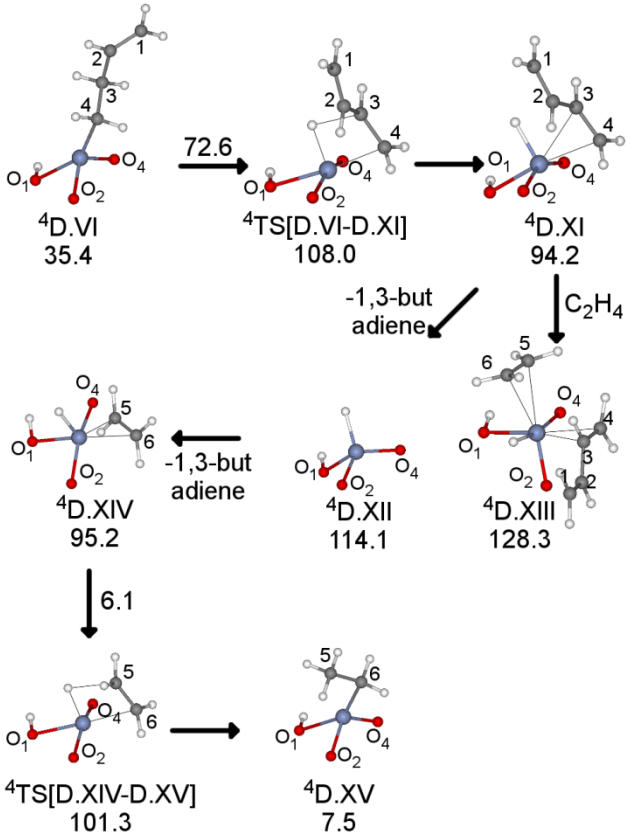

Figure 2.18: Stationary points for chain termination by β-H elimination over a Cr(III) site, and free energies (kJ/mol) relative to that of the bare site, ^{4}D.I, at 373 K. ^{4}D.VI, butenylchromium(III); ^{4}TS[D.VI-D.XI], transition state for β-H elimination to Cr; ^{4}D.XI, (1,3-butadiene)(hydrido)chromium(III); ^{4}D.XII, hydridochromium(III); ^{4}D.XIII, (ethylene)(1,3-butadiene)(hydrido)chromium(III); ^{4}D.XIV, (ethylene)(hydrido)chromium(III); ^{4}TS[D.XIV-D.XV], transition state ethylene insertion into the Cr-H bond; ^{4}D.XV, ethylchromium(III)

However, vinyl-assisted proton transfer can potentially be averted if the butenyl ligand becomes an alkyl group. This can be accomplished through β-H elimination (Figure 2.18). The C3 of butenylchromium(III) **^{4}D.VI** transfers a proton to the metal while a bound, conjugated 1,3-butadiene **^{4}D.XI** forms (Bond lengths and angles in Table B.21). The free energy barrier for this reaction is 73 kJ/mol, and the transition state **^{4}TS[D.VI-D.XI]** is only

14 kJ/mol higher than that of the vinyl-assisted proton transfer. At 373 K, the 1,3-butadiene then prefers to desorb (**^{4}D.XII**) prior to ethylene binding (**^{4}D.XIII**). The hydridochromium(III) **^{4}DXII** can then bind ethylene, which then inserts readily and forms the ethylchromium(III) **^{4}D.XV**. Figure 2.19 shows the qualitative nature of polymerization by the proton-transfer activated Cr(III) site. Polymerization on the proton-transfer activated Cr(III) site is therefore precluded because, according to the present single site model, nearly all sites will be trapped in the dormant **^{4}D.III** state.

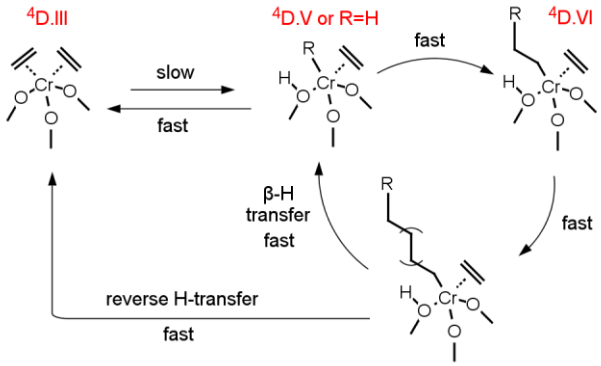

Figure 2.19: Reaction diagram for Cr(III) site initiated by proton transfer. Delley et al. proposed that, after activation by proton transfer, a vinylchromium(III) could be an active polymerization site. Delley et al. proposed the outer loop, but the need to reactivate the site after each polymer chain terminates makes the outer loop exceedingly slow. This work proposes a faster cycle including β-H termination, which can make polymers. However, all steps are many orders of magnitude faster than re-initiation, so the overwhelming majority of sites are trapped in the dormant D.III site.

2.3.7. Cossee-Arlman chain growth at a monoalkylchromium(III) site

Ethylene insertion into the metal-carbon bond of a monoalkylchromium(III) species has long been considered the most likely propagation mechanism for the Phillips catalyst,[1, 6, 10] despite continuing uncertainty over how it might initially be formed. The starting structure for this Cossee-Arlman mechanism, the *n*-butylchromium(III) site **^{4}CA.I** shown in Figure 2.20, was optimized in its high-spin, quartet ground state. It is the reference free energy state for all subsequent structures in this mechanism. Ethylene binds with Cr-C distances of 2.48

and 2.61 Å (**^{4}CA.II**, Table B.22). Relative to **^{4}CA.I**, our calculated binding energy of -52 kJ/mol differs from the -35 kJ/mol calculated by Espelid and Børve.[10] However, both we and they find that this modest binding energy does not offset the entropy penalty for immobilizing free ethylene: we find an overall free energy change of +7 kJ/mol at 373 K and 1 atm, corresponding to a binding constant K of 0.11 atm^{-1}.

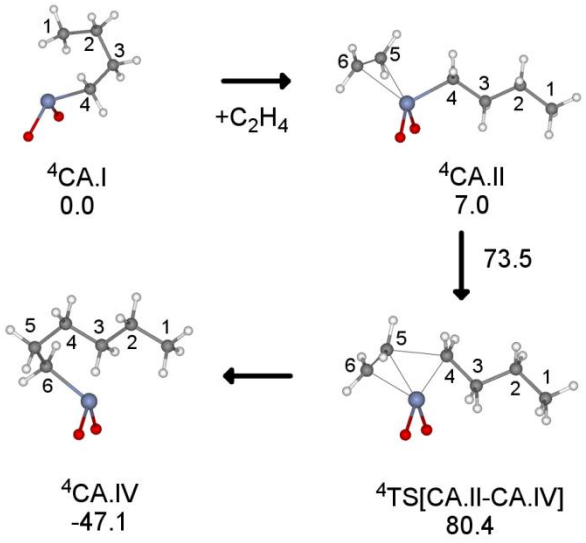

Figure 2.20: Stationary points for Cossee-Arlman propagation on a monoalkylchromium(III) site represented by *n*-butylchromium(III), ^{4}CA.I, and free energies (kJ/mol) relative to that site, at 373 K. ^{4}CA.II, (ethylene)(*n*-butyl)chromium; ^{4}TS[CA.II-CA.IV], transition state for insertion of coordinated ethylene into the Cr-C4 bond; ^{4}CA.IV, *n*-hexylchromium.

As the coordinated monomer prepares to insert, the Cr-C4 bond begins to stretch in the transition state **^{4}TS[CA.II-CA.IV]**. At the same time, a new bond forms as the distance between C4 and C5 shrinks from 3.15 to 2.14 Å. These values match those reported by Espelid and Børve (Table B.22). The overall free energy barrier to traverse the saddle point, 73 kJ/mol relative to **^{4}CA.II**, is low enough for fast propagation, with a calculated rate constant k_{prop} = 4 x 10^2 s^{-1} site^{-1} at 373 K. The activation energy relative to **^{4}CA.II** (64 kJ/mol) also agrees with the value reported by Espelid and Børve (56 kJ/mol).

Chain termination by β-H elimination is shown in Figure 2.21. Migration of a β-H from the alkyl ligand to Cr gives **^{4}CA.III**. In the transition state, **^{4}TS[CA.I-CA.III]**, the β-H approaches Cr at a distance of 1.61 Å. The Cr-C4 bond weakens (Table B.23), while a double-bond begins to develop between C4 and C3. The relative free energy of the transition state, 81 kJ/mol, is just slightly higher than that of the propagation (80 kJ/mol).

The active site is regenerated when 1-butene desorbs from **^{4}CA.III**. The resulting metal hydride intermediate, **^{4}CA.V**, is uphill by 20 kJ/mol relative to **^{4}CA.III**. However, our calculation assumes that 1-butene (representing the polymer product) is present at the standard state pressure of 1 atm. Under realistic operating conditions, the product is present at a much lower pressure than ethylene, and will desorb more readily. In addition, higher α-olefins and long polymer chains gain much more translational entropy from desorption, compared to 1-butene. Thus, all subsequent species in the reaction pathway should be lower in energy.

After ethylene binds to form **^{4}CA.VI**, the free energy of the transition state for the next ethylene insertion, **^{4}TS[CA.VI-CA.VII]**, has a calculated free energy of 81 kJ/mol relative to **^{4}CA.I**. This is indistinguishable from the barrier for β-H elimination. However, the computed free energy of **^{4}TS[CA.VI-CA.VII]** is likely too high, due to the underestimated desorption free energy of the polymer chain (represented by 1-butene) in the previous step. Therefore, the earlier transition state **^{4}TS[CA.I-CA.III]** is probably the main hurdle for the overall chain termination/regeneration process. Overall, the rate coefficient k_{elim} for the reaction **^{4}CA.I** → **^{4}CA.III** is 36 s^{-1} $site^{-1}$.

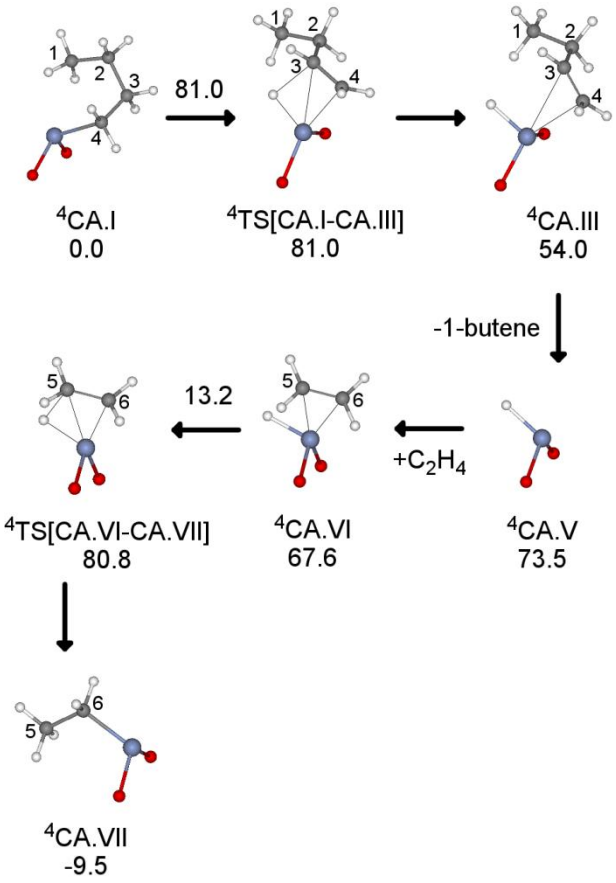

Figure 2.21: Stationary points for chain termination by β-H elimination and subsequent ethylene insertion into the resulting Cr-H bond, at 373 K. ^{4}CA.I, *n*-butylchromium(III); ^{4}TS[CA.I-CA.III], transition state for β-H transfer to Cr; ^{4}CA.III, (1-butene)(hydrido)chromium(III); ^{4}CA.V, hydridochromium(III); ^{4}CA.VI, (ethylene)(hydrido)chromium(III); ^{4}TS[CA.VI-CA.VII], transition state for ethylene insertion into the Cr-H bond; ^{4}CA.VII, ethylchromium(III).

An alternative chain termination reaction is β-H transfer to monomer, in which the bound ethylene in **^{4}CA.II** becomes an ethyl ligand and so transforms the existing alkyl ligand into a bound α-olefin (Figure 2.22). The transition state **^{4}TS[CA.II-CA.IX]** (Table B.24) is 99 kJ/mol higher in free energy than **^{4}CA.II**, corresponding to a rate constant k_{xfer} = 9.8 x 10^{-2} s^{-1} $site^{-1}$ at 373 K. This transition state is also 25 kJ/mol higher in free energy than the β-H elimination transition state **^{4}TS[CA.I-CA.III]**. However, this difference does not immediately determine the dominant termination mechanism for all operating conditions,

because the rate of β-H transfer to monomer increases with ethylene pressure, while that of β-H elimination does not.

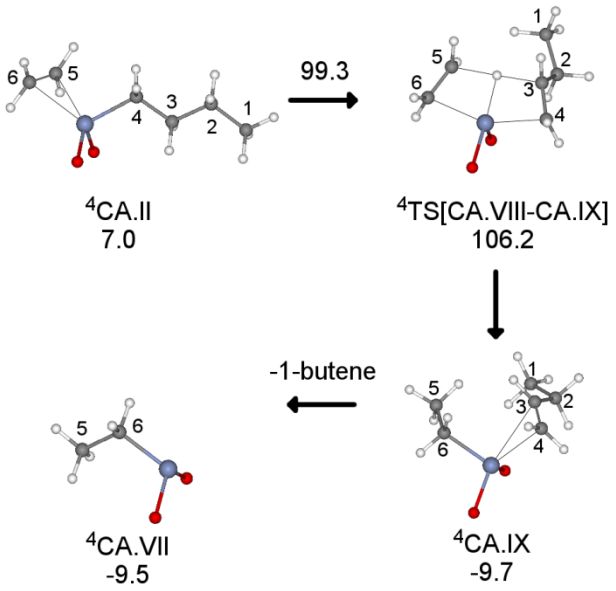

Figure 2.22: Stationary points for β-H transfer to monomer, and free energies (kJ/mol) relative to *n*-butylchromium(III) ^{4}CA.I, at 373 K. ^{4}CA.II, *n*-butylchromium; ^{4}CA.IX, (ethylene)(*n*-butyl)chromium; ^{4}TS[CA.II-CA.IX], transition state for β-H transfer to C5; ^{4}CA.IX, (1-butene)ethylchromium; ^{4}CA.VII, ethylchromium.

A microkinetic model can be built to compute the rate of ethylene consumption and weight-averaged molecular weight. The ethylene consumption rate includes propagation steps and also the consumption from β-H transfer to ethylene monomers. At steady state, the ethylene consumption rate is (derivation in C.2):

$$-r_{C2H4} = k_{prop}\frac{K_1P}{1+K_1P} + k_{xfer}\frac{K_1P}{1+K_1P}\left(\frac{k_{prop}K_1P}{k_{prop}K_1P+k_{e\lim}} + \frac{k_{prop}K_1P\left(k_{xfer}K_1P+k_{e\lim}\right)}{\left(k_{prop}K_1P+k_{e\lim}\right)\left(k_{prop}K_1P+k_{xfer}K_1P+k_{e\lim}\right)}\right) \quad (2.2.4)$$

The first term represents insertion of ethylene into a Cr-C or Cr-H bond (both of which are assumed to be the same). The smaller second term represents β-H transfer to monomer

for all sites except for hydridochromium(III) **^{4}CA.V** and ethylchromium(III) **^{4}CA.VII**, because the former has no β-H and the latter produces ethylene when it transfer H to a monomer. The rate is plotted as function of pressure in Figure 2.23, which shows that the majority of ethylene consumption is due to insertion. At 373 K and 40 atm, the computed consumption rate of ethylene is 3 x 10^{2} C_2H_4*s^{-1} $site^{-1}$, which is close to the experimental value of 2 x 10^{3} C_2H_4*s^{-1} Cr^{-1} (0.01 wt % Cr).[36] Because the proton-transfering-step β-H elimination contributes only 0.02 % of the rate, a kinetic isotope effect is not expected in this mechanism.

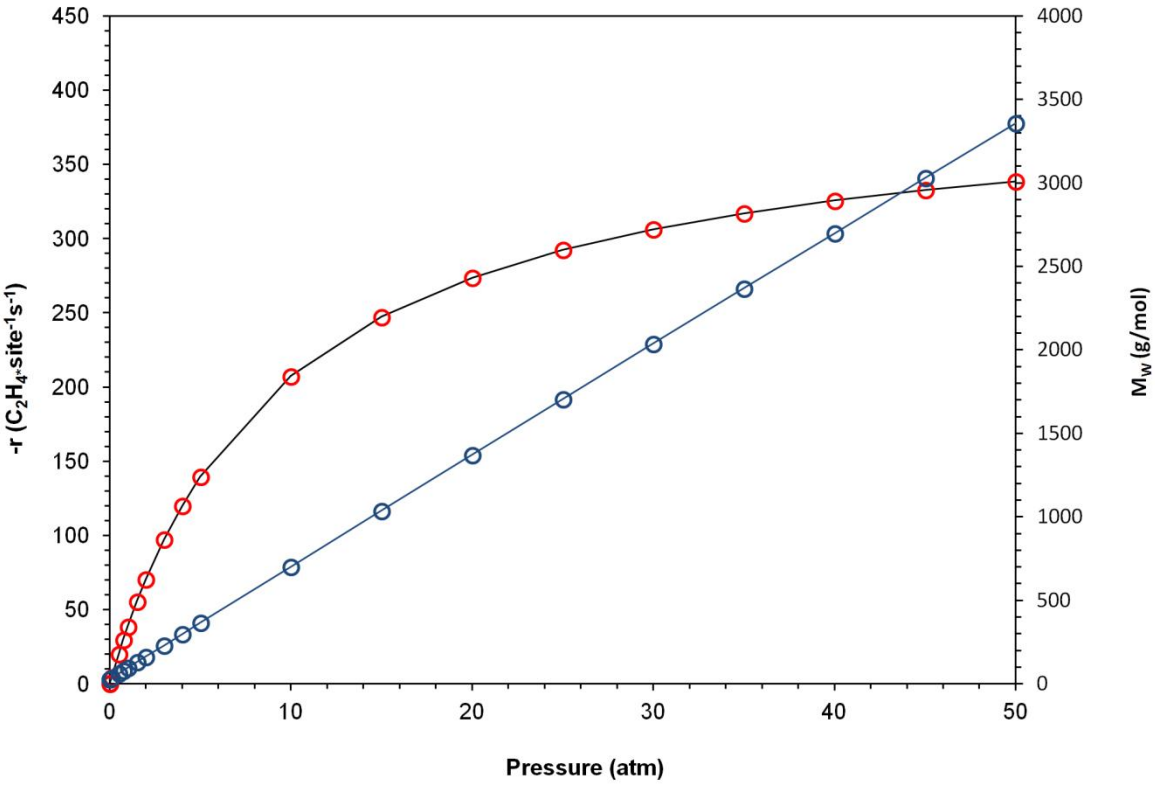

Figure 2.23: Ethylene Rate of Consumption and Weight Average Molecular Weight vs Pressure. Black: total ethylene consumption rate. Red Circles: ethylene insertion rate. Blue: weight average molecular weight

The weight average molecular weight ($P > 0$) is determined by the ratio of propagation and termination[75, 76] as seen in equation 2.2.5:

$$M_w = 2\frac{k_{xfer}K_1P + 2k_{prop}K_1P + k_{e\lim}}{k_{xfer}K_1P + k_{e\lim}} \tag{2.2.5}$$

At 373 K and pressures in the range 1-40 atm, the predicted weight-averaged molecular weight ranges from 100 to 3000 g/mol, which is only a few orders off from the ca. 10^5 g/mol reported for the Phillips catalyst.[1, 77, 78] In addition, the molecular weight is nearly linear in pressure, suggesting β-elimination is the dominant termination mechanism. This is not observed experimentally, because the molecular weight does not extrapolate to zero at zero pressure.[1, 79, 80] Furthermore, at high enough pressure (~40 atm) all alkylchromium(III) sites should bind ethylene like species **^{4}CA.II**, which can only β-H transfer to monomer. Eventually M_w should level off to:

$$M_{w,highP} = 2\frac{k_{xfer} + 2k_{prop}}{k_{xfer}} \tag{2.2.6}$$

which is approximately 2 x 10^5 g/mol. At an extremely high 3 x 10^4 atm, the molecular weight is within 10% of this value. Our cluster model is only a single site catalyst with a polydispersity of nearly two, and small errors in DFT can have large effects on predicted rate coefficients and molecular weight. In particular, an underestimated binding energy of ethylene can cause the predicted plateau in molecular weight to occur at pressures which are too high. The relative free energy difference between the transition states for β-elimination and β-H transfer to monomer is also only 25 kJ/mol, so different sites may terminate via different mechanism and give different molecular weights.

2.4. Conclusions

The calculated free energy barriers for initiation, propagation, and termination for each mechanism in this study are summarized in Table 2.2. For the monochromium site investigated here, the barriers for the metallacycle and Green-Rooney mechanisms are too high to account for observed polymerization rates, in agreement with the earlier conclusions of Espelid and Børve.[10] The oxachromacycle mechanism has a sufficiently low propagation barrier of 97 kJ/mol, but initiates too slowly with a barrier of 165 kJ/mol. The Cossee-Arlman mechanism with a bridging hydroxyl through proton transfer initiates too slowly for both Cr(II) and Cr(III), and only short oligomers form.

Table 2.2: Summary of free energy barriers (kJ/mol) for various proposed Phillips mechanisms

Mechanism	$\Delta G^{\ddagger}_{init}$	$\Delta G^{\ddagger}_{prop}$	$\Delta G^{\ddagger}_{term}$	**Comments**
Metallacycle	-	149-189	114	$\Delta G^{\ddagger}_{prop}$ too high; $\Delta G^{\ddagger}_{prop} > \Delta G^{\ddagger}_{term}$
Oxachromacycle	165	97	-	$\Delta G^{\ddagger}_{init}$ too high
Green-Rooney	-	226	-	$\Delta G^{\ddagger}_{prop}$ too high
Cossee-Arlman mech.				
Si(OH)Cr(II)	152	86	48	$\Delta G^{\ddagger}_{prop} > \Delta G^{\ddagger}_{term}$ (oligomers only)
Si(OH)Cr(III)	151	83	80-88	1) $\Delta G^{\ddagger}_{init}$ too high and re-initiation required 2) some sites make oligomers only
$(\equiv SiO)_2Cr(III)$	-	79	80	1) termination leaves still active site, 2) some sites make oligomers, 3) unknown initiation

Thus far, Cossee-Arlman propagation at a monoalkylchromium(III) site without a bridging hydroxyl is the only viable mechanism we (or others) have identified, although the reactions that lead to its initial formation remain unknown. Fast termination also occurs in this Cossee-Arlman mechanism, but the resulting site remains active with no need for re-initiation, as required by McDaniel's postulates.[17] At 373 K, the calculated overall free energy barriers for propagation and termination by β-H elimination are 79 and 80 kJ/mol, respectively, suggesting that long polymer chains will not form. However, the model we have chosen for the site may be configured to generate oligomers. Recently, Goldsmith et al.[81] showed how subtle structural variations in sites present on amorphous SiO_2 can lead to substantial changes in reactivity, and by extension, to changes in the degree of polymerization. Future work using that systematic approach may help us to understand the structural differences that distinguish sites with different reactivities and selectivities. The Phillips catalyst is also usually made with amorphous silica, and the high polydispersity indicates a very broad range of active sites. In this sense, it is reasonable to expect that a single site model will not be capable of modeling all aspects of Phillips polymerization. Of course, further experimental and computational studies are also needed to understand the Cossee-Arlman initiation mechanism.

2.5. Acknowledgements

This work was supported by the National Science Foundation, award no. CBET08-54425.

We thank Horia Metiu for helpful discussions. Thank PRF and DOE?

2.6. References

1. McDaniel, M. P., *Advances in Catalysis, Vol 53* **2010,** *53*, 123-606.
2. McDaniel, M. P.; Welch, M. B., *Journal of Catalysis* **1983,** *82* (1), 98-109.
3. McDaniel, M. P., *Advances in Catalysis* **1985,** *33*, 47-98.

4. McDaniel, M. P.; Welch, M. B.; Dreiling, M. J., *Journal of Catalysis* **1983,** *82* (1), 118-126.
5. Pullukat, T. J.; Hoff, R. E.; Shida, M., *Journal of Polymer Science Part a-Polymer Chemistry* **1980,** *18* (9), 2857-2866.
6. Hogan, J. P., *Journal of Polymer Science Part a-1-Polymer Chemistry* **1970,** *8* (9), 2637-&.
7. Cossee, P., *Journal of Catalysis* **1964,** *3* (1), 80-88.
8. Groppo, E.; Lamberti, C.; Bordiga, S.; Spoto, G.; Zecchina, A., *Chemical Reviews* **2005,** *105* (1), 115-183.
9. McGuinness, D. S.; Davies, N. W.; Horne, J.; Ivanov, I., *Organometallics* **2010,** *29* (22), 6111-6116.
10. Espelid, O.; Borve, K. J., *Journal of Catalysis* **2000,** *195* (1), 125-139.
11. McDaniel, M. P.; Cantor, D. M., *Journal of Polymer Science Part a-Polymer Chemistry* **1983,** *21* (4), 1217-1221.
12. Ghiotti, G.; Garrone, E.; Zecchina, A., *Journal of Molecular Catalysis* **1988,** *46* (1-3), 61-77.
13. Kantcheva, M.; Dallalana, I. G.; Szymura, J. A., *Journal of Catalysis* **1995,** *154* (2), 329-334.
14. Conley, M. P.; Delley, M. F.; Siddiqi, G.; Lapadula, G.; Norsic, S.; Monteil, V.; Safonova, O. V.; Coperet, C., *Angewandte Chemie-International Edition* **2014,** *53* (7), 1872-1876.
15. Delley, M. F.; Nunez-Zarur, F.; Conley, M. P.; Comas-Vives, A.; Siddiqi, G.; Norsic, S.; Monteil, V.; Safonova, O. V.; Coperet, C., *Proceedings of the National Academy of Sciences 111* (32), 11624-11629.
16. Cheng, R. H.; Xu, C.; Liu, Z.; Dong, Q.; He, X. L.; Fang, Y. W.; Terano, M.; Hu, Y. T.; Pullukat, T. J.; Liu, B. P., *Journal of Catalysis* **2010,** *273* (2), 103-115.
17. McDaniel, M. P., Review of the Phillips Chromium Catalyst for Ethylene Polymerization. In *Handbook of Heterogeneous Catalysis*, Wiley-VCH Verlag GmbH & Co. KGaA: 2008.
18. Delley, M. F.; Conley, M. P.; Coperet, C., *Catalysis Letters* **2014,** *144* (5), 805-808.
19. Kuran, W., *Principles of coordination polymerisation : heterogeneous and homogeneous catalysis in polymer chemistry-polymerisation of hydrocarbon, heterocyclic, and heterounsaturated monomers*. Wiley: Chicthester ; New York, 2001; p xxi, 522 p.
20. Merryfield, R.; Mcdaniel, M.; Parks, G., *Journal of Catalysis* **1982,** *77* (2), 348-359.
21. Zecchina, A.; Groppo, E., *Proceedings of the Royal Society a-Mathematical Physical and Engineering Sciences* **2012,** *468* (2143), 2087-2098.
22. M. J. Frisch, G. W. T., H. B. Schlegel, G. E. Scuseria, M. A. Robb, J. R. Cheeseman, G. Scalmani, V. Barone, B. Mennucci, G. A. Petersson, H. Nakatsuji, M. Caricato, X. Li, H. P. Hratchian, A. F. Izmaylov, J. Bloino, G. Zheng, J. L. Sonnenberg, M. Hada, M. Ehara, K. Toyota, R. Fukuda, J. Hasegawa, M. Ishida, T. Nakajima, Y. Honda, O. Kitao, H. Nakai, T. Vreven, J. A. Montgomery, Jr., J. E. Peralta, F. Ogliaro, M. Bearpark, J. J. Heyd, E. Brothers, K. N. Kudin, V. N. Staroverov, R. Kobayashi, J. Normand, K. Raghavachari, A. Rendell, J. C. Burant, S. S. Iyengar, J. Tomasi, M. Cossi, N. Rega, J. M. Millam, M. Klene, J. E. Knox, J. B. Cross, V. Bakken, C. Adamo, J. Jaramillo, R. Gomperts, R. E. Stratmann, O. Yazyev, A. J.

Austin, R. Cammi, C. Pomelli, J. W. Ochterski, R. L. Martin, K. Morokuma, V. G. Zakrzewski, G. A. Voth, P. Salvador, J. J. Dannenberg, S. Dapprich, A. D. Daniels, Ö. Farkas, J. B. Foresman, J. V. Ortiz, J. Cioslowski, and D. J. Fox *Gaussian 09, Revision A.1*, Gaussian, Inc.: Wallingford CT, 2009.
23. Chai, J. D.; Head-Gordon, M., *Physical Chemistry Chemical Physics* **2008,** *10* (44), 6615-6620.
24. Goerigk, L.; Grimme, S., *Physical Chemistry Chemical Physics* **2011,** *13* (14), 6670-6688.
25. Schenker, S.; Schneider, C.; Tsogoeva, S. B.; Clark, T., *Journal of Chemical Theory and Computation* **2011,** *7* (11), 3586-3595.
26. Zhao, Y.; Truhlar, D. G., *Journal of Chemical Theory and Computation* **2011,** *7* (3), 669-676.
27. Yang, K.; Zheng, J. J.; Zhao, Y.; Truhlar, D. G., *Journal of Chemical Physics* **2010,** *132* (16).
28. Minenkov, Y.; Singstad, A.; Occhipinti, G.; Jensen, V. R., *Dalton Transactions* **2012,** *41* (18), 5526-5541.
29. Feller, D., *Journal of Computational Chemistry* **1996,** *17* (13), 1571-1586.
30. Schuchardt, K. L.; Didier, B. T.; Elsethagen, T.; Sun, L. S.; Gurumoorthi, V.; Chase, J.; Li, J.; Windus, T. L., *Journal of Chemical Information and Modeling* **2007,** *47* (3), 1045-1052.
31. Godbout, N.; Salahub, D. R.; Andzelm, J.; Wimmer, E., *Canadian Journal of Chemistry-Revue Canadienne De Chimie* **1992,** *70* (2), 560-571.
32. Schlegel, H. B., *Journal of Computational Chemistry* **1982,** *3* (2), 214-218.
33. Baker, J., *Journal of Computational Chemistry* **1986,** *7* (4), 385-395.
34. Jensen, F., *Introduction to computational chemistry*. Wiley: Chichester ; New York, 1999; p xvi, 429 p.
35. McDaniel, M. P.; Rohlfing, D. C.; Benham, E. A., *Polymer Reaction Engineering* **2003,** *11* (2), 101-132.
36. Leach, B. E., *Applied industrial catalysis*. Academic Press: New York, 1983.
37. Weckhuysen, B. M.; Schoonheydt, R. A., *Catalysis Today* **1999,** *51* (2), 215-221.
38. Zhong, L.; Liu, Z.; Cheng, R. H.; Tang, S. Y.; Qiu, P. Y.; He, X. L.; Terano, M.; Liu, B. P., *Chemcatchem* **2012,** *4* (6), 872-881.
39. Thune, P. C.; Loos, J.; Chen, X. H.; van Kimmenade, E. M. E.; Kong, B.; Niemantsverdriet, J. W. H., *Topics in Catalysis* **2007,** *46* (1-2), 239-245.
40. Demmelmaier, C. A.; White, R. E.; van Bokhoven, J. A.; Scott, S. L., *Journal of Catalysis* **2009,** *262* (1), 44-56.
41. Waddell, W. H.; Evans, L. R., Silica, Amorphous Silica. In *Kirk-Othmer Encyclopedia of Chemical Technology*, John Wiley & Sons, Inc.: 2000.
42. Gaskell, P. H.; Parker, J. M.; Davis, E. A.; Society of Glass Technology., *The Structure of non-crystalline materials, 1982 : proceedings of the second international conference held in Cambridge, UK on 12-15 July 1982*. International Publications Service, Taylor & Francis, on behalf of the Society of Glass Technology: New York, 1983; p xiii, 609 p.
43. Lee, C. T.; Yang, W. T.; Parr, R. G., *Physical Review B* **1988,** *37* (2), 785-789.
44. Becke, A. D., *Journal of Chemical Physics* **1993,** *98* (7), 5648-5652.
45. Hay, P. J.; Wadt, W. R., *Journal of Chemical Physics* **1985,** *82* (1), 299-310.

46. Hay, P. J.; Wadt, W. R., *Journal of Chemical Physics* **1985,** *82* (1), 270-283.
47. Wadt, W. R.; Hay, P. J., *Journal of Chemical Physics* **1985,** *82* (1), 284-298.
48. Mclean, A. D.; Chandler, G. S., *Journal of Chemical Physics* **1980,** *72* (10), 5639-5648.
49. Krishnan, R.; Binkley, J. S.; Seeger, R.; Pople, J. A., *Journal of Chemical Physics* **1980,** *72* (1), 650-654.
50. Ehlers, A. W.; Bohme, M.; Dapprich, S.; Gobbi, A.; Hollwarth, A.; Jonas, V.; Kohler, K. F.; Stegmann, R.; Veldkamp, A.; Frenking, G., *Chemical Physics Letters* **1993,** *208* (1-2), 111-114.
51. Roy, L. E.; Hay, P. J.; Martin, R. L., *Journal of Chemical Theory and Computation* **2008,** *4* (7), 1029-1031.
52. Clark, T.; Chandrasekhar, J.; Spitznagel, G. W.; Schleyer, P. V., *Journal of Computational Chemistry* **1983,** *4* (3), 294-301.
53. Grimme, S.; Ehrlich, S.; Goerigk, L., *Journal of Computational Chemistry* **2011,** *32* (7), 1456-1465.
54. Grimme, S.; Antony, J.; Ehrlich, S.; Krieg, H., *Journal of Chemical Physics* **2010,** *132* (15).
55. Schmid, R.; Ziegler, T., *Canadian Journal of Chemistry-Revue Canadienne De Chimie* **2000,** *78* (2), 265-269.
56. Perdew, J. P., *Physical Review B* **1986,** *33* (12), 8822-8824.
57. Vosko, S. H.; Wilk, L.; Nusair, M., *Canadian Journal of Physics* **1980,** *58* (8), 1200-1211.
58. Cheng, R. H.; Liu, Z.; Qiu, P. Y.; Zhang, S. L.; Liu, B. P., *Chinese Journal of Polymer Science* **2008,** *26* (5), 579-587.
59. Liu, Z.; Zhong, L.; Yang, Y.; Cheng, R. H.; Liu, B. P., *Journal of Physical Chemistry A* **2011,** *115* (28), 8131-8141.
60. Dixon, J. T.; Green, M. J.; Hess, F. M.; Morgan, D. H., *Journal of Organometallic Chemistry* **2004,** *689* (23), 3641-3668.
61. McGuinness, D. S., *Chemical Reviews* **2011,** *111* (3), 2321-2341.
62. Ghiotti, G.; Garrone, E.; Zecchina, A., *Journal of Molecular Catalysis* **1991,** *65* (1-2), 73-83.
63. Groppo, E.; Lamberti, C.; Bordiga, S.; Spoto, G.; Zecchina, A., *Journal of Catalysis* **2006,** *240* (2), 172-181.
64. Ajjou, J. A. N.; Scott, S. L.; Paquet, V., *Journal of the American Chemical Society* **1998,** *120* (2), 415-416.
65. Ruddick, V. J.; Badyal, J. P. S., *Journal of Physical Chemistry B* **1998,** *102* (16), 2991-2994.
66. van Rensburg, W. J.; Grove, C.; Steynberg, J. P.; Stark, K. B.; Huyser, J. J.; Steynberg, P. J., *Organometallics* **2004,** *23* (6), 1207-1222.
67. Yang, Y.; Liu, Z.; Cheng, R. H.; He, X. L.; Liu, B. P., *Organometallics* **2014,** *33* (10), 2599-2607.
68. Baker, L. M.; Carrick, W. L., *Journal of Organic Chemistry* **1970,** *35* (3), 774-&.
69. Ivin, K. J.; Rooney, J. J.; Stewart, C. D.; Green, M. L. H.; Mahtab, R., *Journal of the Chemical Society-Chemical Communications* **1978,** (14), 604-606.
70. Turner, H. W.; Schrock, R. R., *Journal of the American Chemical Society* **1982,** *104* (8), 2331-2333.

71. Turner, H. W.; Schrock, R. R.; Fellmann, J. D.; Holmes, S. J., *Journal of the American Chemical Society* **1983,** *105* (15), 4942-4950.
72. Fang, Y.; Liu, B.; Terano, M., *Kinetics and Catalysis* **2006,** *47* (2), 295-302.
73. Ajjou, J. A. N.; Scott, S. L., *Journal of the American Chemical Society* **2000,** *122* (37), 8968-8976.
74. Theopold, K. H., *European Journal of Inorganic Chemistry* **1998,** (1), 15-24.
75. Keii, T., *Heterogeneous kinetics : theory of Ziegler-Natta-Kaminsky polymerization*. Kodansha ;
Springer: Tokyo
Berlin ; New York, 2004; p xiii, 249 p.
76. Tonosaki, K.; Taniike, T.; Terano, M., *Journal of Molecular Catalysis a-Chemical* **2011,** *340* (1-2), 33-38.
77. Kim, C. S.; Woo, S. I.; Jeong, D. J.; Oh, J. S., *Polymer Bulletin* **1992,** *29* (1-2), 205-212.
78. Kissin, Y. V.; Brandolini, A. J.; Garlick, J. L., *Journal of Polymer Science Part a-Polymer Chemistry* **2008,** *46* (16), 5315-5329.
79. Clark, A.; Bailey, G. C., *Journal of Catalysis* **1963,** *2* (3), 241-247.
80. Hoff, R. E.; Mathers, R. T., *Handbook of transition metal polymerization catalysts*. Wiley: Hoboken, N.J., p xxi, 575 p.
81. Goldsmith, B. R.; Sanderson, E. D.; Bean, D.; Peters, B., *Journal of Chemical Physics* **2013,** *138* (20).

Chapter 3

Note: This chapter is based on an experimental and computational collaboration between Alessandro Gallo and Anthony Fong.

Dramatic enhancement of olefin metathesis activity for CH_3ReO_3 upon chlorination of γ-Al_2O_3

3.1. Introduction

Olefin metathesis is an important reaction for the production of propylene, detergent-range α-olefins and functionalized olefins. It is a key component of the well-known Phillips Triolefin Process[1] and the Shell Higher Olefins Process (SHOP).[2] The supported Mo and W oxides that are used as catalysts in these large-scale industrial applications work at temperatures up to 500 °C.[3] WO_3/γ-Al_2O_3 (SiO_2) is the major component of the metathesis catalyst for the Triolefin Process, and requires an operating temperature higher than 350 °C. Re oxide-based heterogeneous catalysts, while promising due to their high activity near room temperature and functional group tolerance,[4] have yet to be widely exploited commercially. Some of the barriers include the high cost of Re, the high Re loading required, rapid catalyst deactivation, and the volatility of Re_2O_7. The development of a highly active, robust and regenerable Re-based catalyst would be a major advance.

The acidity of the support is a key factor in the activation of Re-based pre-catalysts. Both Brønsted[5,6] and Lewis [7] acidity have been reported to be involved in their activation. While there are many highly active catalysts based on molecular complexes, or molecular complexes grafted onto oxide surfaces,[8-10] that do not require such activation, their use in

large-scale continuous processing is often impractical. Heterogeneous catalysts based on supported methyltrioxorhenium (MTO) have been proposed as alternatives to purely oxide-based catalysts, due to the development of facile and efficient methods of MTO synthesis.[11-14] Moreover, supported MTO can be generated (or regenerated) in situ from inorganic perrhenates by treatment with methylating agents such as $AlMe_3$ or $SnMe_4$.[15] MTO-based catalysts are very active at low Re loadings (1-3 wt %), while conventional Re/Al_2O_3 catalysts require at least 10 wt % Re. MTO can be activated in solution by a Lewis acid,[16] such as $AlCl_xMe_y$,[17] however, it is also activated efficiently simply by deposition onto an acidic oxide support such as alumina, silica-alumina, or niobia.[18-22] The activation appears to involve interaction with surface Lewis acid sites; our work showed that Brønsted acid sites are not only ineffective, but are implicated in decreased stability and selectivity.[23]

In principle, the catalytic activity of Re-based heterogeneous catalysts may be enhanced by increasing either the intrinsic activity of the active sites, or their fraction, or both. Understanding the nature of these sites is challenging, including those involving well-defined organorhenium complexes grafted onto high surface area supports. The intrinsic heterogeneity of the surface results in the presence of numerous grafted sites,[24] and the active sites may represent only a small fraction of the total.[25, 26] Supported MTO exemplifies a common problem with organometallic-derived catalysts with highly heterogeneous sites, with a low fraction that are metathesis-active. For example, the activity for MTO on silica-alumina at Re loadings 1 and 10 wt% are identical.[23] Despite general agreement that a terminal Re carbene is required in the active site, this species has not been detected on any support, although a minor species interacting through a bridging $Re\text{-}CH_2\text{-}Al$ alkylidene (analogous to Tebbe's reagent) was proposed to be a precursor of the true active site.[27, 28]

Previously, we reported that γ-Al_2O_3 is much less effective than either SiO_2-Al_2O_3 or Nb_2O_5, although better than SiO_2, in activating MTO for olefin metathesis.[21] While silica-alumina generates the most active catalyst, its high Brønsted acidity results in numerous undesired side-reactions (principally, olefin isomerization and oligomerization).[23] Recently, $ZnCl_2$ was reported to promote the metathesis activity of MTO/γ-Al_2O_3.[29] Upon further investigation, the presence of $ZnCl_2$ causes the fraction of active Re sites to increase, as well as the per-site activity.[30] While both Zn^{2+} and Cl^- have been presumed necessary, and the Lewis acidity of the Zn^{2+} ions have been implicated in the activity enhancement,[31, 32] the presence of Zn^{2+} is likely to interfere with catalyst regeneration. Similar promotion effect have also been observed by using group 13 metal chloride, such as $GaCl_3$.[30] However, the molecular structure of the active species is yet not established, particularly the role of Zn^{2+} or Ga^{3+} and Cl^-. Understanding chlorine promotion of the supported Re catalysts for olefin metathesis is of fundamental interest. Novel insights can be obtained by comparing the structure and catalytic performance of MTO/γ-Al_2O_3 with MTO supported on chlorinated γ-Al_2O_3.[33] Hence, we decided to graft MTO onto this modified and non-modified support in order to gain important structural information concerning the presence of chlorine and its effect of the catalytic activity in olefin metathesis.

3.2 Methods

3.2.1: Computational Details

Likely structures were investigated computationally with a simple cluster model of Al_2Cl_6 (Figure 3.1), which was chosen in order to approximate the surface and take into account the relatively high Cl concentration on the surface and low OH presence. In particular both terminal and bridging Cl atoms were included in the model. To model the

rigid solid support, most of the terminal chlorine atoms were fixed in space. However, in order to model reactions with terminal and not only bridging chlorine atoms, Cl3 was allowed to move freely in space. All bond angles and lengths are summarized in Table 3.1. All geometry optimizations were done with Gaussian 09 and the basis set used was def2-TZVP[34, 35] for Re and TZVP[36] for all other atoms. Reported free energies include translational, rotational, and vibration contributions at 298.15 K. All reported 13-C NMR chemical shifts were calculated with the GIAO method[37, 38] with a calibration curve based on shifts of a series of Re compounds[39] and their computed shielding values (Figure D.1 and Table D.1 in Appendix D). All chemical shifts for MTO on Cl2AlO3 appear in Table D.2.

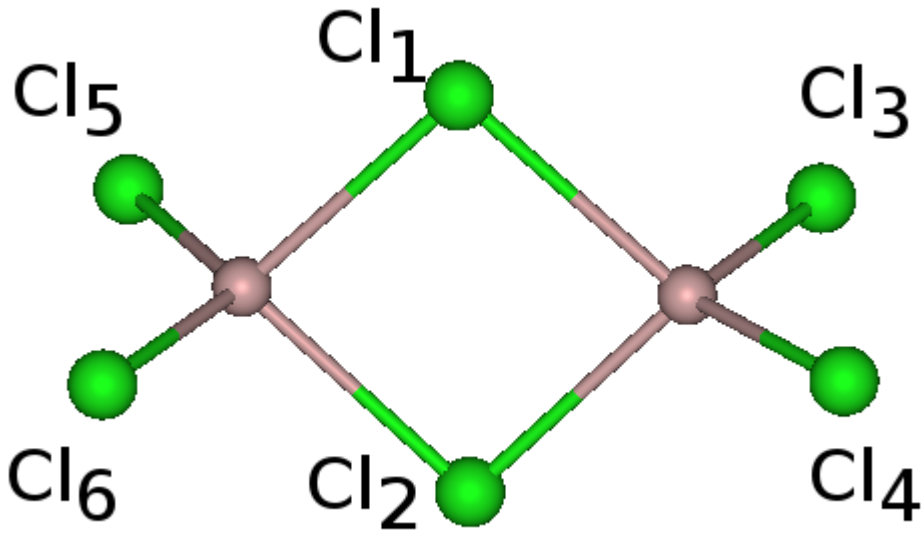

Figure 3.1: Cluster Model for Al_2Cl_6. Cl: green, Al: purple

Table 3.1: Key inter-atomic distances (Å) and bond angles (°) for Al_2Cl_6 cluster

Parameter	Value
*r*Al-Cl1	2.31
*r*Al-Cl2	2.31
*r*Al-Cl3	2.09
*r*Al-Cl4	2.12
∠Al-Cl1-Al	93
∠Al-Cl2-Al	93
∠Cl1-Al-Cl3	107
∠Cl1-Al-Cl4	116

3.2.1: Catalyst Preparation

γ-Al_2O_3 (Strem , 200 m^2/g) was calcined at 450 °C for 4 hours in air and then evacuated under dynamic vacuum (10^{-4} Torr) overnight. The chlorination procedure was performed contacting the alumina in a fixed bed reactor kept at 300 °C with CCl_4 (Sigma-Aldrich) saturated N_2 (Praxair, 99.5 %) (saturated at 25 °C; 10 mL/min) for 1 hour. After chlorination, the support was evacuated at 200 °C for 3 hours and at 450 °C overnight. MTO (Sigma-Aldrich) was grafted at room temperature by subliming it at 10^{-4} Torr into a reactor containing the Cl-Al_2O_3. The solid was vigorously shaken to promote a uniform deposition. After grafting the sample was evacuated at room temperature overnight to remove eventually physisorbed MTO. A reference sample of MTO on γ-Al_2O_3 calcined and evacuated at 450 °C was synthesized following the same procedure, for comparison.

3.2.2: Catalytic test and active sites counting

The batch reaction was performed in a 120 mL Pyrex reactor at 0 °C. 10 mg of catalyst were transferred into the reactor inside an Ar glove-box and after evacuation, 50 Torr of propene were admitted into the reactor (PRAX Air, 99.8%). Propylene was further purified using molecular sieves and Cu containing catalysts. The reaction products were analyzed by means of a GC-FID (Shimadzu equipped with a sulfated alumina capillary column Supelco Alumina Sulfate plot, 30 m x 0.32 mm). Propane was used as internal standard.

Active site counting was performed in a 120 mL batch reactor. 100 mg of sample were loaded into the reactor inside an Ar glove box and after evacuation 120 Torr of 2-butenes mixture were admitted into the reactor at 0 °C and allowed react for 3 hours. After evacuation at RT for 30 min, the 2-butenes (Sigma-Aldrich) mixture addition was repeated. After overnight evacuation at room temperature, 120 Torr of ethene (PRAX Air, 5% propane was used as internal standard) were introduced into the reactor and let react for 3 hours at 0 °C. The amount of propene produced was analyzed by GC-FID.

3.2.3: Solid State NMR

To enhance sensitivity in ^{13}C CP-MAS NMR experiments, labeled $^{13}CH_3ReO_3$ (>99% ^{13}C) according to a literature procedure.[40] The sample was packed inside an Ar glove-box into a 4 mm zirconia rotor and sealed with an O-ring cap. The spinning rate was 10 kHz and the measurement was performed at room temperature on a Bruker AVANCE 300 NMR spectrometer operating at 75.4577 MHz for ^{13}C. The highly air-sensitive samples were packed under an argon atmosphere in a glovebox equipped with O_2- and moisture-sensors into 4 mm zirconia MAS rotor with tightly fitting caps sealed with Kel-F O-rings (Wilmad). ^{13}C CPMAS spectra were recorded using a 90° pulse length of 3.5 μs, a contact time of 3

ms, an acquisition time of 21 ms, and a recycle delay of 2 s and a high power proton decoupling during detection. ^{13}C chemical shifts was referenced to tetrakis(trimethylsilyl)silane (TKMS).

3.2.4: Re Analysis

Re loadings were determined by quantitative extraction, followed by UV spectrophotometric analysis. Samples containing ca. 30 mg of silica-alumina and <3 wt % Re were first weighed in an inert atmosphere. Re was extracted as perrhenate by stirring overnight in air with 5 mL of 3 M NaOH. Samples were diluted to 25 mL with 3 M H_2SO_4 and filtered, and their UV spectra were recorded on a Shimadzu UV2401PC spectrophotometer. Re concentration was determined at 224 nm, using a calibration curve prepared with NH_4ReO_4 (Sigma-Aldrich). Cl was quantified by Columbia Analytical (Tucson, AZ).

3.2.5: FT-IR

FT-IR spectra of self supporting pellets pressed inside an Ar dry-box were collected using a Bruker Alpha-FT-R located inside the Dry-box in the range 4000-400 cm^{-1} with a resolution of 4 cm^{-1}, accumulating 32 scans.

IR-monitored Pyridine adsorption was performed in an air-free Pyrex cell equipped with two KBr windows. A self-supporting pellet of Cl-Al_2O_3 was pressed inside a Ar Glove-box and transferred into the air-free Pyrex cell. The FT-IR spectra were collected using a Shimadzu IRPrestige-21, collecting 32 scans in the 4000-400 cm^{-1} region with a 4 cm^{-1} resolution.

3.2.6: XAS

X-Ray absorption spectra at the L_I (12527 eV) and L_{III} (10535 eV) edges were collected at Stanford Synchrotron Radiation Laboratory on beam-line 4-1 operating at 3.0 GeV with a current of 500 mA. The samples were analyzed at liquid helium temperature to avoid decomposition and handled under inert atmosphere in fluorescence mode using a Lytle detector filled with Ar. The data were analyzed using the Athena and Artemis softwares in order to obtain the coordination number (N), the distance of the scattering atoms (R) and the disorder factor (σ^2) of the neighboring scattering atoms.[41]

3.3. Results

3.3.1: A More Active and Selective MTO Catalyst

When MTO is grafted onto γ-Al_2O_3 (2.4 wt% Re), its activity for gas-phase propene homo-metathesis is very low, Figure 3.2. The reaction is first-order in both propene and Re, with a second-order rate constant at 0 °C of k = 2.9 s^{-1} $(g_{Re})^{-1}$. For comparison, the comparable rate constant for MTO/SiO_2-Al_2O_3 (1.0 wt% Re) is 30 s^{-1} $(g_{Re})^{-1}$.[23] Using γ-Al_2O_3 promoted with $ZnCl_2$ causes the activity to increase; the enhancement is related to the Al/Zn ratio. At 0 °C, the corresponding rate constants are 18 and 45 s^{-1} $(g_{Re})^{-1}$ for Al/Zn ratios of 48 and 16, respectively.[30]

The propene homo-metathesis activity increases dramatically when MTO is grafted directly onto Cl-Al_2O_3 (2.3 wt% Re). At 0 °C, equilibrium was reached after 7 min, compared to more than 60 min for MTO/γ-Al_2O_3 (2.4 wt% Re) (Figure 3.2b). Although the Cl content of the modified Al_2O_3 (4.0 wt%) is comparable to that of the $ZnCl_2$-promoted catalyst (Al/Zn = 16, 5.0 wt% Cl), the second-order rate constant is considerably higher, at 98 s^{-1} $(g_{Re})^{-1}$. Therefore, we infer that the promotion effect is principally due to the presence

of Cl; the additional Lewis acidity contributed by Zn^{2+} is not necessary to achieve a significant increase in the catalytic activity. Indeed, direct chlorination of the support leads to a considerably more active metathesis catalyst. Traces amount of C_5, C_6 and C_7 olefin side-products were formed over MTO/Cl-Al_2O_3 at 0 °C and 50 Torr propylene, while no byproducts were detected by GC-MS for MTO/ γ-Al_2O_3.

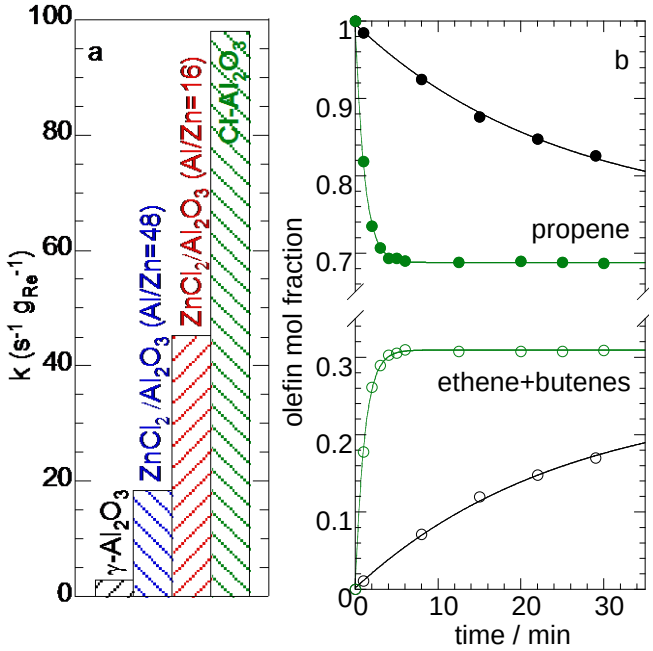

Figure 3.2: Comparison of (a) second-order rate constants for gas-phase propene homo-metathesis at 0 °C, by CH_3ReO_3 supported on γ-Al_2O_3 (2.4 wt% Re), $ZnCl_2$/γ-Al_2O_3 (Al/Zn = 48, 2.3 wt% Re), $ZnCl_2$/γ-Al_2O_3 (Al/Zn = 16, 2.3 wt% Re), and Cl-Al_2O_3 (2.3 wt% Re); and (b) kinetic profiles for propene consumption (filled circles) and product formation (ethene+2-butenes, open circles), for MTO supported on γ-Al_2O_3 (black) and Cl-Al_2O_3 (green). Conditions: 50 Torr propene, 0 °C, 10 mg catalyst in a batch reactor.

The improved catalytic activity for MTO/Cl-Al_2O_3 may be the result of either an increase in the fraction of active sites, or an increase in the per-site activity, or both. In order to identify the origin of the effect, we performed active-site counting experiments[42] for MTO supported on both chlorinated and unmodified aluminas. Each catalyst was first exposed to a mixture of *cis*- and *trans*-2-butene, evacuated, then treated with ethene, all at 0

°C. The amount of propene formed in the last step corresponds to the number of ethylidene sites present after activation with 2-butene, and is equated to the number of active sites. There is some uncertainty involved in this measurement, due to strong retention of olefins on the surface: insufficiently long evacuation times can lead to overestimation of the active site count, while excessive evacuation times may result in decomposition of the active sites. Using multiple experiments, we conclude that on unmodified γ-Al_2O_3, ca. 2 % of Re sites are active, while 12-16% of Re sites are active on Cl-Al_2O_3. Thus the active site fraction increases ca. 7-9 times, which is nevertheless lower than the increase in the second-order rate constant (ca. 30 times). Chlorination of γ-Al_2O_3 therefore enhances both the number of active sites *and* the average per-site activity, as we previously reported for the $ZnCl_2$-promoted catalyst.[30] This further implies that at least some of the active sites present on Cl-Al_2O_3 are distinctly different from those present on γ-Al_2O_3.[27]

3.3.2: Effect of chlorination on the catalyst support

In order to investigate the effect of chlorination on MTO on the stability of the catalyst, we studied how the chlorination procedure changes the surface of the alumina support and the modification of the coordination sphere of Rhenium in the active specie. Chlorination is known to increase the surface acidity, and to affect the distribution and nature of the surface hydroxyls. However, the nature of the surface modification depends strongly on the chlorinating agent and on the reaction conditions. While mild chlorination with HCl leads to replacement of only surface OH groups,[43] more extensive chlorination using CCl_4 causes replacement of lattice oxygen atoms as well,[44] and eventually produces volatile $AlCl_3$ which sublimes from the surface. Our procedure involves treatment in flowing CCl_4 at 300 °C for 0.5 h, followed by evacuation first at 200 °C for 2 h, then at 450 °C overnight. The result is

extensive surface chlorination: the solid contains 4.0 wt% Cl, corresponding to an estimated surface density of 3.8 Cl/nm^2 and a decrease of the surface O/Al from 1.7 to 1.3. In addition, volatile $AlCl_3$ was observed to condense at the reactor outlet.[45]

IR spectra of γ-Al_2O_3 and Cl-Al_2O_3 are compared in Figure 3.3. The former shows two higher frequency bands at 3790 and 3773 cm^{-1}, assigned to the stretching modes of terminal OH groups, while bridging OH groups appear at 3730, 3693 and 3676 cm^{-1}.[46] Their reactivity is determined by their coordination: bridging OH groups are acidic, while terminal OH groups are basic, and are more prone to condensation and substitution reactions.[47] Chlorination of γ-Al_2O_3 leads to major changes in the IR spectrum in the O-H stretching region. The bands attributed to terminal OH groups disappear completely, as also evidenced by ^{1}H MAS NMR (*vide infra*). Previous theoretical calculations showed that the most energetically favorable substitution reaction is one in which terminal OH groups are replaced by Cl.[48] The bands for bridging OH groups decrease noticeably in intensity. While a small peak at 3730 cm^{-1} is still visible, the others are obscured by a very broad band centered at 3500 cm^{-1}, arising from a hydrogen-bonded hydroxyl network. Substitution of terminal OH groups by Cl affects this network and results in broadening of the residual O-H stretching bands.[49] Similar results were reported when γ-Al_2O_3 was chlorinated with CH_2Cl_2 at 250 °C.[50] There is no evidence that $AlCl_3$ remains on the surface, as judged by the absence of a characteristic IR band at ca. 1380 cm^{-1}.[45]

Solid-state ^{1}H MAS NMR spectra provide a more quantitative assessment of the effect of chlorination on both the number and nature of the surface hydroxyl groups. The spectrum of γ-Al_2O_3 (dehydrated and partially dehydroxylated at 450 °C) consists of two signals at 1.8 and -0.4 ppm assigned to bridging and terminal hydroxyl groups, respectively, Figure 3.4.[51]

The dramatic reduction in overall signal intensity upon chlorination indicates a decrease in the total number of hydroxyl groups, while the disappearance of the signal at -0.4 ppm confirms that the terminal hydroxyls are effectively eliminated. We estimate that the total hydroxyl population is reduced by ca. 75 %. The remaining signals are very broad and shifted downfield, presumably due to residual bridging hydroxyls whose environment is perturbed by the presence of chlorine.

We have shown previously that combined homonuclear (^{1}H-^{1}H) and heteronuclear (^{1}H-^{27}Al) solid state NMR is a powerful technique that brings high degree of understanding of the partially dehydrated γ-Al_2O_3 surface hydroxyl network. Through correlations relying on dipolar interaction, we have demonstrated that is possible to use NMR as a surface selective technique, that filters out the ^{27}Al signal from the bulk thanks to surface protons as a source of magnetization transfer.

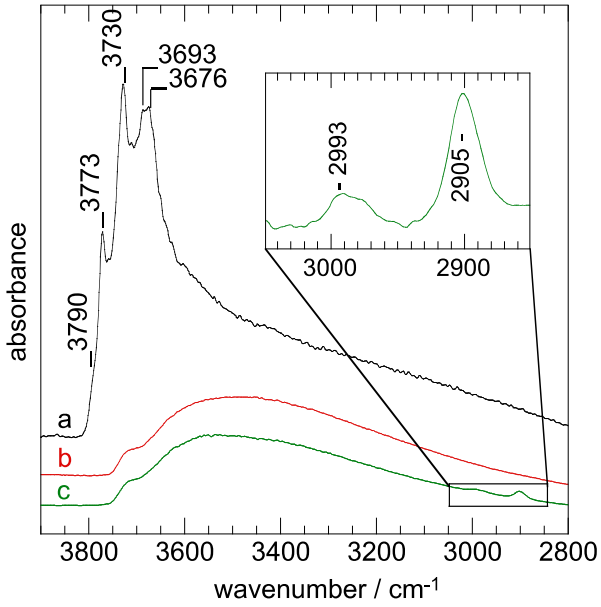

Figure 3.3: Transmission IR spectra of γ-Al_2O_3: (a) after pretreatment *in vacuo* at 450 °C (black); (b) after extensive chlorination (Cl-Al_2O_3, 4.0 wt % Cl, red); and (c) after grafting of MTO (2.5 wt% Re) onto Cl-Al_2O_3 (green). The inset shows the baseline-corrected CH_x stretching modes.

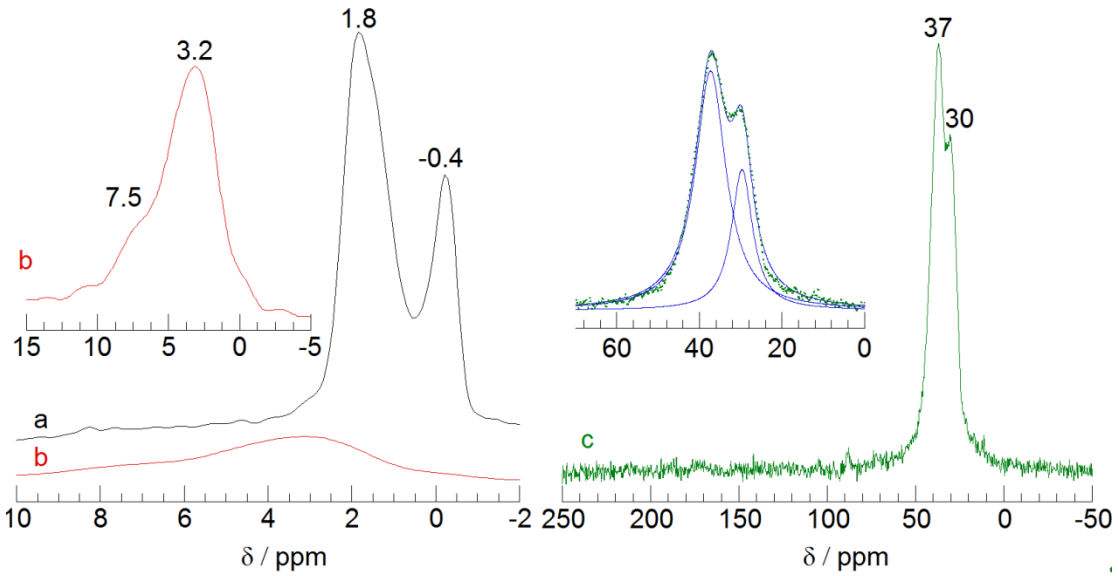

Figure 3.4: ^{1}H MAS NMR spectra for: (a) γ-Al_2O_3, pretreated at 450 °C; and (b) Cl-Al_2O_3 (4.0 wt % Cl). The inset shows the locations of the broad residual signals after chlorination. (c) ^{13}C CP-MAS NMR spectrum of MTO supported on Cl-Al_2O_3 (2.4 wt % Re). The inset shows the spectrum deconvoluted with two Lorentzian components (blue). Spinning rate 10 kHz.

Indeed, we have shown that main hydroxyl groups on γ-Al_2O_3 treated at 500°C comprises terminal hydroxyl groups on tetrahedral aluminum centers, along with doubly and triply bridging hydroxyls, that are connected to all types of aluminum coordination type, in the following order: Al_{VI}>Al_{IV}=Al_V (Figure 3.5). Furthermore, we have also seen that these AlOH are organized in non-random fashion, with specific arrangements. The validity of this approach was demonstrated in the case of the reaction of CO_2 with the basic, terminal Al_{IV}-OH.

Regarding Cl-Al_2O_3, ^{1}H NMR shows globally shifted signals from bridging hydroxyls from 1.7 (FWHM : 1.6 ppm) to 3.0 ppm (FWHM : 5 ppm) due to chloride effects, with a shoulder from 9 to 6 ppm. This modification of chemical shift range illustrates the electron deficiency caused by the chloride substituents on the surface in close proximity to the AlOH. Furthermore, the high field signal accounting for terminal hydroxyl species on

tetracoordinated aluminum centers is no longer observed. This is line with their higher basicity and thus higher reactivity toward chlorination.

In the ^{1}H-^{1}H double quantum correlation spectrum DQ MAS, three main regions can be distinguished. The first one corresponds to the chemical shift range of doubly and triply bridging hydroxyl groups, described as "native" Al_2O_3 on Figure 3.5. The second region overlaps the former and extends up to 7 ppm, associating protons in the [6 - 1.8] ppm range with those in the [4 – 1.6] ppm region.

As seen on slices (Figure 3.5), the shape of the cross peaks evolves from well defined (doublet-like) to unresolved interactions, which indicates a greater structural distribution when evolving toward higher chemical shifts. This may be related to stronger interactions with Al-Cl entities. It may be tempting, when considering the unresolved, broad AlOH elongation signal in the IR spectrum, to conclude that there is H-bonding of various strength between the Al-Cl and the hydroxyls. Observation of dipolar interaction between OH groups indicates that these exist as blocks on the surface, and that they are not (or not only) present as isolated entities.

The third pattern is an on-diagonal signal spreading from 8.5 to 5 ppm, the nature of which is still to be determined. The most unusual CS range and the analogy with alumina argues for triply bridging centers, which are the most acidic protons on the surface, and for which less reactivity toward chlorinating agents is expected. However, it is unlikely that such groups would give rise to self correlation, as this implies chemical shift equivalence, and thus, identical chemical environment. To find such precisely defined pairs of AlOH is not expected, which tends to rule out this hypothesis. A further assignment is the presence of water strongly adsorbed onto Al centers. These H_2O molecules are expected to form during

chlorination by CCl_4: reaction with AlOH gives $CCl_3(OH)$, then in a second stage $CCl_2(OH)_2$, which is dehydrated into phosgene + H_2O. The high CS would be due to coordination onto highly electrophilic centers, and as the two protons would be equivalent, they would give rise to self correlation observed in the spectrum.

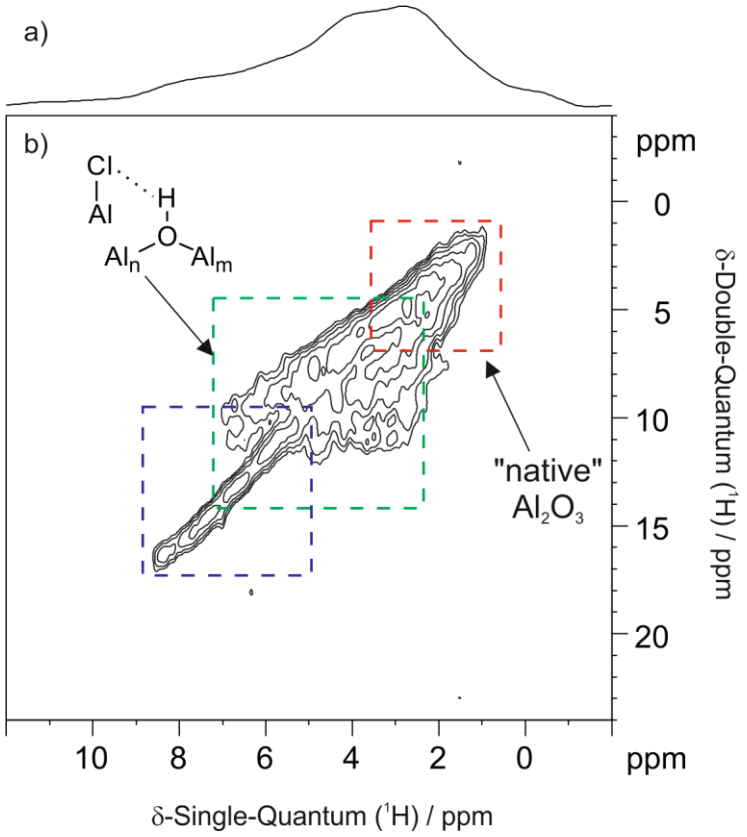

Figure 3.5: Cl-Al_2O_3: a) ^{1}H MAS NMR ; b) ^{1}H-^{1}H DQ-SQ MAS NMR (18.8 T, spinning speed 20 kHz, recycling delay 120s, recoupling time)

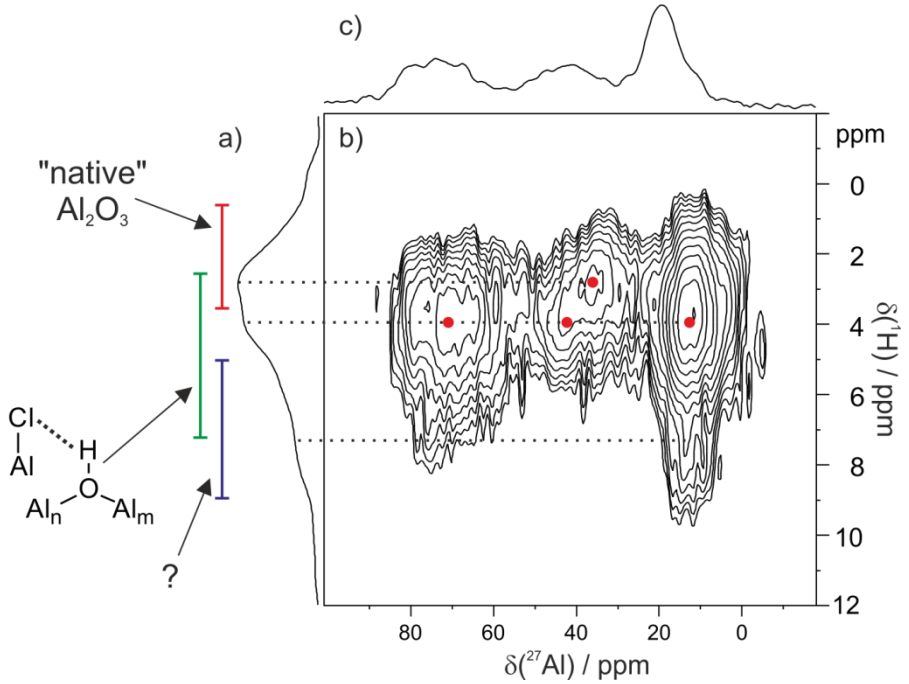

Figure 3.6: Cl-Al_2O_3: a) ^{1}H MAS NMR ; b) ^{1}H-^{27}Al D-HMQC MAS NMR (18.8 T, spinning speed 20 kHz, recycling delay 1s, recoupling time) and c) calculated ^{27}Al projection

The ^{1}H-^{27}Al D-HMQC correlation spectrum (Figure 3.6) reveals the presence of tetra-, penta- and hexa-coordinated aluminum centers, distinguished by their distinct chemical shift range. It confirms the consumption of terminal tetracoordinated aluminum hydroxide. The aluminum centers correlate with different types of protons (centered at 2.8, 3.9 and 7.5 ppm), as illustrated in figure 3.6. The correlation tendency is comparable to that of Al_2O_3-450, with an obvious broadening in the ^{1}H dimension towards high CS values. The major pattern that is observed in alumina for doubly bridging hydroxyls (correlating with the three types of Al, as Al_{VI}> Al_{IV}>Al_V) is also detected in this case, though spread over higher and wider chemical shift ranges, mostly as a signature of chloride proximity, as seen above. The higher range of Al_{IV} (doubly bridging hydroxyl groups) is shifted 6 ppm downfield compared to Al_2O_3-450 (up to 84 ppm), most probably as a consequence of electro-

withdrawing chloride centers in the vicinity. The same tendency is observed for Al_{VI}, though to a lesser extent (2 ppm difference).

The width of the Al signals for tetrahedral and pentahedral aluminum, which present some second-order quadrupolar broadenings, is indicative of large local constraints on the Al centers, as observed in pristine alumina. The main ^{27}Al NMR parameters (CS and CQ, that are connected to coordination number and local constraints, respectively) are overall retained, which is in line with minor modification of the surface Al-OH configuration in the bridging hydroxyl region. A slight shift toward higher chemical shift by about 5 ppm for tetra and penta coordinated sites is consistent with coordination of chloride on the aluminum sites bearing hydroxyl groups as reported in literature.[52]

Alumina reacts with CCl_4 by consumption of terminal hydroxyl groups and some of the bridging hydroxyls. The remaining hydroxyl network is close to that of $Al_2O_{3\text{-}450}$. The network of the latter is maintained regarding local arrangements of hydroxyl groups. The surface of this material may thus be seen as mostly being aluminum chloride, except for islands/clusters of hydroxyl groups.

Lewis acidity in γ-Al_2O_3 arises due to distorted tetra- and penta-coordinated Al ions present on the surface.[48] The number and/or strength of these Lewis acid sites increases when alumina is chlorinated.[53-55] Indeed, the high outgassing temperature that follows chlorination results in dehydration that converts some Brønsted acidic OH sites into Lewis acid sites.[56, 57] It is clear that severe chlorination causes a profound restructuring of the alumina surface, associated with the appearance of Al_xCl_y groups.[58] New, strong Lewis acid sites associated with these bridging Cl sites are also formed.[53] When pyridine was adsorbed onto our Cl-Al_2O_3, the IR spectrum showed only Lewis acid sites (Figure D.2), consistent

with previous reports.[53] This suggests that few Brønsted acid sites remain, and/or that they are incapable of forming pyridinium ions.[59, 60]

3.3.3: Fate of MTO grafted onto chlorinated alumina

Upon grafting MTO onto Cl-Al_2O_3, two new IR bands appear at 2993 and 2906 cm^{-1}, Figure 3.3c. They are assigned to the symmetric and asymmetric stretching of the methyl group of MTO, and are slightly shifted compared to those of crystalline MTO.[21] Similar observations were made when MTO was supported on SiO_2-Al_2O_3,[21] and on γ-Al_2O_3,[27] confirming that the methyl group is preserved upon grafting on all of these oxides. No perturbation of the O-H stretching modes is detected in Figure 3.3c, and no vibrations of terminal (Re=CH_2) or bridging (Re-CH_2-Al) are observed (nor have they been reported on γ-Al_2O_3). No methane evolution was revealed by either gas phase IR or GC during the grafting procedure.

The ^{13}C CP-MAS spectrum of ^{13}C-labeled MTO on Cl-Al_2O_3 consists of a broad signal between 50 and 25 ppm, with two resolved maxima at 30 and 37 ppm, Figure 3.4c. The minor signal at 30 ppm has been previously reported, and is assigned to MTO coordinated to Lewis acid sites on γ-Al_2O_3 (Figure 3.7A),[27] and on SiO_2-Al_2O_3 (Figure 3.7C).[21]

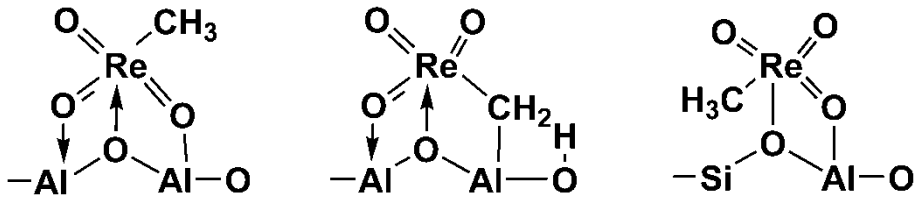

Figure 3.7: Proposed structures for MTO grafted on γ-Al_2O_3[27] (A and B) and SiO_2-Al_2O_3.[23]

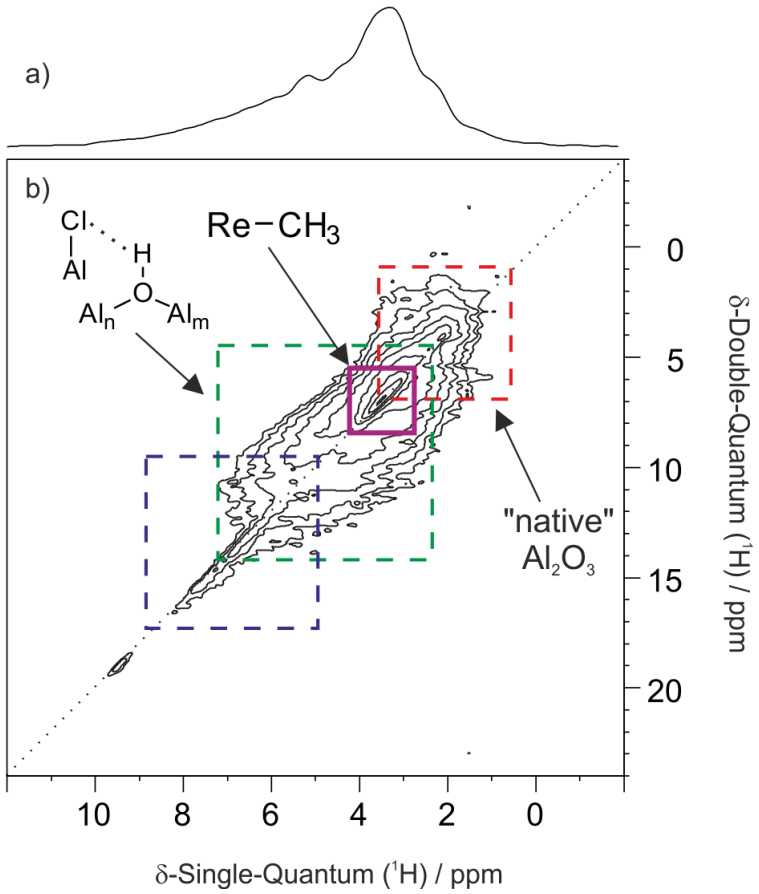

Figure 3.8: MTO-Cl-Al_2O_3: a) ^{1}H MAS NMR ; b) ^{1}H-^{1}H DQ-SQ MAS NMR (18.8 T, spinning speed 20 kHz, recycling delay 2s, recoupling time)

For comparison, the ^{13}C chemical shift spectrum of MTO dissolved in $CDCl_3$ is 19 ppm;[61] interaction with a Lewis acid results in a strong downfield shift. The major signal for MTO/Cl-Al_2O_3, at 37 ppm, has not previously been reported, and is presumably related to new Re sites interacting with Cl, and/or with even stronger Lewis acid sites on Cl-Al_2O_3. This evidence confirms that a new surface Re species is present on Cl-Al_2O_3, associated with its dramatic increase in metathesis activity. The absence of any signal at ca. 65 ppm (previously suggested to be due to bridging methylene sites O_3Re-CH_2-Al (Figure 3.7B)),[27] allows us to completely exclude the presence of such species on Cl-Al_2O_3. This signal is

also absent for MTO/SiO_2-Al_2O_3, although it is likewise much more active than MTO/γ-Al_2O_3.[21]

Upon reaction with MTO, the ^{1}H MAS NMR spectrum (Figure 3.8a) is slightly modified with respect to that of Al_2O_3-Cl, including a new contribution centered at 3.3 ppm, and a minor one at 5.2 ppm.

The DQ MAS NMR (Figure 3.8b) confirms our assignment of the signal at 3.3 ppm to the methyl group from MTO, as intense on diagonal signals are indeed observed at 3.9-3.1 ppm. For comparison, MTO on alumina is centered at 1.8 ppm. Other features emerge from the 2D ^{1}H-^{1}H correlation: overall, the pair-like distribution from the hydroxyl network remains mostly unchanged, but the main pair-wise interaction is now spread over an extended range, up to 14 ppm in the indirect dimension; the low field signal that spanned from 8.5 to 5 ppm is also observed. A further on diagonal, sharp signal is centered at 9.5 ppm and does not appear on the 1D NMR spectrum. These elements indicate that the main consequence of grafting MTO onto Cl-Al_2O_3 is increased distribution of ^{1}H NMR signals from the hydroxyl network. This suggests long range interactions with MTO groups (or grafted organometallic centers), and no direct bonding/strong interaction between rhenium centers and AlOH groups. In turn, this implies that MTO interacts mostly with chlorinated aluminum sites.

Regarding the ^{1}H-^{27}Al HMQC spectrum, similar patterns are observed, as expected from the DQ MAS that gave similar information about the AlOH network, even if minor differences can be observed (the presence of slightly stronger Al_V. component, Figure 3.9). No efficient dipolar transfer between the Re-Me protons and the surface aluminum can be detected, most probably due to longer distances (and weaker dipolar interactions) than Al-

OH, or to bonding on different sites that blurs the information. Thus, it further confirms that reaction of MTO with the surface of chlorinated alumina does not significantly affect the non-chlorinated area of the surface.

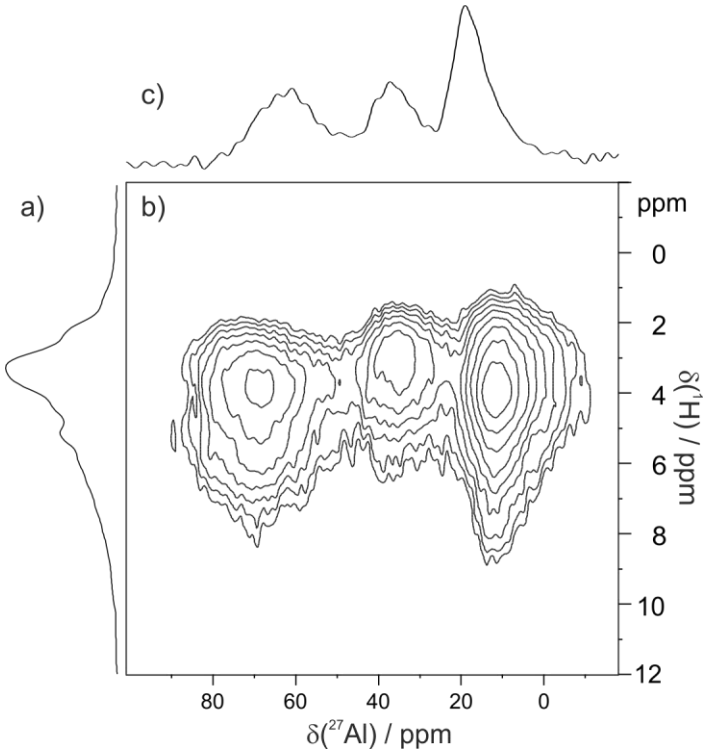

Figure 3.9: MTO-Cl-Al_2O_3: a) ^{1}H MAS NMR ; b) ^{1}H-^{27}Al D-HMQC MAS NMR (18.8 T, spinning speed 20 kHz, recycling delay 1s, recoupling time) and c) calculated ^{27}Al projection

The coordination environment of Re in MTO/Cl-Al_2O_3 was investigated by analysis of its Re *L*-edge X-ray absorption spectra. The Re L_{I}- and L_{III}-edge energies, 12,539 and 10,542 keV, respectively, are consistent with the presence of Re(VII) (Figures D.3 and D.4).[43] The Re L_{III}-edge EXAFS consists of a broad peak between 1.0 and 1.5 Å in *R*-space, Figure 3.10, very similar to that of crystalline MTO, MTO/γ-Al_2O_3 and MTO/SiO_2-Al_2O_3.[21, 27] It arises due to single-scattering by light atoms (C, O) located in the first coordination sphere of Re. However, for MTO/Cl-Al_2O_3, the peak intensity is significantly suppressed, suggesting

either a lower coordination number or, more likely, a lower symmetry that results in more destructive interference between similar paths.

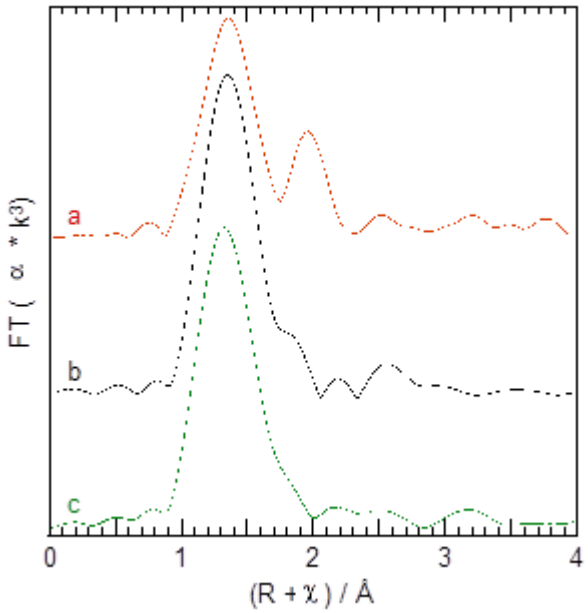

Figure 3.10: Comparison of EXAFS FT magnitudes in k^3-weighted non-phase-corrected *R*-space, for MTO grafted onto Cl-Al_2O_3 (2.4 wt % Re, red) or γ-Al_2O_3 (2.4 wt % Re, black), as well as crystalline MTO diluted in BN (3 wt % Re, green).

In addition, there is a prominent new feature at ca. 2 Å, whose location and intensity suggest a heavier scatterer, e.g., a Re-Cl path. There are several well-defined examples of facile Cl-O ligand exchange involving MTO, such as the reaction of perrhenate with $(CH_3)_3SiCl$ in THF, which yields $ReO_3Cl(THF)_2$.[62] Similarly, when Re_2O_7 was dissolved in thionyl chloride at room temperature, $ReO_3Cl(SO_2Cl_2)$ was isolated.[63] Furthermore, while MTO itself is not active for olefin metathesis in solution, it can be activated by $AlCl_3$,[15] for which Cl-O exchange was inferred.[64] Therefore it seems plausible that Cl-Al_2O_3 may act as a chlorinating agent for MTO, in addition to providing strong Lewis acidity.

The EXAFS curvefit for MTO/γ-Al_2O_3, shown in Figure D.5 and Table 3.2, is consistent with three short Re=O bonds, a Re-C bond, as well as a much longer Re-O path at 2.47 Å. The latter presumably involves a support oxygen. Thus the structure of MTO changes only slightly upon grafting. In order to construct a model for MTO/Cl-Al_2O_3, we took into account the presence of a heavier scattering atom at a higher distance to create the second well-resolved peak, via inclusion of a Re-Cl scattering path. The curvefit is also reported in Figure D.5 and Table 3.2. The Re=O distance is almost identical to that of molecular MTO, and comparable to those found for MTO grafted onto SiO_2-Al_2O_3 and /γ-Al_2O_3.[21, 27] Similarly, the Re-C distance is hardly affected by the surface interaction or O-Cl ligand exchange. MTO interacts with the alumina surface through an O atom at a distance of 2.3 Å, comparable to the Re-O distance for coordinated THF in $ReO_3Cl(THF)_2$, 2.26 Å,[62] and for the Re-O bonds in Re(VII) hydrogendiolato complexes (2.28 - 2.39 Å).[65] However, the mean-square displacement for this path, 0.019 $Å^2$, is very large. The intrinsic heterogeneity of the disordered chlorinated alumina surface, as well as the presence of an intense Re-Cl scattering path at the same distance make it more difficult to identify a much weaker long Re-O path. The Re-Cl distance, 2.31 Å, is in the range of a terminal Cl bonded to Re, and was also confirmed by DFT calculation (*vide infra*). For comparison, $ReO_3Cl(THF)_2$ has a terminal Re-Cl bond at 2.43 Å,[62] while the distance is 2.29 Å in $ReNCl_4$.[66]

Table 3.2: Comparison of curvefit parameters[a] for the Re L_{III}-edge EXAFS of MTO/γ-Al_2O_3 and MTO/Cl-Al_2O_3

Path	N[a]	R (Å)	σ^2 ($Å^2$)
Re=O	2 (s)	1.68 (0.01)	0.0027 (0.0003)
Re-C	1 (s)	2.08 (0.02)	0.0023 (0.0022)
Re-O	1 (s)	2.3 (0.1)	0.018 (0.017)
Re-Cl	1 (s)	2.31 (0.01)	0.005 (0.002)

[a] ΔE_0 was refined as a global fit parameter, (6.1 ± 3.2) eV, while S_0^2 was held fixed at 1. [b] Coordination numbers (N) were fixed at their integer values to give physical meaning to the σ^2 values.

3.3.4. Computational Assessment of MTO Chlorination

Possible structures for the grafted MTO sites were investigated computationally. In the absence of more detailed information about the surface structure of extensively chlorinated (and consequently highly dehydroxylated) alumina, we chose a simple cluster model, Al_2Cl_6, which contains both bridging and terminal chlorides. As noted above, "$AlCl_3$" is capable of activating MTO for olefin metathesis in solution,[15] although the structure of the active complex is not known.

Figure 3.11 shows the structures and relative free energies of several possible stable adducts. The free energy of the O-bound adduct of MTO with intact Al_2Cl_6, structure **I**, is only -0.7 kcal/mol relative to separate reactants. The Re-O1(Al) distance (1.73 Å) is elongated relative to the Re=O2 distance (1.69 Å) bond (Table 3.3), but is still much shorter than the 2.3 Å path observed by EXAFS. Another possible species involves an interaction with a terminal chloride (**II**), resulting in a slightly longer Re-O1 bond of 1.85 Å. However, this species is slightly uphill in free energy at +8.7 kcal/mol. Instead, it is more favorable for MTO to disrupt one of the chloride bridges between the Al atoms (**III**), yielding an MTO adduct coordinated via a bridging oxo ligand (-7.0 kcal/mol). Structure **IV**, in which a second oxo ligand of MTO interacts with the other Al site and Cl transfers to Re, is similarly downhill in free energy (-3.1 kcal/mol), although neither **III** nor **IV** possesses a long Re-O bond (~1.80 Å, Table 3.3). No stable Cl-bound adduct involving MTO and Al_2Cl_6 was found. However, ligand exchange involving a bridging chloride of Al_2Cl_6 was observed (**V**). For **V**, the elongated Re-O1 distance involving the bridging oxygen is 1.94 Å, which is closest to the EXAFS value of all the computed structures; the simplicity of the model cluster and the uncertainty in the EXAFS fit may account for some of the discrepancy. Since

all of the computed species have energies within a few kcal/mol of each other, several may co-exist in the catalyst.

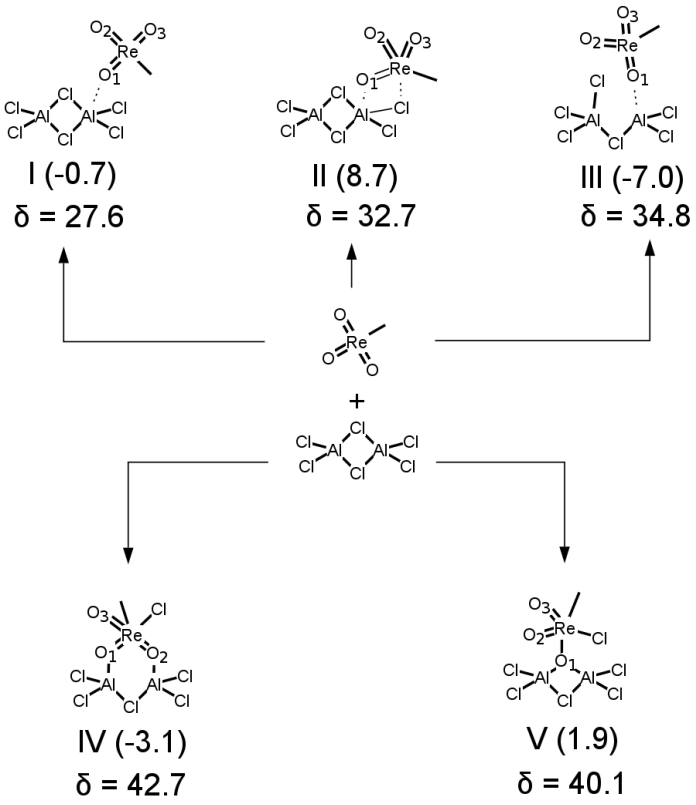

Figure 3.11: DFT-optimized species for MTO interacting with Al_2Cl_6 as a model for the surface of chlorinated alumina. Free energies (parentheses) in kcal/mol. Chemical shifts for ^{13}C NMR in ppm.

Table 3.3: DFT-optimized bond lengths (Å) for MTO interacting with Al_2Cl_6 as a model for the surface of chlorinated alumina

	MTO	**I**	**II**	**III**	**IV**	**V**
*r*Re-O1	1.69	1.73	1.85	1.76	1.78	1.94
*r*Re-O2	1.69	1.68	1.67	1.67	1.78	1.67
*r*Re-O3	1.69	1.68	1.67	1.67	1.66	1.66
*r*Re-Cl	--	2.02	2.49	3.06	2.31	2.41
*r*Re-C	--	2.07	2.14	2.09	2.14	2.13

The calculated ^{13}C chemical shifts for species **I - V** range from 26 to 50 ppm, within the 30-60 ppm range seen experimentally in Figure 3.4c. Interestingly, the chemical shifts of the most energetically favorable structures **III** and **IV** are 34.8 and 42.7 ppm, respectively, which compare well to the experimentally observed maxima at 30 and 37 ppm. Even the 40.1 chemical shift for structure **V** is within range.

The EXAFS finding that a major Re site contains a terminal chloride ligand, and the calculations above showing that chloride exchange between Al and Re is possible, raises the question of how chloride promotes the formation of the initiating carbene. The tautomerization reaction was modeled by transferring a proton from the methyl group of the grafted MTO to one of the cluster oxygens. Without the chloride ligand on Re, tautomerization is very significantly uphill, especially when the proton acceptor site is Re=O (Figure 3.12). For example, such proton transfers in **I** and **IV** are unfavorable in free energy by 16 and 20 kcal/mol (**Ia** and **IVa**), respectively. In contrast, proton transfer to the bridging oxygen (AlORe) in **IV** is nearly isoenergetic (**IVb**) . The interaction with Al, following the exchange of chloride with Re, weakens the Re-O bond making the oxygen more basic. Similarly, species **V** prefers to transfer the proton to an oxygen near Al. Forming from transfer of a proton to Re=O, species **Va**, with an additional interaction between the Cl on Re and Al at 2.56 Å, is 12.4 kcal/mol uphill in energy. On the other hand, **Vb**, with an interaction between the bridging O and Al at 1.92 Å, is 1 kcal/mol downhill. No such reaction was found for **III**, suggesting that the chloride ligand is an important component of the active site.

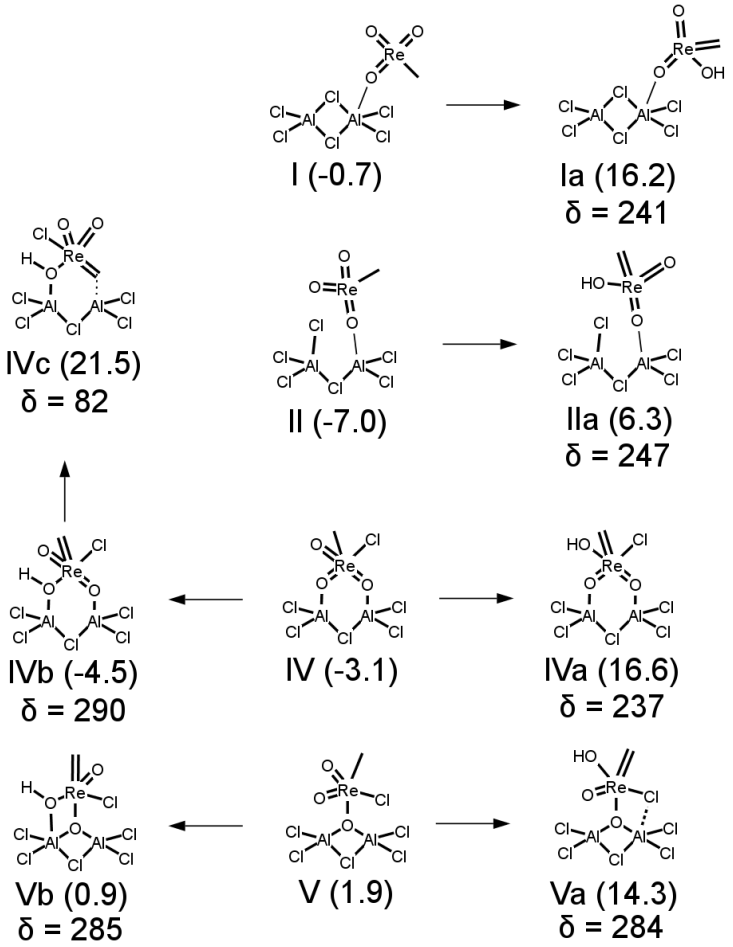

Figure 3.12: DFT-optimized species for various carbenes MTO interacting with Al_2Cl_6 as a model for the surface of chlorinated alumina. Free energies (parentheses) in kcal/mol. Chemical shifts for ^{13}C NMR in ppm.

Experimental ^{13}C NMR chemical shifts[67] for such terminal carbenes are in the range 240-310 ppm. Since none were observed, we conclude that such intermediates are not abundant enough to be spectroscopically observable, consistent with the calculations that show their formation to be uphill. A bridging methylidene ($ReCH_2Al$), derived from **IV**, was also investigated (**IVc**). Its ^{13}C NMR chemical shift is near 80 ppm, although no signal was detected at this location in the experimental spectrum. However, its formation is highly

unfavorable at 26.0 kcal/mol relative to **IVb**. No analogous species was found to form with either species **Va** or **Vb**.

Transition states involved in forming the most stable carbene, **IVb**, were also located (Figure 3.13). Direct transfer of H from the methyl to an oxygen near Al, **TS[IV-IVb]**, involves a high barrier of 50.6 kcal/mol for this four-membered transition state. However, chlorination of the alumina may leave traces of HCl on the surface, which can facilitate the proton transfer. Inclusion of HCl at the **TS[IV+HCl-IVb]**, involving a less strained six-membered transition state, lowers this barrier by 7.5 kcal/mol to 43.0 kcal/mol.

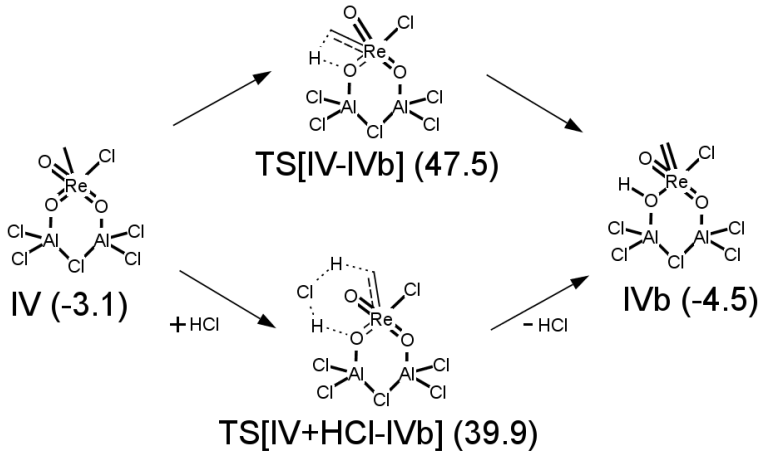

Figure 3.13: Direct H-transfer from methyl to surface oxygen with and without the presence of HCl. Free energies (parantheses) in kcal/mol.

3.4 Conclusions

Extensive chlorination of alumina results in much more efficient activation of MTO for olefin metathesis. The dramatic increase in catalytic activity is associated with both an overall increase in the Lewis acidity of the support as well as direct chlorination of MTO. EXAFS and solid state NMR, as well as DFT calculations, support such a ligand exchange between Al and Re, similar to the presumed role of $AlCl_3$ in solution as a co-catalyst for

MTO in olefin metathesis. Chlorination lowers the energies of carbene tautomers, leading to a much higher fraction of active sites. HCl, which could exist in trace amounts from chlorination of the support, was shown to lead to a lower energy pathway for tautomerization.

3.5 Acknowledgements.

J.R. is grateful for a Fulbright scholarship. Financial support of the U.S. Department of Energy, Office of Science, Office of Basic Energy Sciences, under the Catalysis Science Initiative (DE-FG-02-03ER15467) is gratefully acknowledged. Portions of this work made use of facilities of UCSB's Materials Research Laboratory (MRL), supported by the NSF MRSEC Program under award DMR1121053. Use of the Stanford Synchrotron Radiation Lightsource, SLAC National Accelerator Laboratory, is supported by the U.S. Department of Energy, Office of Science, Office of Basic Energy Sciences, under Contract DE-AC02-76SF00515. Ask alessandro what "J.R." means

3.6 References

1. Mol, J. C., *Journal of Molecular Catalysis A: Chemical* **2004,** *213* (1), 39-45.
2. Keim, W., *Angewandte Chemie, International Edition* **2013,** *52* (48), 12492-12496.
3. Lwin, S.; Wachs, I. E., *ACS Catalysis* **2014,** *4* (8), 2505-2520.
4. Bakala, P. C.; Briot, E.; Millot, Y.; Piquemal, J.-Y.; Bregeault, J.-M., *Journal of Catalysis* **2008,** *258* (1), 61-70.
5. Xu, X.; Boelhouwer, C.; Vonk, D.; Benecke, J. I.; Mol, J. C., *Journal of Molecular Catalysis* **1986,** *36* (1-2), 47-66.
6. Boelhouwer, C., *Journal of Molecular Catalysis* **1988,** *46* (1-3), 297-303.
7. Schekler-Nahama, F.; Clause, O.; Commereuc, D.; Saussey, J., *Applied Catalysis, A: General* **1998,** *167* (2), 237-245.
8. Rhers, B.; Salameh, A.; Baudouin, A.; Quadrelli, E. A.; Taoufik, M.; Coperet, C.; Lefebvre, F.; Basset, J.-M.; Solans-Monfort, X.; Eisenstein, O.; Lukens, W. W.; Lopez, L. P. H.; Sinha, A.; Schrock, R. R., *Organometallics* **2006,** *25* (15), 3554-3557.

9. Blanc, F.; Berthoud, R.; Salameh, A.; Basset, J.-M.; Coperet, C.; Singh, R.; Schrock, R. R., *Journal of the American Chemical Society* **2007,** *129* (27), 8434-8435.
10. Chabanas, M.; Coperet, C.; Basset, J.-M., *Chemistry - A European Journal* **2003,** *9* (4), 971-975.
11. Herrmann, W. A.; Rost, A. M. J.; Mitterpleininger, J. K. M.; Szesni, N.; Sturm, S.; Fischer, R. W.; Kuehn, F. E., *Angewandte Chemie, International Edition* **2007,** *46* (38), 7301-7303.
12. Tosh, E.; Mitterpleininger, J. K. M.; Rost, A. M. J.; Veljanovski, D.; Herrmann, W. A.; Kuehn, F. E., *Green Chemistry* **2007,** *9* (12), 1296-1298.
13. Szesni, N.; Sturm, S.; Fischer, R. Improved procedure for preparation of methyl trioxorhenium (MTO) as catalyst for oxidation and metathesis reactions. 2009-EP90332010075972, 20091216., 2010.
14. Szesni, N.; Sturm, S.; Fischer, R.; Hermann, W.-A. Improved process for preparing methyltrioxorhenium and organorhenium(vii) oxides. 2007-EP79902009036775, 20070913., 2009.
15. Herrmann, W. A.; Kuchler, J.; Felixberger, J. K.; Herdtweck, E.; Wagner, W., *Angewandte Chemie* **1988,** *100* (3), 420-2.
16. Lai, Y.-Y.; Bornand, M.; Chen, P., *Organometallics* **2012,** *31* (21), 7558-7565.
17. Herrmann, W. A.; Wagner, W.; Flessner, U. N.; Vokhardt, U.; Komber, H., *Angewandte Chemie* **1991,** *103* (12), 1704-6 (See also Angew Chem , Int Ed Engl , 1991, 30(12) 1636-8).
18. Rost, A. M. J.; Schneider, H.; Zoller, J. P.; Herrmann, W. A.; Kuehn, F. E., *Journal of Organometallic Chemistry* **2005,** *690* (21-22), 4712-4718.
19. Burron, R.; Auroux, A.; Lefebvre, F.; Leconte, M.; Choplin, A.; Basset, J. M.; Herrmann, W. A., *Journal of Molecular Catalysis* **1992,** *76* (1-3), 287-95.
20. Salameh, A.; Baudouin, A.; Soulivong, D.; Boehm, V.; Roeper, M.; Basset, J.-M.; Coperet, C., *Journal of Catalysis* **2008,** *253* (1), 180-190.
21. Moses, A. W.; Ramsahye, N. A.; Raab, C.; Leifeste, H. D.; Chattopadhyay, S.; Chmelka, B. F.; Eckert, J.; Scott, S. L., *Organometallics* **2006,** *25* (9), 2157-2165.
22. Stekrova, M.; Zdenkova, R.; Vesley, M.; Vykocilova, E.; Cerveny, L., *Materials* **2014,** *7*, 2650-2668.
23. Moses, A. W.; Raab, C.; Nelson, R. C.; Leifeste, H. D.; Ramsahye, N. A.; Chattopadhyay, S.; Eckert, J.; Chmelka, B. F.; Scott, S. L., *Journal of the American Chemical Society* **2007,** *129* (28), 8912-8920.
24. Popoff, N.; Mazoyer, E.; Pelletier, J.; Gauvin, R. M.; Taoufik, M., *Chemical Society Reviews* **2013,** *42* (23), 9035-9054.
25. Gajan, D.; Coperet, C., *New Journal of Chemistry* **2011,** *35* (11), 2403-2408.
26. Joubert, J.; Delbecq, F.; Sautet, P.; Le Roux, E.; Taoufik, M.; Thieuleux, C.; Blanc, F.; Coperet, C.; Thivolle-Cazat, J.; Basset, J.-M., *Journal of the American Chemical Society* **2006,** *128* (28), 9157-9169.
27. Salameh, A.; Joubert, J.; Baudouin, A.; Lukens, W.; Delbecq, F.; Sautet, P.; Basset, J. M.; Coperet, C., *Angewandte Chemie, International Edition* **2007,** *46* (21), 3870-3873.
28. Wischert, R.; Coperet, C.; Delbecq, F.; Sautet, P., *ChemCatChem* **2010,** *2* (7), 812-815.

29. Oikawa, T.; Masui, Y.; Tanaka, T.; Chujo, Y.; Onaka, M., *Journal of Organometallic Chemistry* **2007,** *692* (1-3), 554-561.
30. Tovar, T. M.; Stewart, S. M.; Scott, S. L., *Topics in Catalysis* **2012,** *55* (7-10), 530-537.
31. Pillai, S. K.; Hamoudi, S.; Belkacemi, K., *Applied Catalysis, A: General* **2013,** *455*, 155-163.
32. Pillai, S. K.; Hamoudi, S.; Belkacemi, K., *Fuel* **2013,** *110*, 32-39.
33. Cornet, D.; Goupil, J.-M.; Szabo, G.; Poirier, J.-L.; Clet, G., *Applied Catalysis, A: General* **1996,** *141* (1-2), 193-205.
34. Feller, D., *Journal of Computational Chemistry* **1996,** *17* (13), 1571-1586.
35. Schuchardt, K. L.; Didier, B. T.; Elsethagen, T.; Sun, L. S.; Gurumoorthi, V.; Chase, J.; Li, J.; Windus, T. L., *Journal of Chemical Information and Modeling* **2007,** *47* (3), 1045-1052.
36. Godbout, N.; Salahub, D. R.; Andzelm, J.; Wimmer, E., *Canadian Journal of Chemistry-Revue Canadienne De Chimie* **1992,** *70* (2), 560-571.
37. Forsyth, D. A.; Sebag, A. B., *Journal of the American Chemical Society* **1997,** *119* (40), 9483-9494.
38. White, R. E.; Hanusa, T. P., *Organometallics* **2006,** *25* (23), 5621-5630.
39. Cai, S.; Hoffman, D. M.; Wierda, D. A., *Organometallics* **1996,** *15* (3), 1023-1032.
40. Morris, L. J.; Downs, A. J.; Greene, T. M.; McGrady, S. G.; Herrmann, W. A.; Sirsch, P.; Scherer, W.; Gropen, O., *Organometallics* **2001,** *20* (11), 2344-2352.
41. Ravel, B., *Journal of Synchrotron Radiation* **2001,** *8*, 314-316.
42. Chauvin, Y.; Commereuc, D., *Journal of the Chemical Society, Chemical Communications* **1992,** (6), 462-4.
43. Kytokivi, A.; Lindblad, M.; Root, A., *Journal of the Chemical Society, Faraday Transactions* **1995,** *91* (5), 941-8.
44. Thomson, J.; Webb, G.; Winfield, J. M., *Journal of Molecular Catalysis* **1991,** *67* (1), 117-26.
45. Rohner, M. C.; Sharma, V. K.; Richarz, W., *Chemical Engineering & Technology* **1989,** *12* (1), 27-32.
46. Knoezinger, H.; Ratnasamy, P., *Catalysis Reviews - Science and Engineering* **1978,** *17* (1), 31-69.
47. Peri, J. B., *Journal of Physical Chemistry* **1965,** *69* (1), 211-19.
48. Digne, M.; Sautet, P.; Raybaud, P.; Euzen, P.; Toulhoat, H., *Journal of Catalysis* **2002,** *211* (1), 1-5.
49. Digne, M.; Raybaud, P.; Sautet, P.; Guillaume, D.; Toulhoat, H., *Journal of the American Chemical Society* **2008,** *130* (33), 11030-11039.
50. Van Den Brink, R. W.; Mulder, P.; Louw, R.; Sinquin, G.; Petit, C.; Hindermann, J.-P., *Journal of Catalysis* **1998,** *180* (2), 153-160.
51. DeCanio, E. C.; Edwards, J. C.; Bruno, J. W., *Journal of Catalysis* **1994,** *148* (1), 76-83.
52. Benn, R.; Janssen, E.; Lehmkuhl, H.; Rufinska, A., *Journal of Organometallic Chemistry* **1987,** *333* (2), 155-168.
53. Ayame, A.; Sawada, G.; Sato, H.; Zhang, G.; Ota, T.; Izumizawa, T., *Applied Catalysis* **1989,** *48* (1), 25-35.
54. Frederick, B. G.; Apai, G.; Rhodin, T. N., *Surface Science* **1992,** *277* (3), 337-50.

55. Samoila, P.; Epron, F.; Marecot, P.; Especel, C., *Applied Catalysis, A: General* **2013,** *462-463*, 207-219.
56. Sang, H.; Chu, H. Y.; Lunsford, J. H., *Catalysis Letters* **1994,** *26* (3-4), 235-46.
57. Hughes, T. R.; White, H. M.; White, R. J., *Journal of Catalysis* **1969,** *13* (1), 58-64.
58. Zhang, W.; Sun, M.; Prins, R., *Journal of Physical Chemistry B* **2002,** *106* (45), 11805-11809.
59. Shen, Y.-F.; Suib, S. L.; Deeba, M.; Koermer, G. S., *Journal of Catalysis* **1994,** *146* (2), 483-90.
60. Berteau, P.; Kellens, M. A.; Delmon, B., *Journal of the Chemical Society, Faraday Transactions* **1991,** *87* (9), 1425-31.
61. Herrmann, W. A.; Kiprof, P.; Rypdal, K.; Tremmel, J.; Blom, R.; Alberto, R.; Behm, J.; Albach, R. W.; Bock, H.; et al., *Journal of the American Chemical Society* **1991,** *113* (17), 6527-37.
62. Noh, W.; Girolami, G. S., *Dalton Transactions* **2007,** (6), 674-679.
63. Bagnall, K. W.; Brown, D.; Colton, R., *Journal of the Chemical Society* **1964,** (Sept.), 3017-20.
64. Herrmann, W. A., *Angewandte Chemie* **1988,** *100* (10), 1269-86.
65. Edwards, P. G.; Jokela, J.; Lehtonen, A.; Sillanpaa, R., *Journal of the Chemical Society, Dalton Transactions: Inorganic Chemistry* **1998,** (19), 3287-3294.
66. Binder, A.; Maichle-Moessmer, C.; Niquet, E.; Staehle, J., *Zeitschrift fuer Anorganische und Allgemeine Chemie* **2008,** *634* (8), 1326-1328.
67. Lotz, S.; Landman, M.; Olivier, A. J.; Bezuidenhout, D. I.; Liles, D. C.; Palmer, E. R., *Dalton Transactions* **2011,** *40* (37), 9394-9403.

Chapter 4

Conclusions

Reaction mechanisms for two metal oxide catalysts have been modeled here. Through density functional theory, reaction energies and barrier have been calculated. From there, elementary rate coefficients and equilibrium constants have also been estimated for the Phillips catalyst. Where applicable, microkinetic models were constructed to compare theoretical results with those from experiment.

In Chapter 2, the Phillips supported chromium polymerization catalyst was investigated. The metallacycle and alternating metallacycle/carbene were eliminated because of the high propagation barriers. The high barriers match experimental results: homogeneous metallacycles oligomerize ethylene only, and the expected kinetic isotope effect for the carbene mechanism is also not observed experimentally. Two other mechanisms were investigated: oxachromacycle ring growth and Cossee-Arlman chain growth at a Cr(II) site initiated by proton transfer. Both mechanisms were found to have high initiation barriers. The Cossee-Arlman chain-growth at Cr(II) also could not produce long polymers. In analogy with Cr(II), a Cr(III) site that has been recently proposed to be a viable mechanism was also eliminated by similar calculations. The concluding results of Chapter 2 suggests a $(\equiv SiO)_2Cr(III)R$ site is the most likely site for polymerization. Future work concerns how such a Cr(III) site arises from an inorganic precursor.

Chapter 3 concerns activation of a rhenium oxide (MTO) supported on chlorinated alumina. Ligand exchange between chlorine and oxygen on MTO was shown to be possible, leading to multiple species that could lead to the active carbene. MTO was then found to favorably transfer a proton to a support oxygen near Lewis-acid aluminum, and after the chlorination of rhenium. The barrier for direct proton transfer from MTO to an oxygen was found to be high. However, a more favorable pathway was found with HCl, which could exist in trace amounts from chlorination of the support.

Appendix A

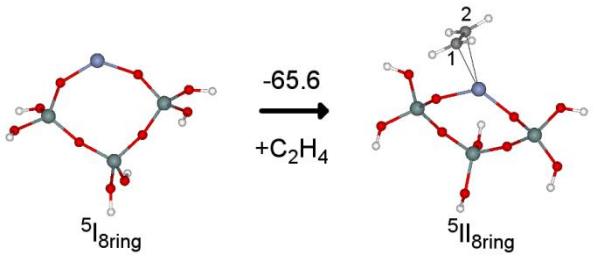

Figure A.1: Binding of Ethylene to Cluster with a Wider O-Cr-O angle. The cluster involves a larger eight member ring involving chromium. The binding energy (not free energy) of -65.6 kJ/mol is reduced relative to the -83.8 kJ/mol for the six member ring (see Figure 2.7)

Appendix B

Table B.1: Computed Gibbs Free Energy of Reaction and Activation (kJ/mol) at 298 K for Cr(III) (Section 2.3.6). Refer to figures 2.15 (initiation), 2.16 (propagation), 2.17 (termination by proton transfer), 2.18 (termination by β-H elimination). Values are listed from ωB97X-D, B3LYP-D3 (this work), and B3LYP-D3 (Delley et al.[1] where available).

	ΔG	$\Delta G^{\ddagger}$
^{4}D.I → ^{4}D.I	-25.1	-
	-36.3	-
	-37.7	-
^{4}D.II → ^{4}D.III	0.4	-
	-11.3	-
	-13.0	-
^{4}D.III → ^{4}D.V	98.9	150.3
	94.9	151.4
	100.0	153.1
^{4}D.V → ^{4}D.VI	-59.0	36.2
	-37.6	45.4
	-41.8	39.3
^{4}D.VI → ^{4}D.VIII	-62.1	69.4
	-52.5	64.3
	-46.0	54.0
^{4}D.VI → ^{4}D.VII	3.1	-
	-6.4	-
	-7.5	-
^{4}D.VII → ^{4}D.VIII	-65.3	66.3
	-46.1	70.7
	-	-
^{4}D.VII → ^{4}D.IX	-85.6	68.2
	-80.1	67.6
	-	-
^{4}D.VI → ^{4}D.X	-74.1	96.8
	-67.7	97.6
	-66.9	99.2

Table B.1 (cont): Computed Gibbs Free Energy of Reaction and Activation (kJ/mol) at 298 K for Cr(III). (Section 2.3.6).

	ΔG	ΔG‡
^{4}D.VI → ^{4}D.VIb	-25.4	-
	-28.9	-
	-	-
^{4}D.VIb → ^{4}D.Xb	-98.3	78.9
	-89.8	80.9
	-	-
^{4}D.VI → ^{4}D.XI	69.0	69.0
	56.6	56.6
	54.8	64.4
^{4}D.XI → ^{4}D.XII	32.2	-
	48.5	-
	51.8	-
^{4}D.XI → ^{4}D.XIII	21.8	-
	10.7	-
	-	-
^{4}D.XII → ^{4}D.XIV	-30.9	-
	-45.0	-
	-	-
^{4}D.XIV → ^{4}D.XV	-85.8	4.7
	-74.5	7.8
	-	-

Table B.2: Key inter-atomic distances (Å) and bond angles for ethylene complexes of Cr(II): II, mono(ethylene) complex; III, *bis*(ethylene) complex (Section 2.3.1 and Figure 2.7). Values in parentheses computed by Espelid and Børve.[2]

	^{5}II	^{5}III	^{3}II	^{3}III
*r*Cr-C1	2.40 (2.36)	2.48	2.04 (2.02)	2.10
*r*Cr-C2	2.40 (2.38)	2.48	2.03 (2.03)	2.25
*r*Cr-C3	-	2.48	-	2.35
*r*Cr-C4	-	2.48	-	2.16
*r*C1-C2	1.35 (1.36)	1.34	1.42 (1.45)	1.38
*r*C3-C4	-	1.34	-	1.37
*r*Cr-O	1.84-1.86 (1.83-1.86)	1.88	1.79 (1.78)	1.82
∠O1-Cr-O2	104 (107)	98	110 (113)	101

Table B.3: Key inter-atomic distances (Å) and bond angles for ethylene complexes of in a eight-member ring of Cr(II): $^5I_{8ring}$, bare site; $^5II_{8ring}$, mono(ethylene) complex. (Appendix A and Figure A.1)

	$^5I_{8ring}$	$^5II_{8ring}$
*r*Cr-C1	--	2.43
*r*Cr-C2	--	2.40
*r*C1-C2	--	1.34
*r*Cr-O1	1.82	1.86
*r*Cr-O2	1.81	1.85
∠O1-Cr-O2	132	124

Table B.4: Key inter-atomic distances (Å) for propagation by the chromacycle mechanism (Section 2.3.2 and Figure 2.8). The imaginary frequency for the transition state has units of *i* cm^{-1}. Values in parentheses are from Espelid and Børve.[2]

	^{3}M.IV	^{3}TS[M.IV-M.V]	^{3}M.V
*r*Cr-C4	1.99 (2.02)	2.99 (2.21)	3.05
*r*Cr-C5	-	2.75 (2.36)	2.92 (2.89)
*r*Cr-C6	-	2.23 (2.19)	1.97 (2.00)
*r*C4-C5	-	2.55 (1.99)	1.54 (1.55)
*r*C5-C6	-	1.36 (1.43)	1.53 (1.53)
ω	-	241	-

Table B.5: Key inter-atomic distances (Å) for termination and second insertion in the chromacycle mechanism (Section 2.3.2 and Figure 2.9). The imaginary frequency for the transition state has units of i cm^{-1}.

	^{3}M.V	^{3}TS[M.V-M.VI]	^{3}M.VI	^{3}TS[M.V-M.VII]	^{3}M.VII
*r*Cr-C1	1.99	2.02	2.03	-	-
*r*Cr-C2	2.91	2.18	2.06	-	-
*r*Cr-C6	1.97	2.18	-	3.11	3.54
*r*Cr-H_{C2}	3.00	1.64	-	-	-
*r*C1-C2	1.53	1.44	-	-	-
*r*C5-C6	1.53	1.54	1.52	-	-
*r*C2-H_{C2}	1.09	1.38	-	-	-
*r*C6-H_{C2}	2.81	1.46	1.09	-	-
*r*Cr-C7	-	-	-	2.83	3.04
*r*Cr-C8	-	-	-	2.22	1.98
*r*C6-C7	-	-	-	2.43	1.53
*r*C7-C8	-	-	-	1.37	1.52
ω	-	911	-	331	-

Table B.6: Key interatomic distances (Å) for initiation in the oxachromacycle mechanism (Section 2.3.3 and Figure 2.10). The imaginary frequency for the transition state has units of i cm^{-1}.

	^{5}III	^{5}TS[III-O.IV]	^{5}O.IV
*r*Cr-C1	-	-	-
*r*Cr-C2	2.48	2.22	2.13
*r*C1-C2	1.34	1.41	1.51
*r*C1-O1	2.95	1.83	1.50
*r*Cr-O1	1.88	1.96	2.03
*r*Cr-O2	1.88	1.92	1.95
ω	-	344	-

Table B.7: Key interatomic distances (Å) for ethylene insertion into the Cr-C bond of the oxachromacycle (Section 2.3.3 and Figure 2.10). The imaginary frequency for the transition state has units of i cm^{-1}.

	^{5}O.IV	^{5}TS[O.IV- O.V]	^{5}O.V
*r*Cr-C2	2.13	2.22	3.31
*r*Cr-C3	2.38	2.34	3.09
*r*Cr-C4	2.38	2.09	2.10
*r*C2-C3	3.58	2.07	1.53
*r*C3-C4	1.34	1.42	1.53
*r*Cr-O1	2.03	2.12	2.07
*r*Cr-O2	1.95	1.92	1.93
ω	-	334	-

Table B.8: Key inter-atomic distances (Å) for the conversion of a mono(ethylene) complex to a carbene (Section 2.3.4 and Figure 2.11). The imaginary frequency for the transition state has units of *i* cm^{-1}.

	^{3}C.III	^{3}TS[C.III-C.IV	^{3}C.IV
*r*Cr-C1	2.03	3.07	3.00
*r*Cr-C2	2.04	1.93	1.86
*r*Cr-H_{C2}	-	2.64	3.06
*r*C1-H_{C2}	-	1.38	1.09
*r*C2-H_{C2}	1.09	1.24	2.16
ω	-	1648	-

Table B.9: Key inter-atomic distances (Å) for the conversion of a chromacyclobutane to a carbene complex via H transfer from C4 to C2, in the Green-Rooney mechanism (Section 2.3.4 and Figure 2.11). The imaginary frequency for the transition state has units of *i* cm^{-1}. Values in parentheses are from Espelid and Børve.[2]

	^{3}C.IV	^{3}C.V	^{3}TS[C.V-C.VI]	^{3}C.VI
*r*Cr-C2	1.86 (1.82)	1.94 (1.98)	2.24 (2.23)	3.30 (4.26)
*r*Cr-C3	-	2.27 (2.34)	2.56 (2.54)	3.04 (3.01)
*r*Cr-C4	-	1.94 (1.99)	1.89 (2.23)	1.87 (1.82)
*r*Cr-H_{C4}	-	2.60 (2.61)	1.72 (1.70)	3.16
*r*C2-H_{C4}	-	3.05 (2.93)	1.49 (1.44)	1.09 (1.10)
*r*C4-H_{C4}	-	1.09 (1.10)	1.37 (1.63)	2.82
ω	-	-	1632	-

Table B.10: Key inter-atomic distances (Å) for conversion of a chromacyclobutane to a carbene complex via H transfer from C2 to C4, in the Green-Rooney mechanism (Section 2.3.4 and Figure 2.11). The imaginary frequency for the transition state has units of *i* cm^{-1}. Values in parentheses are from Espelid and Børve.[2]

	^{3}C.V	^{3}TS[C.V-C.VII]	^{3}C.VII
*r*Cr-C2	1.94 (1.98)	1.88	1.86
*r*Cr-C3	2.27 (2.34)	2.50	3.06
*r*Cr-C4	1.94 (1.99)	2.19	3.39
*r*Cr-H_{C2}	2.59	1.71	3.27
*r*C2-H_{C2}	1.09	1.55	2.87
*r*C4-H_{C2}	3.41	1.45	1.09
ω	-	1542	-

Table B.11: Key inter-atomic distances (Å) for Cossee-Arlman initiation at a Cr(II) site (Section 2.3.5 and Figure 2.13). The imaginary frequency of the transition state has units of *i* cm^{-1}.

	^{5}III	^{5}TS[III-H.V]	^{5}H.V
*r*Cr-C1	2.48	3.14	3.07
*r*Cr-C2	2.48	2.22	2.09
*r*Cr-H_{C2}	2.74	1.96	2.53
*r*C2-H_{C2}	1.08	1.50	2.53
*r*O2-H_{C2}	2.62	1.15	0.97
*r*Cr-O2	1.88	1.98	2.09
*r*Cr-O1	1.88	1.91	1.95
ω	-	1202	-

Table B.12: Key inter-atomic distances (Å) for Cossee-Arlman propagation at a Cr(II) site (Section 2.3.5 and Figure 2.13). The imaginary frequency of the transition state has units of *i* cm^{-1}.

	^{5}H.V	^{5}TS[H.V-H.VI]	^{5}H.VI
*r*Cr-C2	2.09	2.13	4.49
*r*Cr-C3	2.41	2.36	3.11
*r*Cr-C4	2.41	2.12	2.11
*r*C2-C3	3.30	2.02	1.50
*r*C3-C4	1.34	1.41	1.54
*r*Cr-O2	2.09	2.18	2.07
*r*Cr-O1	1.95	1.92	1.93
ω	-	402	-

Table B.13: Key inter-atomic distances (Å) for chain termination at a monoalkylchromium(II) site (Section 2.3.5 and Figure 2.13). The imaginary frequency of the transition state has units of i cm^{-1}.

	^{5}H.VII	^{5}TS[H.VII-H.VIII]	^{5}H.VIII	^{5}TS[H.VI-H.VIII]
*r*Cr-C1	2.44	2.44	2.38	--
*r*Cr-C2	2.44	2.37	2.44	--
*r*Cr-C4	2.13	2.25	3.42	2.21
*r*C1-C2	1.34	1.34	1.35	1.56
*r*Cr-H_{O2}	2.57	1.90	2.88	1.97
*r*C4-H_{O2}	2.79	1.55	1.10	1.59
*r*O2-H_{O2}	0.96	1.14	3.50	1.12
*r*Cr-O2	2.10	1.98	1.85	1.99
*r*Cr-O1	1.96	1.90	1.86	1.89
ω	--	1173	--	1143

Table B.14. Key inter-atomic distances (Å) for formation of a bridging alkoxy ligand at a monoalkylchromium(II) site (Section 2.3.5 and Figure 2.14). The imaginary frequency of the transition state has units of i cm^{-1}.

	^{5}H.V	^{5}TS[H. V-H.IX]	^{5}H.IX	^{5}TS[H.V-H. X]	^{5}H. X
*r*C3-C4	1.34	1.38	1.51	1.40	1.51
*r*C3-O1	-	-	-	2.04	1.46
*r*C3-O2	-	2.30	1.46	-	-
*r*C4-H_{O2}	-	1.22	1.10	1.34	1.10
*r*O2-H_{O2}	0.97	1.66	2.71	1.30	4.70
*r*Cr-O2	2.09	1.98	2.09	2.06	1.92
*r*Cr-O1	1.95	1.92	1.92	1.97	2.09
ω	-	1000	-	1263	-

Table B.15: Key inter-atomic distances (Å) for Cossee-Arlman initiation at a Cr(III) site through proton transfer (Section 2.3.6 and Figure 2.15). The imaginary frequency of the transition state has units of i cm^{-1}. Values in parentheses are from Delley et al.[1]

	^{4}D.II	^{4}TS[D.II-D.IV]	^{4}D.IV	^{4}D.III	^{4}TS[D.III-D.V]	^{4}D.V
*r*Cr-C1	2.61 (2.68)	3.03	2.84	2.66 (2.71)	3.12	2.92
*r*Cr-C2	2.47 (2.49)	2.13 (2.15)	1.99 (1.99)	2.64 (2.72)	2.17 (2.18)	2.00 (2.00)
*r*Cr-H_{C2}	2.86	1.95 (1.98)	2.55	2.86	1.96 (1.98)	2.55
*r*C1-C2	1.34 (1.34)	1.34 (1.34)	1.33 (1.33)	1.33 (1.34)	1.34 (1.34)	1.33 (1.33)
*r*C2-H_{C2}	1.09	1.53 (1.53)	2.85	1.09	1.48 (1.48)	2.72
*r*O1-H_{C2}	3.59	1.14 (1.15)	0.96	2.64	1.15 (1.16)	0.96
*r*Cr-C3	-	-	-	2.65 (2.72)	2.48 (2.53)	2.51 (2.55)
*r*Cr-C4	-	-	-	2.65 (2.69)	2.53 (2.59)	2.48 (2.52)
ω	-	1326	-	-	1310	-

Table B.16: Key inter-atomic distances (Å) for Cossee-Arlman insertion into an ethenylchromium(III) site formed through proton transfer (Section 2.3.6 and Figure 2.15). The imaginary frequency of the transition state has units of i cm^{-1}. Values in parentheses are from Delley et al.[1]

	^{4}D.V	^{4}TS[D.V-D.VI]	^{4}D.VI
*r*Cr-C2	2.00 (2.00)	2.09 (2.06)	4.26
*r*Cr-C3	2.51 (2.55)	2.38	2.88
*r*Cr-C4	2.48 (2.52)	2.11 (2.14)	1.99
*r*C2-C3	2.98	2.14 (2.10)	1.50
*r*C3-C4	1.34 (1.34)	1.39 (1.40)	1.53
ω	-	367	-

Table B.17: Key inter-atomic distances (Å) for Cossee-Arlman insertion into a butenylchromium(III) site formed through proton transfer (Section 2.3.6 and Figure 2.16). The imaginary frequency of the transition state has units of i cm^{-1}. Values in parentheses are from Delley et al.[1]

	^{4}D.VI	^{4}D.VII	^{4}TS[D.VII-D.VIII]	^{4}D.VIII
*r*Cr-C4	1.99	2.03 (2.05)	2.16 (2.19)	3.43
*r*Cr-C5	-	2.55 (2.60)	2.35	2.39
*r*Cr-C6	-	2.47 (2.52)	2.11 (2.11)	1.98 (2.00)
*r*C4-C5	-	3.10	2.25 (2.16)	1.53
*r*C5-C6	-	1.34 (1.34)	1.38 (1.40)	1.51
ω	-	-	320	-

Table B.18: Key inter-atomic distances (Å) for direct reverse proton transfer termination at a butenylchromium(III) site (Section 2.3.6 and Figure 2.17). The imaginary frequency of the transition state has units of *i* cm^{-1}. Values in parentheses are from Delley et al.[1]

	^{4}D.VI	^{4}TS[D.VI-D.X]	^{4}D.X
*r*Cr-C4	1.99	2.17 (2.20)	2.62 (2.64)
*r*Cr-H_{O1}	2.86	1.91 (1.93)	-
*r*C4- H_{O1}	4.58	1.55 (1.55)	-
*r*O1- H_{O1}	0.96	1.12 (1.13)	-
ω	-	1252	-

Table B.19: Key inter-atomic distances (Å) for ethylene-assisted reverse proton transfer termination at a butenylchromium(III) site (Section 2.3.6 and Figure 2.17). The imaginary frequency of the transition state has units of *i* cm^{-1}.

	^{4}D.VII	^{4}TS[D.VII-D.IX]	^{4}D.IX
*r*Cr-C4	2.03	2.20	3.14
*r*Cr-C5	2.55	2.49	2.52
*r*Cr-C6	2.47	2.54	2.61
*r*Cr-H_{O1}	2.54	1.92	-
*r*C4- H_{O1}	3.06	1.50	-
*r*O1- H_{O1}	0.97	1.14	-
ω	-	1252	-

Table B.20: Key inter-atomic distances (Å) for vinyl-assisted reverse proton transfer termination at a butenylchromium(III) site (Section 2.3.6 and Figure 2.17). The imaginary frequency of the transition state has units of *i* cm^{-1}.

	^{4}D.VIb	^{4}TS[D.VIb-D.Xb]	^{4}D.Xb
*r*Cr-C1	2.48	2.47	2.38
*r*Cr-C2	2.43	2.42	2.67
*r*Cr-C4	2.02	2.21	3.80
*r*Cr-H_{O1}	2.53	1.91	-
*r*C4- H_{O1}	3.24	1.54	-
*r*O1- H_{O1}	0.97	1.13	-
ω	-	1209	-

Table B.21: Key inter-atomic distances (Å) for β-H elimination from a butenylchromium(III) site (Section 2.3.6 and Figure 2.18). The imaginary frequency of the transition state has units of i cm^{-1}. Values in parentheses are from Delley et al.[1]

	^{4}D.VI	^{4}TS[D.VI-D.XI]	^{4}D.XI	^{4}D.XIII	^{4}D.XII	^{4}D.XIV	^{4}TS[D.XIV-D.XV]	^{4}D.XV
*r*Cr-C3	2.88	2.41	2.56 (2.59)	2.61	-	-	-	-
*r*Cr-C4	1.99	2.12 (2.21)	2.37 (2.38)	2.37	-	-	-	-
*r*Cr-H_{C3}	2.96	1.60 (1.58)	1.57	1.62	1.60 (1.57)	1.58	1.59	3.06
*r*C3- H_{C3}	1.10	1.83 (1.82)	2.47	2.51	-	-	-	-
*r*C3- C4	1.53	1.38 (1.38)	1.35	1.35	-	-	-	-
*r*Cr-C5	-	-	-	2.57	-	2.45	2.39	2.84
*r*Cr-C6	-	-	-	2.51	-	2.39	2.25	1.99
*r*C5-H_{Cr}	-	-	-	2.32	-	2.33	1.94	1.09
*r*C5-C6	-	-	-	1.34	-	1.34	1.36	1.53
ω	-	483	-	-	-	-	280	-

Table B.22. Key inter-atomic distances (Å) for the Cossee-Arlman propagation mechanism starting from a monoalkylchromium(III) site (Section 2.3.7 and Figure 2.20). The imaginary frequency of the transition state has units of i cm^{-1}. Values in parentheses are from Espelid and Børve.[2]

	^{4}CA.I	^{4}CA.II	^{4}TS[CA.II-CA.IV]	^{4}CA.IV
*r*Cr-C4	2.00 (2.01)	2.01(2.03)	2.13(2.19)	3.35(4.42)
*r*Cr-C5	-	2.61(2.57)	2.30(2.32)	2.93(3.03)
*r*Cr-C6	-	2.48(2.37)	2.06(2.05)	2.00(2.01)
*r*C4-C5	-	3.15(3.07)	2.14(2.09)	1.53(1.54)
*r*C5-C6	-	1.34(1.36)	1.41(1.43)	1.53(1.52)
ω	-	-	275	-

Table B.23. Key interatomic distances (Å) for β-H elimination from a monoalkylchromium(III) site (Section 2.3.7 and Figure 2.21). The imaginary frequencies of the transition states have units of i cm^{-1}.

	^{4}CA.I	^{4}TS[CA.I-CA.III]	^{4}CA.III	^{4}CA.V	CA.VI	^{4}TS[CA.VI-CA.VII]	^{4}CA.VII
*r*Cr-C3	2.93	2.39	2.62	-	-	-	-
*r*Cr-C4	2.00	2.17	2.37	-	-	-	-
*r*C3-C4	1.53	1.38	1.35	-	-	-	-
*r*C3-H_{C3}	1.10	1.80	2.70	-	-	-	-
*r*Cr-H_{C3}	3.92	1.61	1.59	1.60	1.59	1.61	3.14
*r*C5-H_{C3}	-	-	-	-	2.60	1.83	1.09
*r*Cr-C5	-	-	-	-	2.53	2.37	2.95
*r*Cr-C6	-	-	-	-	2.44	2.21	1.99
*r*C5-C6	-	-	-	-	1.34	1.37	1.52
ω	-	683	-	-	-	667	-

Table B.24. Key interatomic distances (Å) for β-H transfer to monomer in a monoalkylchromium(III) site (Section 2.3.7 and Figure 2.22). The imaginary frequency of the transition state has units of i cm^{-1}.

	^{4}CA.I	^{4}CA.II	^{4}TS[CA.VIII-CA.IX]	^{4}CA.IX
*r*Cr-C3	2.93	2.97	2.38	2.71
*r*Cr-C4	2.00	2.01	2.15	2.38
*r*Cr-C5	-	2.61	2.35	3.02
*r*Cr-C6	-	2.48	2.18	2.02
*r*C3-C4	1.53	1.52	1.39	1.34
*r*C5-C6	-	1.34	1.39	1.52
*r*Cr-H_{C3}	3.92	3.05	1.74	3.26
*r*C3-H_{C3}	1.10	1.10	1.60	2.94
*r*C5-H_{C3}	-	4.82	1.60	1.09
ω	-	-	1109	-

Appendix C

C.1: Microkinetic Model for Cr(III) Site Initiated by Proton Transfer

C.1.1: Microkinetic Model for Species Fractions

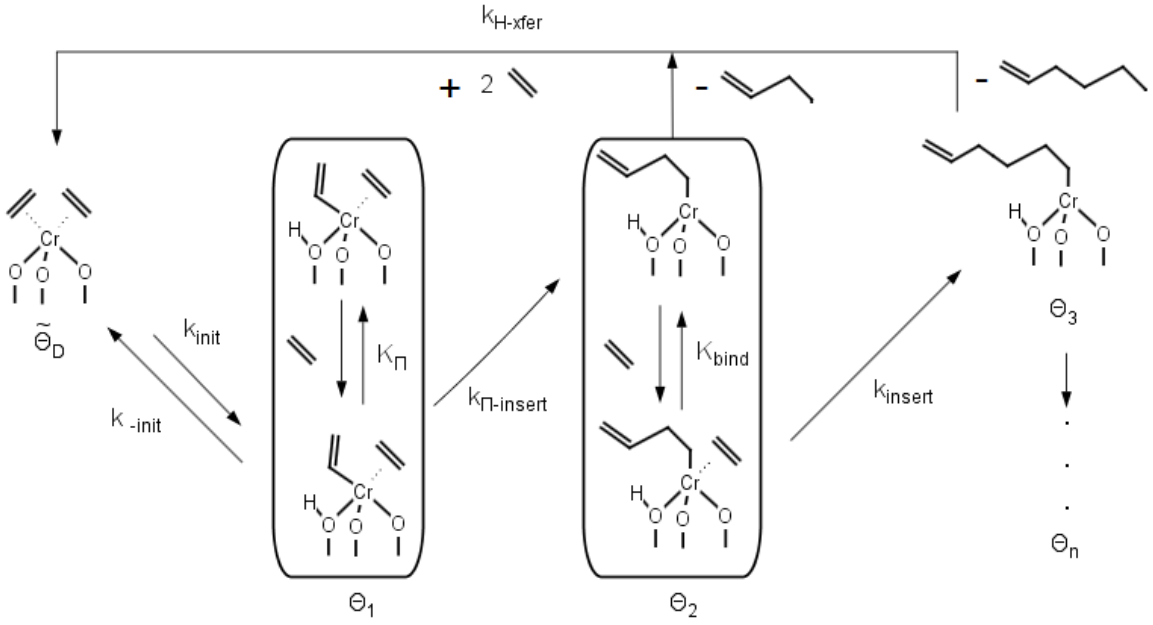

Figure C.1: Reaction Network for Proposed Cr(III) Initiation through Proton Transfer. In a reversible reaction, species "D" transfers a proton to a surface oxygen while a vinyl group forms on Cr (k_{init}). Ethylene then inserts ($k_{\pi\text{-}insert}$) into the Cr-vinyl bond of species "1," yielding species butenylchromium(III) species "2." Species "2" can then proton transfer to form an oligomer (top path with $k_{H\text{-}xfer}$) or continue to insert (k_{insert}).

Species $\tilde{\theta}_D$ is the initiating diethylene complex. Any other species *n* is a polymer of carbon length 2*n*. For instance, both species in the box for $\tilde{\theta}_1$ correspond to two carbon atoms. All species in a box (a bare polymer and its complex with ethylene) are assumed to be in equilibrium with each other.

The sum of all fractions of species *n*, $\tilde{\theta}_i$, must equal one.

$$\tilde{\theta}_D + \tilde{\theta}_1 + \tilde{\theta}_2 + S = 1 \tag{C.1}$$

S is the sum of all species with the number of carbon atoms greater than 2*n*.

$$S = \tilde{\theta}_3 + \tilde{\theta}_4 + ... + \tilde{\theta}_\infty \tag{C.2}$$

Pseudo-steady state approximations for species $\tilde{\theta}_D, \tilde{\theta}_1$, and $\tilde{\theta}_2$:

$$-k_{init}\tilde{\theta}_D + k_{-init}\tilde{\theta}_1 \frac{K_\pi P}{1+K_\pi P} + k_{H-xfer}\frac{\tilde{\theta}_2 + S}{1+K_{bind}P} = 0 \tag{C.3}$$

$$k_{init}\tilde{\theta}_D - k_{-init}\tilde{\theta}_1 \frac{K_\pi P}{1+K_\pi P} - k_{\pi-insert}\tilde{\theta}_1 \frac{K_\pi P}{1+K_\pi P} = 0 \tag{C.4}$$

$$k_{\pi-insert}\tilde{\theta}_1 \frac{K_\pi P}{1+K_\pi P} - k_{insert}\tilde{\theta}_2 \frac{K_{bind}P}{1+K_{bind}P} - k_{H-xfer}\frac{\tilde{\theta}_2}{1+K_{bind}P} = 0 \tag{C.5}$$

For instance, the first term in equation C.3 represents the loss of species "D" as it initiates the polymerization (by transferring a proton), forming species '1." Because the reaction is reversible, species "1" can reverse proton transfer and reform species "D," resulting in the second term in C.3. Furthermore, all other species ($\tilde{\theta}_2, \tilde{\theta}_3, .., \tilde{\theta}_\infty$) can also reverse proton transfer, reforming the diethylene complex species "D" (represented by the third term in C.3)

The solution to these equations is the following:

$$\tilde{\theta}_D = \frac{(k_{\pi-insert} + k_{-init})k_{H-xfer}K_\pi P}{k_{init}k_{\pi-insert}K_\pi K_{bind}P^2 + (k_{\pi-insert} + k_{-init} + k_{init})k_{H-xfer}K_\pi P + k_{init}k_{\pi-insert}K_\pi P + k_{init}k_{H-xfer}} \quad \text{(C.6)}$$

$$\tilde{\theta}_1 = \frac{k_{init}k_{H-xfer}(1 + K_\pi P)}{k_{init}k_{\pi-insert}K_\pi K_{bind}P^2 + (k_{\pi-insert} + k_{-init} + k_{init})k_{H-xfer}K_\pi P + k_{init}k_{\pi-insert}K_\pi P + k_{init}k_{H-xfer}} \quad \text{(C.7)}$$

$$\tilde{\theta}_2 = \frac{k_{init}k_{\pi-insert}k_{H-xfer}K_\pi P(1 + K_{bind}P)(k_{insert}K_{bind}P + k_{H-xfer})^{-1}}{k_{init}k_{\pi-insert}K_\pi K_{bind}P^2 + (k_{\pi-insert} + k_{-init} + k_{init})k_{H-xfer}K_\pi P + k_{init}k_{\pi-insert}K_\pi P + k_{init}k_{H-xfer}} \quad \text{(C.8)}$$

$$S = \frac{k_{init}k_{insert}k_{\pi-insert}k_{H-xfer}K_\pi K_{bind}P^2(1 + K_{bind}P)(k_{insert}K_{bind}P + k_{H-xfer})^{-1}}{k_{init}k_{\pi-insert}K_\pi K_{bind}P^2 + (k_{\pi-insert} + k_{-init} + k_{init})k_{H-xfer}K_\pi P + k_{init}k_{\pi-insert}K_\pi P + k_{init}k_{H-xfer}} \quad \text{(C.9)}$$

For $n \geq 3$, the pseudo-steady state approximation simplifies to only three terms.

$$k_{insert}\tilde{\theta}_{n-1}\frac{K_{bind}P}{1 + K_{bind}P} - k_{insert}\tilde{\theta}_n\frac{K_{bind}P}{1 + K_{bind}P} - k_{H-xfer}\frac{\tilde{\theta}_n}{1 + K_{bind}P} = 0 \quad \text{(C.10)}$$

In C.10, the first gain term represents ethylene insertion into a polymer with 2(n-1) carbons, forming a polymer with 2n carbons. The second loss term represents ethylene insertion into a polymer with 2n carbons, forming a polymer of length 2(n+1). The final loss term represents proton transfer from a polymer of length 2n.

The solution to this equation is the following recursion relation:

$$\tilde{\theta}_n = \varphi\tilde{\theta}_{n-1} \quad \text{(C.11)}$$

where

$$\varphi = \frac{k_{insert}K_{bind}P}{k_{insert}K_{bind}P + k_{H-xfer}} \quad \text{(C.12)}$$

C.1.2.: Fraction of Active Sites

Finally the fraction of active sites is given by all sites that are not "D:"

$$\tilde{\theta}_{active} = \tilde{\theta}_1 + \tilde{\theta}_2 + \tilde{\theta}_3 + \tilde{\theta}_4 + ... + \tilde{\theta}_\infty = \tilde{\theta}_1 + \tilde{\theta}_2 + S = 1 - \tilde{\theta}_D$$
$$= \frac{k_{init}(k_{\pi-insert}K_\pi K_{bind}P^2 + k_{H-xfer}K_\pi P + k_{\pi-insert}K_\pi P + k_{H-xfer})}{k_{init}k_{\pi-insert}K_\pi K_{bind}P^2 + (k_{\pi-insert} + k_{-init} + k_{init})k_{H-xfer}K_\pi P + k_{init}k_{\pi-insert}K_\pi P + k_{init}k_{H-xfer}} \quad \text{(C.13)}$$

All terms with k_{init}(~10^{-9} s^{-1}) in the denominator are extremely small, and $k_{\pi\text{-}insert} >> k_{H\text{-}xfer}$ in the numerator. C.13 simplifies to the C.14.

$$\tilde{\theta}_{active} \approx \frac{k_{init}k_{\pi-insert}(1 + K_{bind}P)}{(k_{\pi-insert} + k_{-init})k_{H-xfer}} \quad \text{(C.14)}$$

C.1.3: Polymerization Rate

The polymerization rate is determined by three terms (C.15). The first term represents ethylene insertion into a carbon with a vinyl ligand. The second term represents ethylene insertion into all species with $n > 2$. The final term represents the two ethylene which coordinate to the bare chromium after proton transfer, forming the site "D."

$$-r_{C2H4} = -r_{\pi-insert} - r_{insert} - r_{\theta_2+S\rightarrow\theta_D} \quad \text{(C.15)}$$

$$-r_{\pi-insert} = k_{\pi-insert}\frac{K_\pi P}{1 + K_\pi P}\tilde{\theta}_1 \quad \text{(C.16)}$$

$\tilde{\theta}_1$ is given by a simplified equation C.7

$$-r_{\pi-insert} \approx k_{\pi-insert}\frac{K_\pi P}{1 + K_\pi P}\left(\frac{k_{init}k_{H-xfer}(1 + K_\pi P)}{(k_{\pi-insert} + k_{-init})k_{H-xfer}K_\pi P}\right) \quad \text{(C.17)}$$

$$-r_{\pi-insert} \approx k_{init}\frac{k_{\pi-insert}}{k_{\pi-insert} + k_{-init}} \quad \text{(C.18)}$$

Ethylene insertion into all species with $n \geq 2$:

$$-r_{insert} = k_{insert}\frac{K_{bind}P}{1+K_{bind}P}\sum_{n=2}^{\infty}\tilde{\theta}_n \tag{C.19}$$

$$-r_{insert} \approx k_{insert}\frac{K_{bind}P}{1+K_{bind}P}\left(\frac{k_{init}k_{\pi-insert}K_{\pi}P(1+K_{bind}P)}{(k_{\pi-insert}+k_{-init})k_{H-xfer}K_{\pi}P}\right) \tag{C.20}$$

$$-r_{insert} \approx k_{init}\frac{k_{insert}}{k_{H-xfer}}K_{bind}P\frac{k_{\pi-insert}}{k_{\pi-insert}+k_{-init}} \tag{C.21}$$

Ethylene consumption following proton transfer:

$$-r_{\theta_2+S\rightarrow\theta_D} = 2k_{H-xfer}\sum_{n=2}^{\infty}\tilde{\theta}_n \tag{C.22}$$

$$-r_{\theta_2+S\rightarrow\theta_D} \approx 2k_{H-xfer}\left(\frac{k_{init}k_{\pi-insert}K_{\pi}P(1+K_{bind}P)}{(k_{\pi-insert}+k_{-init})k_{H-xfer}K_{\pi}P}\right) \tag{C.23}$$

$$-r_{\theta_2+S\rightarrow\theta_D} \approx 2k_{init}(1+K_{bind}P)\frac{k_{\pi-insert}}{k_{\pi-insert}+k_{-init}} \tag{C.24}$$

For C.15, the most significant contribution is frrm $-r_{insert}$, because $-r_{\pi-insert}$ (C.18) and $-r_{\theta_2+S\rightarrow\theta_D}$ (C.24) are led by terms with k_{init} (~10^{-9} s^{-1}).

$$-r_{C2H4} \approx k_{init}\frac{k_{insert}}{k_{H-xfer}}K_{bind}P\frac{k_{\pi-insert}}{k_{\pi-insert}+k_{-init}} \tag{C.25}$$

C.1.4: Molecular Weight

Number average molecular weight:

$$M_n = \frac{\sum_{n=2}^{\infty}2n\tilde{\theta}_n}{\sum_{n=2}^{\infty}\tilde{\theta}_n} = \frac{2\tilde{\theta}_2\sum_{n=2}^{\infty}n\varphi^{n-2}}{\tilde{\theta}_2\sum_{n=2}^{\infty}\varphi^{n-2}} \tag{C.26}$$

$$M_n = \frac{2\dfrac{(2-\varphi)}{(1-\varphi)^2}}{\dfrac{1}{\varphi(1-\varphi)}} = \frac{2\varphi(2-\varphi)}{(1-\varphi)} \tag{C.27}$$

Weight average molecular weight

$$M_w = \frac{\sum_{n=2}^{\infty}(2n)^2\tilde{\theta}_n}{\sum_{n=2}^{\infty}2n\tilde{\theta}_n} = \frac{4\tilde{\theta}_2\sum_{n=2}^{\infty}n^2\varphi^{n-2}}{2\tilde{\theta}_2\sum_{n=2}^{\infty}n\varphi^{n-2}} \tag{C.28}$$

$$M_w = \frac{\dfrac{4(4-3\varphi+\varphi^2)}{(1-\varphi)^3}}{2\dfrac{(2-\varphi)}{(1-\varphi)^2}} = \frac{2(4-3\varphi+\varphi^2)}{(2-\varphi)(1-\varphi)} \tag{C.29}$$

C.2: Microkinetic Model for (≡SiO_2)Cr(III) Cossee-Arlman mechanism

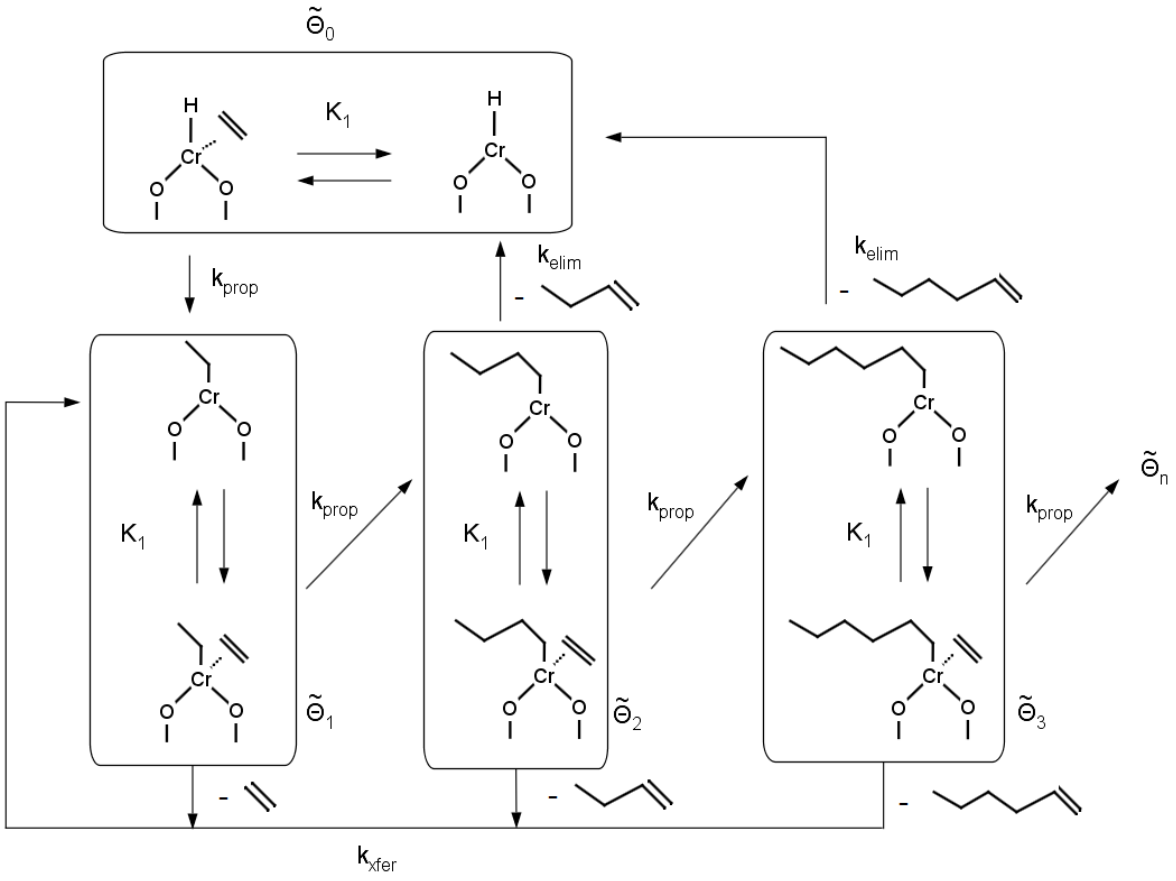

Figure C.2: Reaction Diagram for Cossee-Arlman Mechanism for (≡SiO_2)Cr(III) site. Species $\tilde{\theta}_n$ inserts ethylene to from species $\tilde{\theta}_{n+1}$. For $n \geq 2$, a polymer can eliminate to a hydridochromium $\tilde{\theta}_0$. For $n \geq 1$, a polymer can transfer hydrogen to a bound ethylene, ejecting the chain and forming an ethylchromium $\tilde{\theta}_1$.

C.2.1: Microkinetic Model for Species Fractions

Pseudo-steady state approximations for species $\tilde{\theta}_0$ and $\tilde{\theta}_1$:

$$-k_{prop}\frac{K_1P}{1+K_1P}\tilde{\theta}_0+\frac{k_{elim}}{1+K_1P}S=0 \tag{C.30}$$

$$-k_{prop}\frac{K_1P}{1+K_1P}\tilde{\theta}_1+k_{prop}\frac{K_1P}{1+K_1P}\tilde{\theta}_0+\frac{k_{elim}}{1+K_1P}\tilde{\theta}_1+k_{xfer}\frac{K_1P}{1+K_1P}\left(S-\tilde{\theta}_1\right)=0 \tag{C.31}$$

$$\tilde{\theta}_0+\tilde{\theta}_1+S=0 \tag{C.32}$$

The solution to these equations is:

$$\tilde{\theta}_0=\frac{k_{elim}}{k_{prop}K_1P+k_{elim}} \tag{C.33}$$

$$\tilde{\theta}_1=\frac{k_{prop}K_1P}{k_{prop}K_1P+k_{elim}}\frac{k_{xfer}K_1P+k_{elim}}{k_{prop}K_1P+k_{xfer}K_1P+k_{elim}} \tag{C.34}$$

$$S=\frac{k_{prop}K_1P}{k_{prop}K_1P+k_{elim}} \tag{C.35}$$

For all species $n\geq 2$:

$$-k_{prop}\frac{K_1P}{1+K_1P}\tilde{\theta}_n+k_{prop}\frac{K_1P}{1+K_1P}\tilde{\theta}_{n-1}+\frac{k_{elim}}{1+K_1P}\tilde{\theta}_n+k_{xfer}\frac{K_1P}{1+K_1P}\tilde{\theta}_n=0 \tag{C.36}$$

$$\tilde{\theta}_n=\varphi\tilde{\theta}_{n-1} \tag{C.37}$$

$$\varphi=\frac{k_{prop}K_1P}{k_{prop}K_1P+k_{xfer}K_1P+k_{elim}} \tag{C.38}$$

C.2.2: Polymerization Rate

The polymerization rate includes insertion into all species $i = 0, 1, 2, \ldots, \infty$ and β-H transfer to monomer for all species $i = 2, 3, 4, \ldots, \infty$. Species 0 (hydridochromium) cannot transfer hydrogen to monomer, and species 1 (ethylchromium) produces ethylene when it transfers monomer.

$$-r_{C2H4} = \frac{k_{prop}K_1P}{1+K_1P}(\tilde{\theta}_0 + \tilde{\theta}_1 + \tilde{\theta}_2 + ...) + \frac{k_{xfer}K_1P}{1+K_1P}(\tilde{\theta}_2 + \tilde{\theta}_3 + ...) \tag{C.39}$$

$$-r_{C2H4} = k_{prop}\frac{K_1P}{1+K_1P} + \frac{k_{xfer}K_1P}{1+K_1P}\left(\frac{k_{prop}K_1P}{k_{prop}K_1P + k_{elim}} + \frac{k_{prop}K_1P}{k_{prop}K_1P + k_{elim}}\frac{k_{xfer}K_1P + k_{elim}}{k_{prop}K_1P + k_{xfer}K_1P + k_{elim}}\right) \tag{C.40}$$

C.2.3: Molecular Weight

Number average molecular weight:

$$M_n = \frac{\sum_{n=1}^{\infty} 2n\tilde{\theta}_n}{\sum_{n=1}^{\infty}\tilde{\theta}_n} = \frac{2\tilde{\theta}_1\sum_{n=1}^{\infty} n\varphi^{n-1}}{\tilde{\theta}_1\sum_{n=1}^{\infty}\varphi^{n-1}} \tag{C.41}$$

$$M_n = \frac{2\dfrac{\varphi}{(1-\varphi)^2}}{\dfrac{\varphi}{(1-\varphi)}} = \frac{2}{(1-\varphi)} \tag{C.42}$$

$$M_n = 2\frac{k_{prop}K_1P + k_{xfer}K_1P + k_{elim}}{k_{xfer}K_1P + k_{elim}} \tag{C.43}$$

Weight average molecular weight

$$M_w = \frac{\sum_{n=1}^{\infty}(2n)^2\tilde{\theta}_n}{\sum_{n=1}^{\infty}2n\tilde{\theta}_n} = \frac{4\tilde{\theta}_1\sum_{n=1}^{\infty}n^2\varphi^{n-1}}{2\tilde{\theta}_1\sum_{n=1}^{\infty}n\varphi^{n-1}} \tag{C.44}$$

$$M_w = \frac{4\dfrac{\varphi(1+\varphi)}{(1-\varphi)^3}}{2\dfrac{\varphi}{(1-\varphi)^2}} = 2\frac{(1+\varphi)}{(1-\varphi)} \tag{C.45}$$

$$M_w = 2\frac{2k_{prop}K_1P + k_{xfer}K_1P + k_{elim}}{k_{xfer}K_1P + k_{elim}} \tag{C.46}$$

Appendix D

D.1: Figures

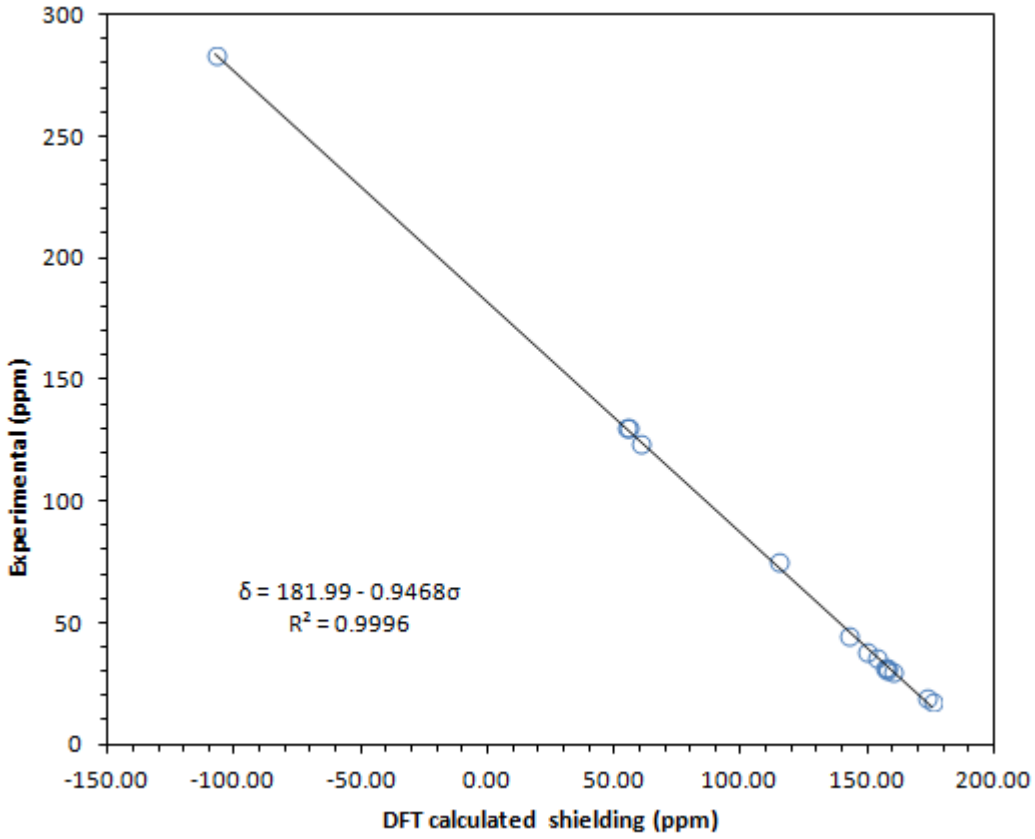

Figure D.1: Calibration Curve for Calculated ^{13}C-NMR Chemical Shifts in Re(7+) compounds: CH3ReO3, [(Me3CCH2)2PhReO2] and [Me3CCH2ReO2(=CHC(CH3)3)].

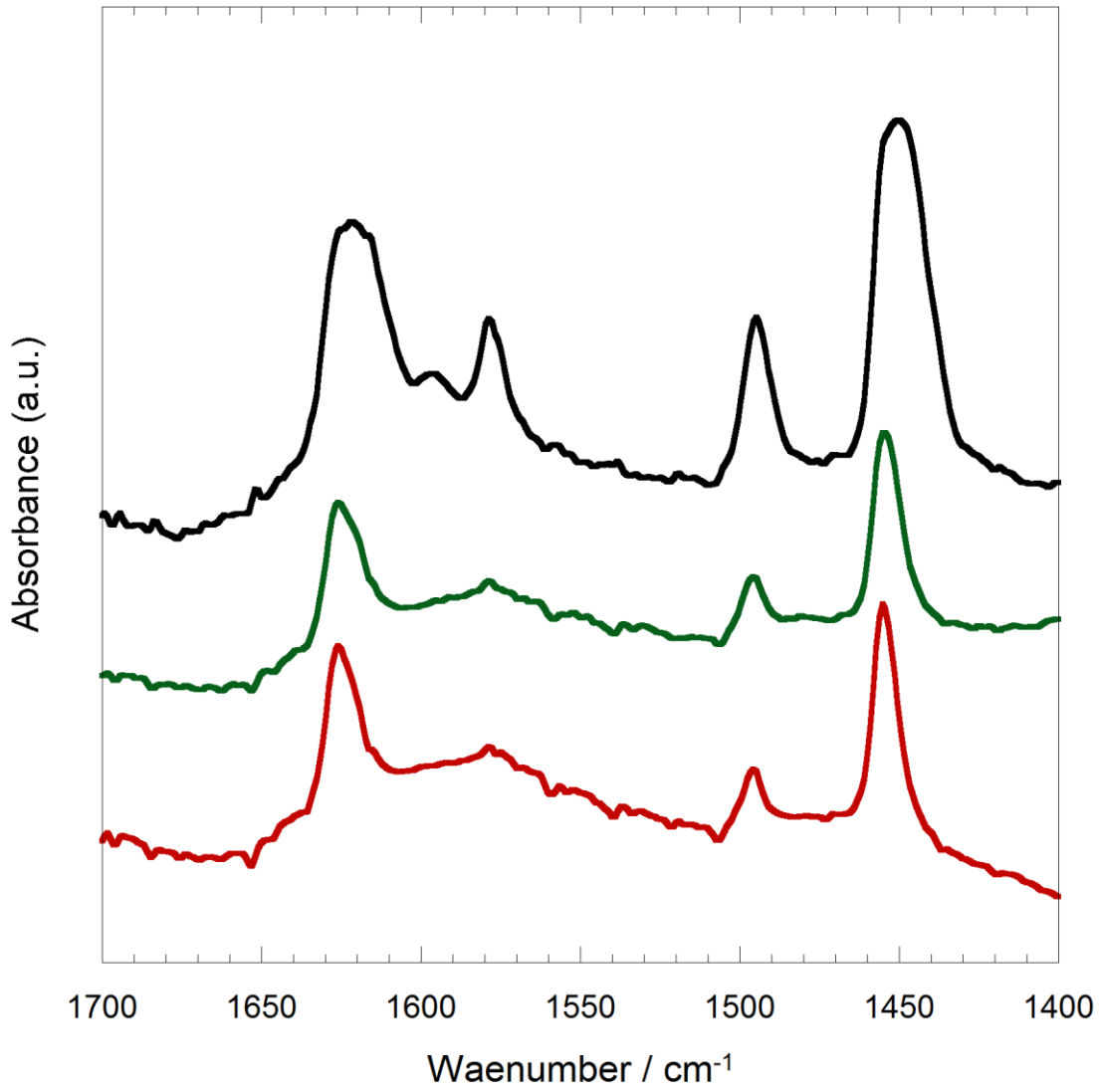

Figure D.2. IR of pyridine adsorbed on Cl-Al_2O_3 at RT and desorbed for 20 min at RT (black line), 200 °C (green line) and 300 °C (red line). The spectra in shows the presence of bands related to Lewis acid sites on the surface of Cl-Al_2O_3 after evacuation at different temperatures at 1455, 1495 and 1625 cm^{-1}.[1] No bands associated with pyridinium ions on the surface were detected at 1540 and 1640 cm^{-1}. In particular a strong band at 1625 cm^{-1}, typical for strong Lewis acid sites, is well visible after desorption at 200 and 300 °C.

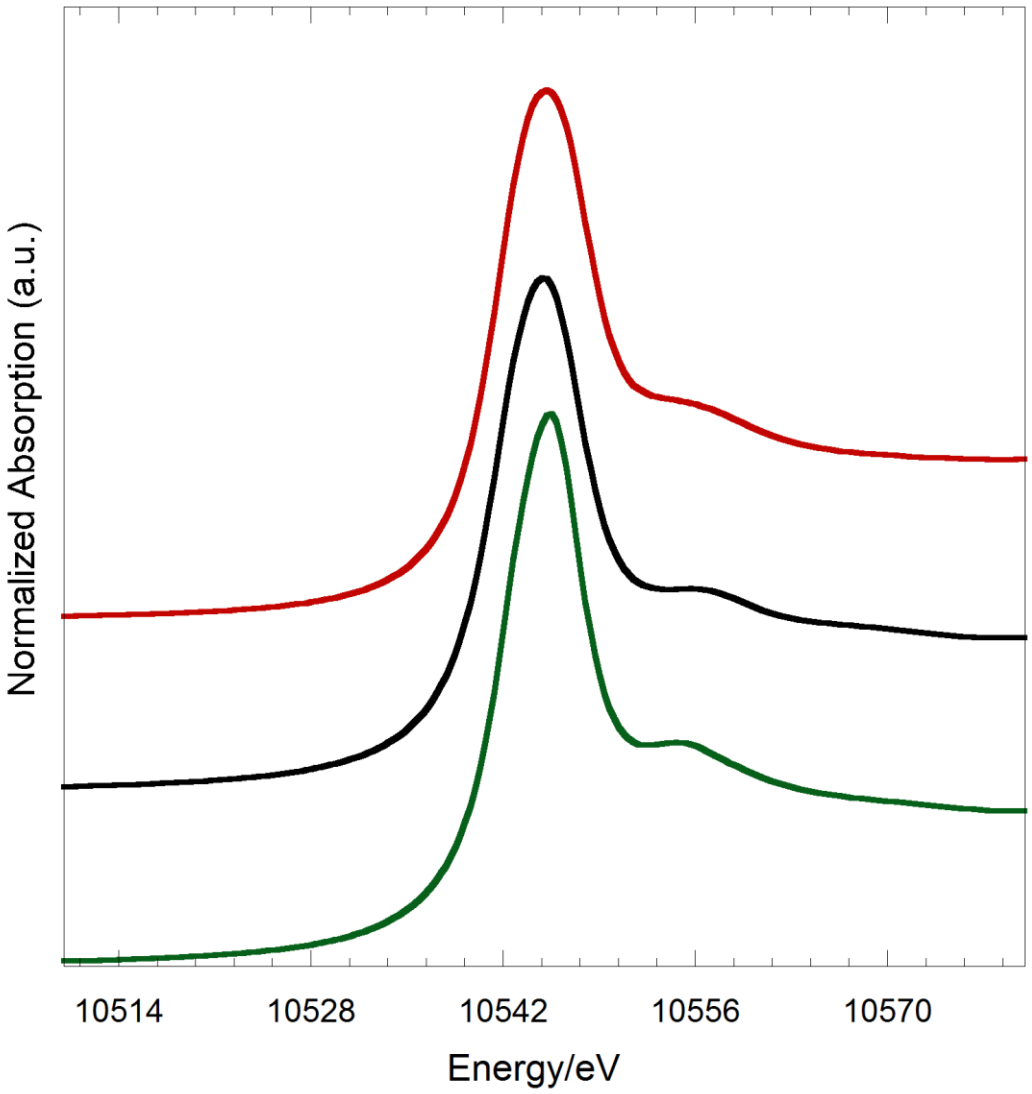

Figure D.3. X-ray Absorption Spectra at Re L_{III} edge for MTO (green line), MTO on γ-Al_2O_3 (black line) and MTO on Cl-Al_2O_3 (red line). A pronounced white line, similar to Re_2O_3 and NH_4ReO_4, signature of a high Re oxidation state, was detected for all samples. The position of the edge at 10542 eV did not appreciably shift after MTO was grafted, both on alumina and chlorinated alumina, confirming that no detectable Re oxidation state change occurred.[2]

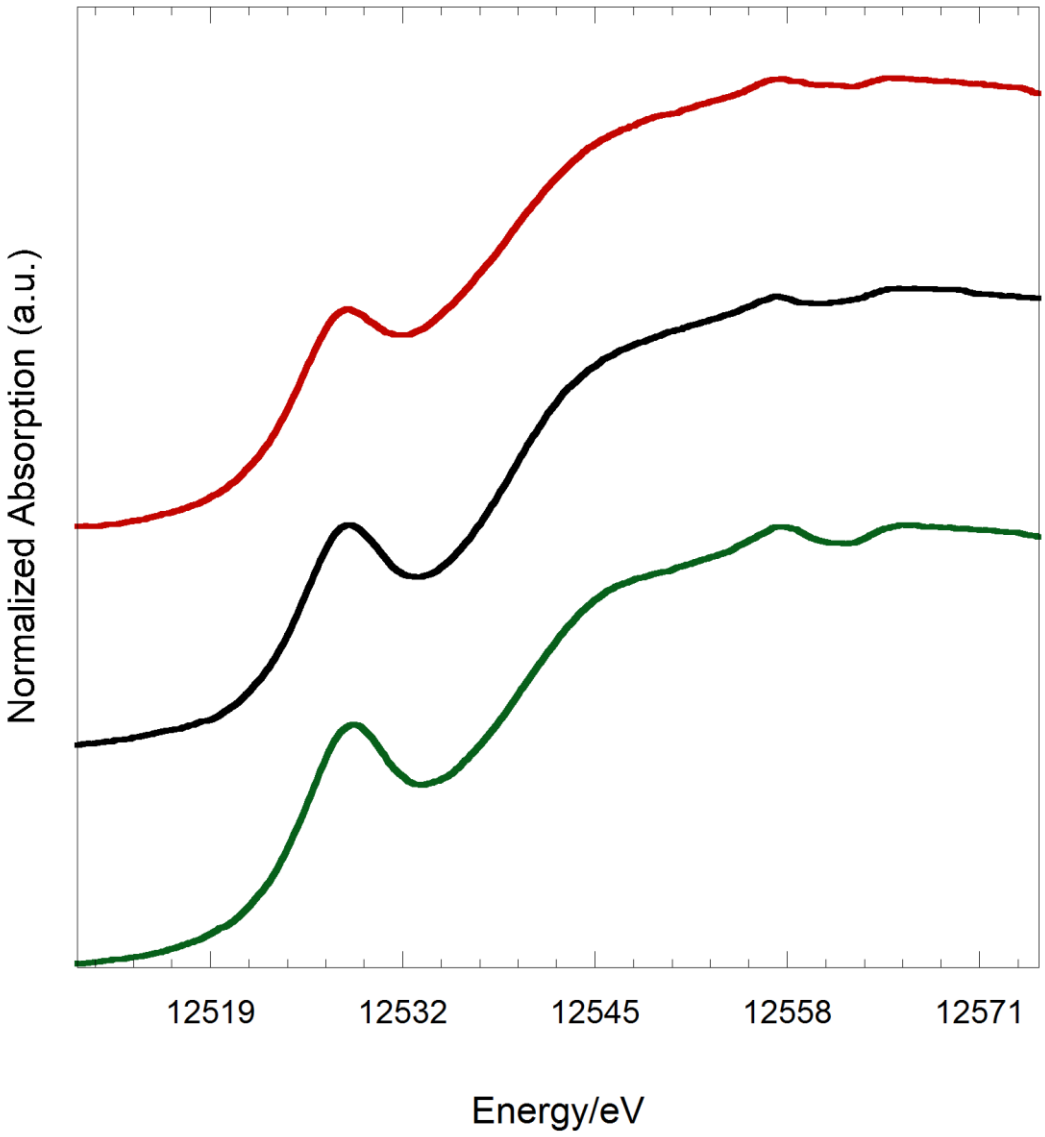

Figure D.4: X-ray Absorption Spectra at Re L_I edge for MTO (green line), MTO on γ-Al_2O_3 (black line) and MTO on Cl-Al_2O_3 (red line). A prominent pre-edge, caused by the dipolar 2s→6p transition, is detected at 12526 eV for all samples revealing a non-centrosymmetric geometry of the Re sites that cause an hybridization of the 5p-6d orbitals. The same pre-edge feature was detected for Re_2O_7 and NH_4ReO_4.[2] The position of the edge at 12539 eV for all samples is compatible with the presence of Re(VII). After grafting of MTO both on alumina and chlorinated alumina no substantial differences among were detected in the spectra.

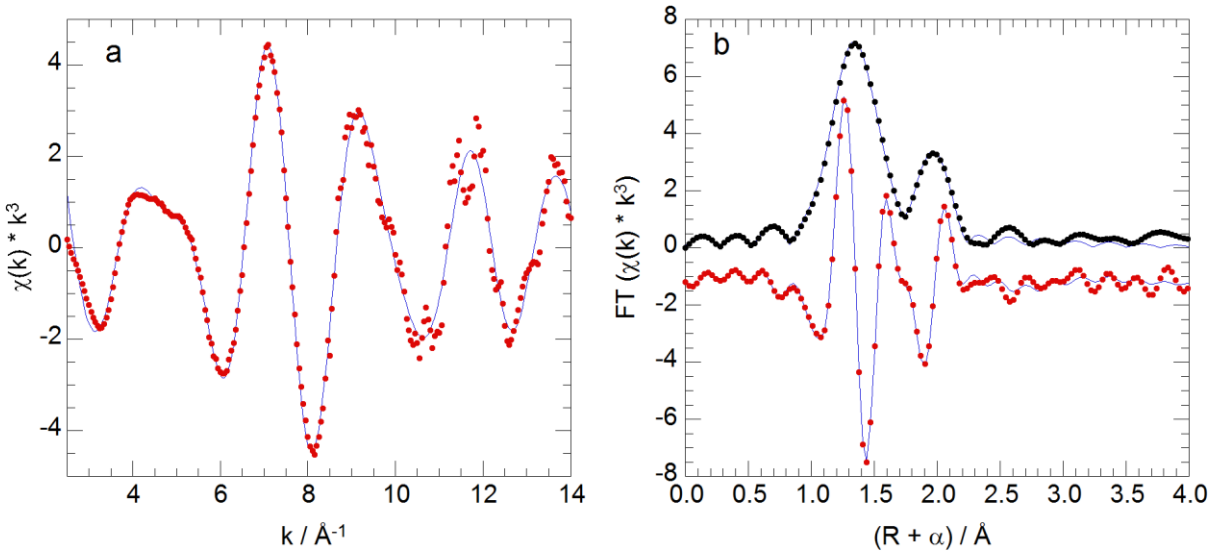

Figure D.5: (a) EXAFS data in (a) k^3-weighted k-space (red points and line) and (b) non-phase-corrected R-space (imaginary, red points; FT magnitude, black points) MTO supported on Cl-γ-Al_2O_3. Parameters for the curve-fit (blue lines) are given in Table 3.2.

D.2 Tables

Table D.1: Calculated ^{13}C chemical shifts (ppm) for molecular organorhenium(VII) compounds used in calibration curve of Figure D.1

compound	solvent	Calculated isotropic shielding	Calculated chemical shift	Observed chemical shift
CH3ReO3	CDCl3	173.5	17.7	19.6
	C6H6	175.6	15.8	18.1
[(Me3CCH2)2PhReO2]	CDCl3	55.7	129.2	131.0 metaC)
		54.5	130.4	130.5 (orthoC)
		60.7	124.5	124.1 (paraC)
		115.1	73.0	75.9 (CH2)
		153.4	36.8	36.4 (CH2C)
		157.8	32.6	31.8 (CH3)
[Me3CCH2ReO2(=CHC(CH3)3)]	CD3C6D5	-107.6	283.9	283.3 (CH)
		142.4	47.7	45.3 (CHC)
		149.6	33.4	38.5 (CH2)
		157.0	32.6	32.1 (CH3)
		157.8	30.5	31.3 (CH2C)
		160.1	30.5	29.9 (CH3)

Table. D.2. Calculated ^{13}C chemical shifts (ppm) for MTO on Cl-Al2O3 and carbene intermediates.

species	Calculated isotropic shielding	Calculated chemical shift
I	163.1	27.6
II	157.7	32.7
III	155.4	34.8
IV	147.1	42.7
V	149.8	40.1
Ia	-62.1	241
IIa	-68.7	247
IVa	-58.5	237
Va	-107.7	284
IVb	-114.1	290
IVc	104.8	82
Vb	-109.7	285

D.3: References

1 Berteau, P., Kellens, J. M., Delmon, B. *J. Chem. Soc. Faraday Trans.* 1991 87 1425.

2 Tougerti, A., Cristol, S., Berrier, E., Briois, V., La Fontaine, C., Villain, F., Joly, Y. *Phys. Rev. B* 2012 85 125136-1.